8-2023

Investigation of VO2 thin films and devices for opto-electromechanical applications

Samee Azad
sameea@clemson.edu

INVESTIGATION OF VO_2 THIN FILMS AND DEVICES FOR OPTO-ELECTROMECHANICAL APPLICATIONS

A Dissertation
Presented to
the Graduate School of
Clemson University

In Partial Fulfillment
of the Requirements for the Degree
Doctorate of Philosophy
Electrical Engineering

---

by
Samee Azad
August 2023

Accepted by:
Dr. Goutam Koley, Committee Chair
Dr. Judson Ryckman
Dr. Pingshan Wang
Dr. Apparao Rao

ABSTRACT

Specialized and optimized low pressure direct oxidation technique have been implemented to synthesize high quality VO_2 thin films on various substrates (sapphire, SiO_2/Si, AT-cut quartz, GaN/AlGaN/GaN/Si and muscovite). Structural and surface characterization methods such as X-ray diffraction, Raman spectroscopy and atomic force microscopy have been administered on the grown VO_2 films which indicate their material quality. Transition of characteristics of the VO_2 films are caused by semiconductor metal transition (SMT). This phenomenon is attributed as the change maker in transition of resistivity and transmitted optical power through the VO_2 films. Apart the substrates mentioned, metal doped VO_2 films have been synthesized and characterized on quartz and muscovite, which are found to have transition temperature near the room temperature level, indicating to the possibility of high sensitive VO_2 based sensors to be manufactured. Also, the VO_2 films on flexible muscovite displays the direct effect of mechanical strain on the electrical and optical characteristics of the films. After metal finger patterning and releasing the VO_2 membranes from the synthesized thin films, combination of all these characteristics of VO_2 thin film is the reason of transmitted infrared beam through the VO_2 membrane being modulated periodically due to implementation of external electric field at different frequencies.

ACKNOWLEDGMENTS

My gratitude goes to the Clemson University for allowing me to be one of its graduate students and providing me with a wide range of research opportunities, which I could not imagine before setting foot on this great campus. I am grateful to my parents and family members for their continuous support and inspiration. I must thank Dr. Goutam Koley from the bottom of my heart for including me into his dynamic research group and taking me under his mentorship and guidance, a rare privilege any researcher in my field would love to compete for. Since the beginning, I am always astounded by his calm and composed attitude, at the same time his zeal and passion and excitement for exploring and implementing innovative research ideas and concepts. His helpfulness towards his disciples is a great relief for us, when I get stuck in my research and start to give up hope, each time I get recharged by the inspiration and enthusiasm from Dr. Koley.

I also count myself lucky to have met and worked with Dr. Ferhat Bayram, Dr. Digangana Khan, Dr. Hongmei Li, Dr. Durga Gajula, Dr. Baaladitya Uppalapati, Lavanya Muthusamy, Andrew Gunn, Rahul Singh, Rackley Wren, Manav Bava and Makhluk Prio in our research group. My time with this great group of scientists and researchers will always be a very important part of my life and career.

TABLE OF CONTENTS

LIST OF TABLES

LIST OF FIGURES

CHAPTER ONE

INTRODUCTION TO PHASE TRANSITION MATERIALS

Different types of materials exist in form of compounds or alloys which can change their structural phase due to some external or internal excitation factors, leading to a drastic change in their multiple properties. The change may be reversible, or irreversible or semi-reversible, but the condition lies that the change of properties has to be drastic and noticeable, and these characteristics have to be inherent property of the pure form of that particular material. For example, an intrinsic silicon can change its conductivity due to external heating, but the change is merely because of the low bandgap of silicon causing electron-hole pair creation due to the thermal effect, and the change of resistivity or conductivity is not more than some percentage. And an extrinsic p-type or n-type silicon does witness a few hundreds of percentage in its conductivity, but its state become impure due to the external doping. However, actual phase transitional oxides and alloys experience change of properties by percentage of up to several hundreds of thousands. These near-abrupt huge transition of properties enable the phase transitioning materials to be utilized for a wide variety of applications related to sensing and switching.

Reversible and irreversible phase transitioning materials

On basis of how the properties of the phase transitioning materials can return to their initial condition when the transition causing external factor is removed, they can be

classified as reversible and irreversible types. Some notable well known reversible phase transitioning materials are different types of oxides of vanadium, for example VO_2, V_2O_3, V_2O_5. While they demonstrate some hysteresis during the forward and reverse directions of their transition, they can return to their initial state and exhibits the initial properties as they had before the transition. This easy reversibility causes the oxides of vanadium to be used as fast switching applications. As shown in Figure 1.1 (a), VO_2 is a reversible phase changing material which has high resistivity during its monoclinic phase, acts like a semiconductor After phase changing, the resistivity becomes low, acts like a metal in rutile phase. Phase transition of polycrystalline monoclinic VO_2 thin film can occur by external factors like heating, electric field, mechanical strain etc. After the removal of the phase transitioning factor, the VO_2 thin film returns to its initial monoclinic phase and polycrystalline structure, retaining its high resistivity during semiconducting state.

However, this is not the case of another phase transitioning material, commonly known as GST (Germanium-Antimony-Telluride). Germanium-Antimony-Telluride is a non-reversible phase changing material [1]. The GST thin film has high resistivity during amorphous phase, and acts like a semiconductor. After the phase transition, the resistivity becomes low, and GST acts like a metal in crystalline phase (FCC and HCP). Phase transition can occur by heating, when the temperature is around 150 C. However, unlike the oxides of Vanadium, merely removing the heat can neither get the GST back to its amorphous structure, nor it can retain its initial high resistivity (Figure 1.1 (b)). In order to reverse the GST back to its initial semiconducting state, the GST needs to be heated

until it reaches melting point (600 °C) and become amorphous. Only after that the cooling of GST can send it back to its initial amorphous structure and semiconducting state. This type of irreversibility allows us to implement GST for memory device applications.

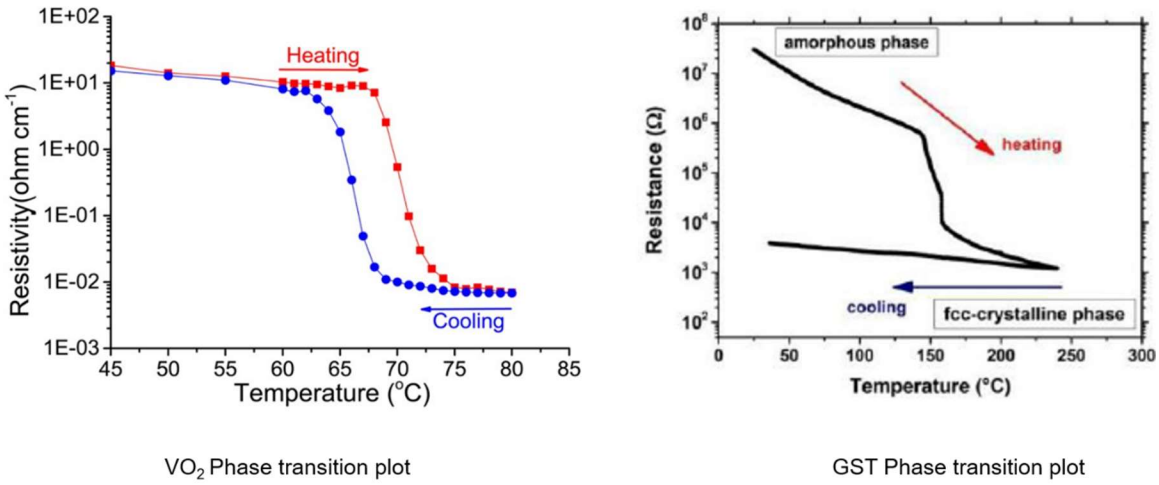

VO_2 Phase transition plot

GST Phase transition plot

Figure 1.1: Change of resistivity during phase transition for (a) VO_2 and (b) GST

Vanadium oxide based phase changing materials (VO_2, V_2O_3, V_2O_5)

Among the reversible phase transitioning materials like oxides of vanadium, the vanadium dioxide (VO_2), vanadium trioxide (V_2O_3) and vanadium pentaoxide (V_2O_5) most commonly found. As shown in Figure 1.2 (a), during the semiconducting state, the VO_2 maintains the monoclinic crystal structure. However, at metallic state, its crystal structure shifts to rutile and returns to monoclinic once the VO_2 comes back to semiconducting state. Crystal structure of V_2O_3 shifts from monoclinic to conundrum during phase transition (Figure 1.2 (b)) [2]. However, the orthorhombic crystal structure

of V2O5 remains unchanged despite its transition from semiconducting to metallic and vice versa (Figure 1.2 (c)) [3].

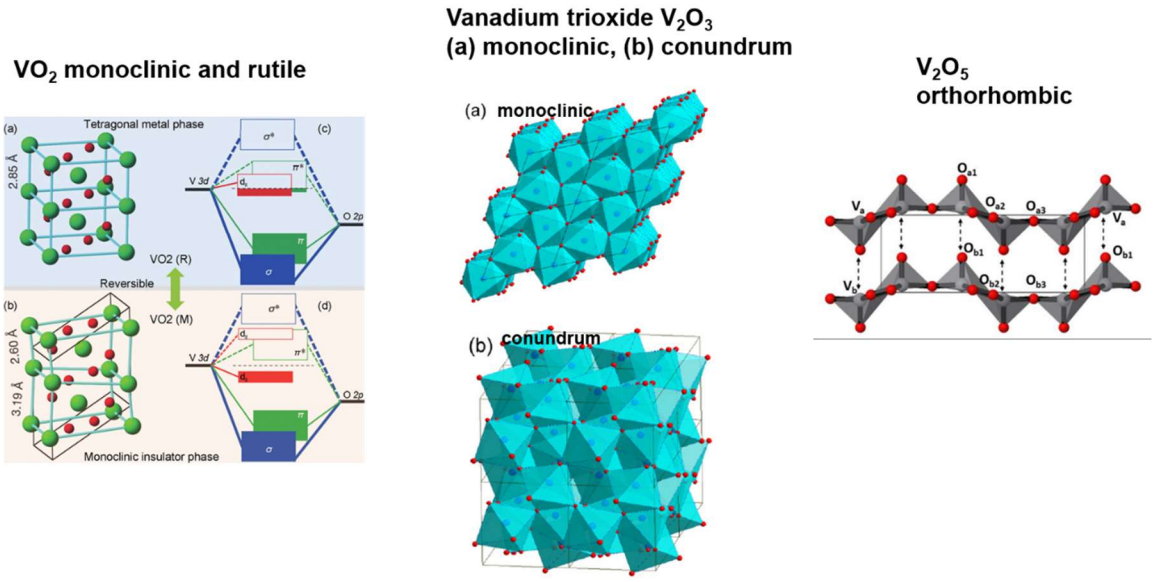

Figure 1.2: Change of crystal structure during phase transition for (a) VO_2, (b) V_2O_3 and (c) V_2O_5

The phase transition characteristics are plotted in Figure 1.3, which shows the transition temperature of VO_2 is around 67 C [4], compared to the phase transition temperature of V_2O_3, which is way below the room temperature (-113 C) [2], and the phase transition temperature of V_2O_5, 280 C [3]. This comparison clearly indicates the convenience of using VO_2 as a fast phase transitioning material because of the easy achievability of its transition temperature.

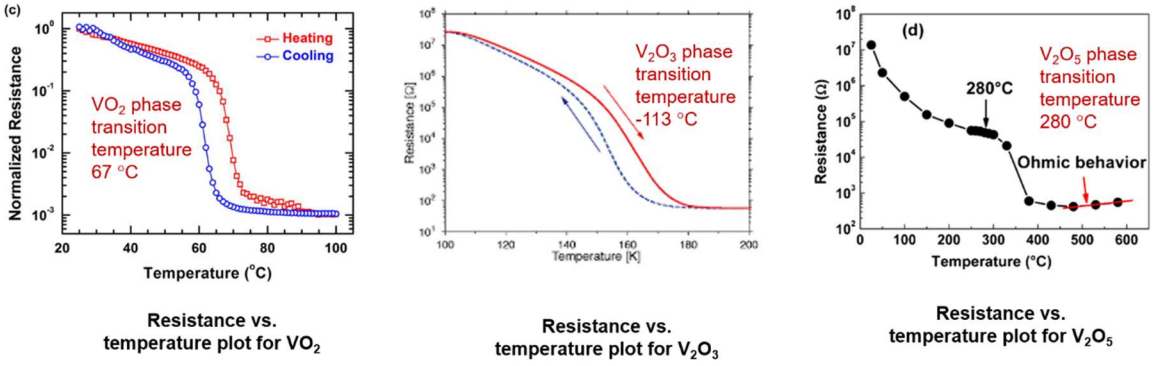

Figure 1.3: Change of resistivity during phase transition for (a) VO_2, (b) V_2O_3 and (c) V_2O_5

Electronic and crystal structure of VO_2

Vanadium can form a variety of lattice structures by transforming into different orientations. Tetragonal (V_2O_4), orthorhombic (V_2O_5), monoclinic and corundum (V_2O_6) are some of the notable orientations. While VO_2 is at the semiconducting state, it arranges into a structure called monoclinic (low temperature), and when the VO_2 is at the metallic state, it assumes a tetragonal (Rutile) structure [6] (high temperature). In Figure 1.4 we observe that, vanadium system has a lattice structure and it contains six oxygen atoms around the vanadium atom. The oxygen atoms assume an octahedral system. When the temperature is below transition level, a dimer combination of two-unit cells (V - V metal bond causes the axial dimerism) takes the monoclinic form. A monoclinic unit cell surrounds the vanadium-vanadium dimer in a lopsided way, with tetragonal structure. This shifted tilting deforms the vanadium-vanadium dimer octahedron structure of oxygen also.

The vanadium dimer is the primary reason for the VO_2 semiconductor to metallic transition (SMT). The vanadium atom ([Ar] $4s^2 3d^5$) orbitals and the two oxygen atoms ($1s^2 2s^2 2p^4$) combine and creates the VO_2 electronic structure. Four electrons from the valence-shell of vanadium ion play role to finish the two oxygen atomic orbitals, and in vanadium ion it leaves behind one electron. This electron occupies the d orbital near the 3d Fermi level.

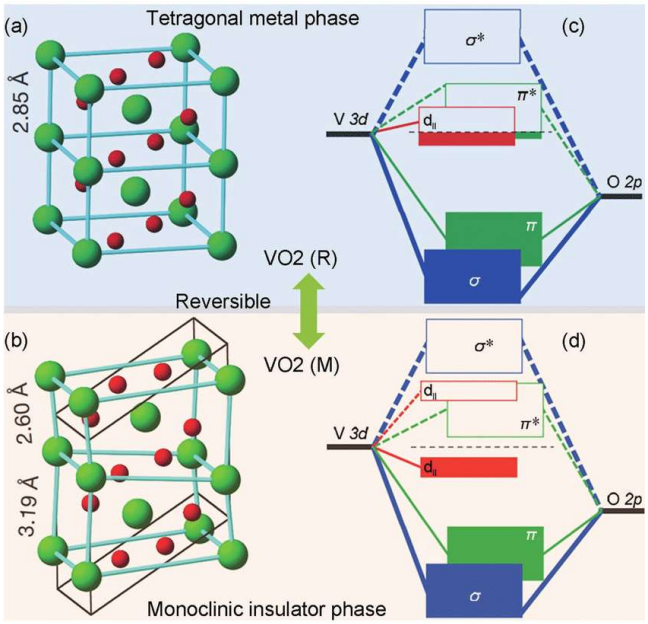

Figure 1.4: Monoclinic and rutile phases of VO_2

The 2p orbital electrons of oxygen plays no contribution for the electrical conductivity. The d orbitals of the vanadium ions are segregated into lower energy t2g and eg s orbitals. The electron orbital is quite below the Fermi level. The t2g orbital

segregates into bonding (a1g) and antibonding (eg p) orbitals. However, the Eg s orbital is in energy state which is higher. Therefore it stays empty. Later, an electron of vanadium ion will occupy the a1g orbital. So, the arrangement of V-V and oxygen cause difference in the bandgap of a1g and Eg p.

Semiconductor to metallic transition mechanism of VO_2

People think that, there is no interaction between an insulator and a metal. But some materials exhibit semiconductor to metal transition or vice versa. This situation is quite interesting because these materials can be good candidates for switching applications.

Various mechanisms may trigger semiconductor to metal transition. Heating, mechanical strain, or electric fields are some of those mechanisms. Material properties such as resistivity or resistance, may undergo semiconductor to metal transition. It is observed VO_2 thin film resistance can shift by three or four orders during semiconductor to metal transition, as displayed in Figure 1.5. External heat can trigger this SMT transition at a particular temperature typically at 67°C for VO_2 [4].

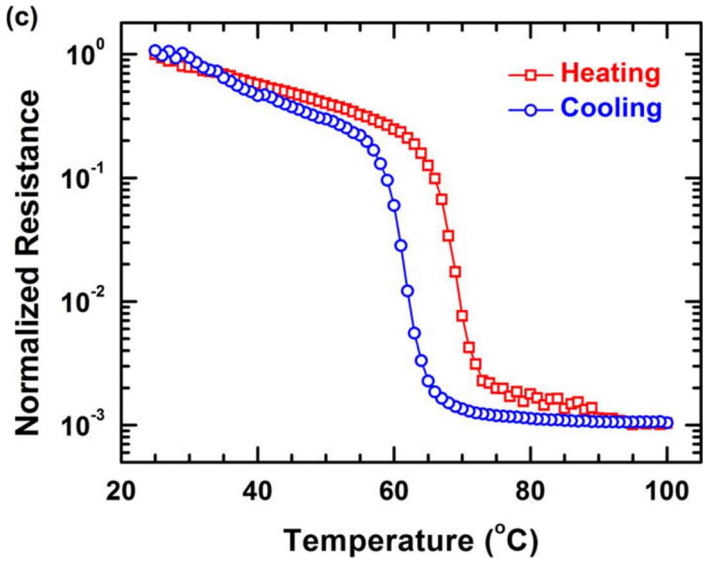

Figure 1.5: Resistance change of VO_2 due to semiconductor to metal transition

Optical properties of the phase transition materials also get changed by semiconductor to metallic transition. It is shown that in Figure 1.6 that the optical power transmission reduces when VO_2 undergoes SMT because of external heating. For various wavelengths and frequencies, the optical power transmittance variation will not be similar.

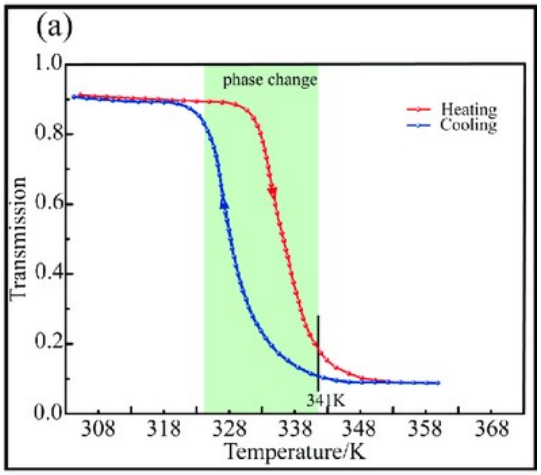

Figure 1.6: Transmitted optical power vs. temperature through VO_2 thin film at laser wavelength 4 μm

It is still debatable why and how exactly SMT occurs, but different theories have been proposed since the last six decades. Presently, there are three theories (Mott, Peierls, Anderson) which are accepted till now. According to Mott [8], when the carrier density overcomes a critical carrier density, n_c, the correlation between electrons take place. We can determine it from $n_c^{1/3}$ aH ~ 0.2 where aH is termed as the Bohr radius of the material. Mott proposes that this transition initiates a phase transition. Within a lattice, when electrons jump from one site then to the immediate beside it, probably that is when the conduction occurs. But, the Coulomb repulsion occurs when an electron is already inside the new location. The electrons are unable to pass through the lattice when their kinetic energy is surpassed by the amount of repulsive energy U. Because of the electrons facing this obstacle, the condition causes two different band groups, UHB (upper Hubbard band) and LHB (lower Hubbard band) get arranged, leading to the VO2 thin film to be in insulating, shown in Figure 1.7. External factors such as mechanical strain can also cause the semiconducting state transit into a metallic state.

Peierls proposes that, when a lattice of the material undergoes a structural change in occurs, it may initiate the transition [9]. A model can be proposed which constitutes a one-dimensional metal. Figure 1.8 shows that because of a lattice constant, a, and an even atomic distance of L_0, the periodic chain experiences deformation, a change in a

repeat distance to L' takes place. Later, the new zone boundary is formed forms at π/ L' at the opening of the band.

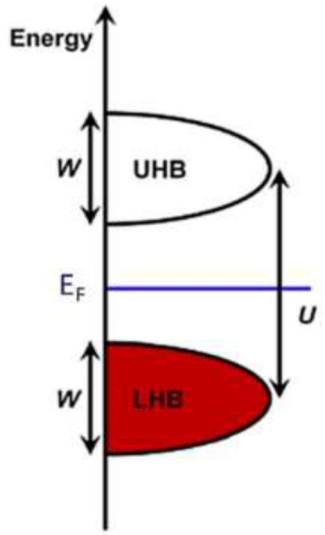

Figure 1.7: Electron correlation forms upper Hubbard band (UHB) and lower Hubbard band (LHB)

For the band gap newly created, lower energy is possessed by the electrons will near the Fermi level. Because of lattice getting deformed, the energy increase caused by elastic energy requires neutralization. The energy reduction in electrons near Fermi level do this, causing transition.

According to Anderson, disorder-induced localization impact can be used to explain semiconductor to metal transition [10]. It is proposed that defects (impurities or vacancies) may be distributed arbitrarily in a lattice, and the conducting electrons can be scattered by them. Localized and extended states can become separated because of non-

uniform lattice potentials due to the defects in the structure. the mobility edge characterizes the border between localized and extended states displayed in Figure 1.9. The transition takes place when the Fermi energy level shifts upward or downward.

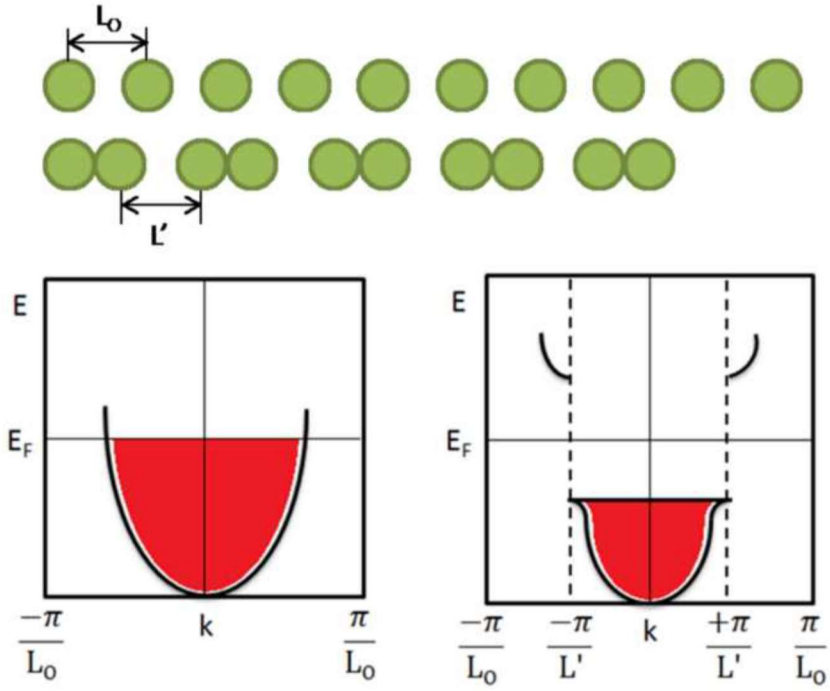

Figure 1.8: The normal lattice and the distorted lattice in a one-dimensional model, and the respective band diagrams

Till now, we are still trying to find a decisive theory to explain the fundamental reason of phase transition in vanadium dioxide. Debate is still prevalent whether the SMT is an outcome of change in structure (Peierls theory) or because of reaction of carriers (the Mott-Hubbard theory).

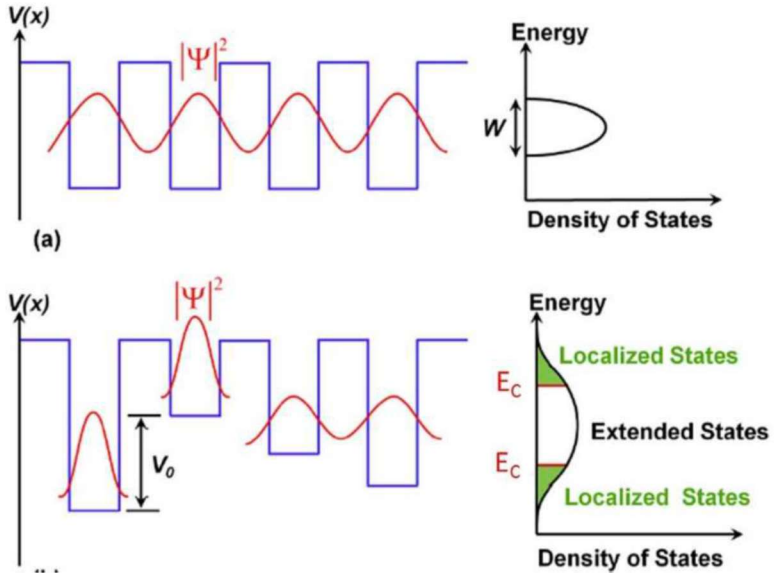

Figure 1.9: For an orderly crystal and imperfect crystal, the lattice energy and the state density

Applications of VO_2

Extensive research is going on vanadium dioxide (VO_2) recently because of its drastic transition in physical properties because of phase transition [11]. This unique characteristic has led rise of diverse applications in different sides such as temperature and infrared (IR) sensing [12], smart windows [13], temperature based optical switch for waveguides at radio frequencies [14], and thermally switched microelectromechanical systems (MEMS) [15], as shown in Figure 1.10. VO_2 can undergo transition from the semiconductor to the metallic because of temperature change, application of electric field, and strain [11-13]. Despite the first two methods having been commonly utilized to

initiate phase transition, strain induced phase change has been investigated to a limited extent and only indirectly [14-15]. However, its wide potential applications in sensing and detection get impeded partly by the difficulty in releasing devices where significant strain change can be applied. In this case, piezoelectric substrates have promising possibilities to implement strain induced phase change just by the applying an appropriate external electric field.

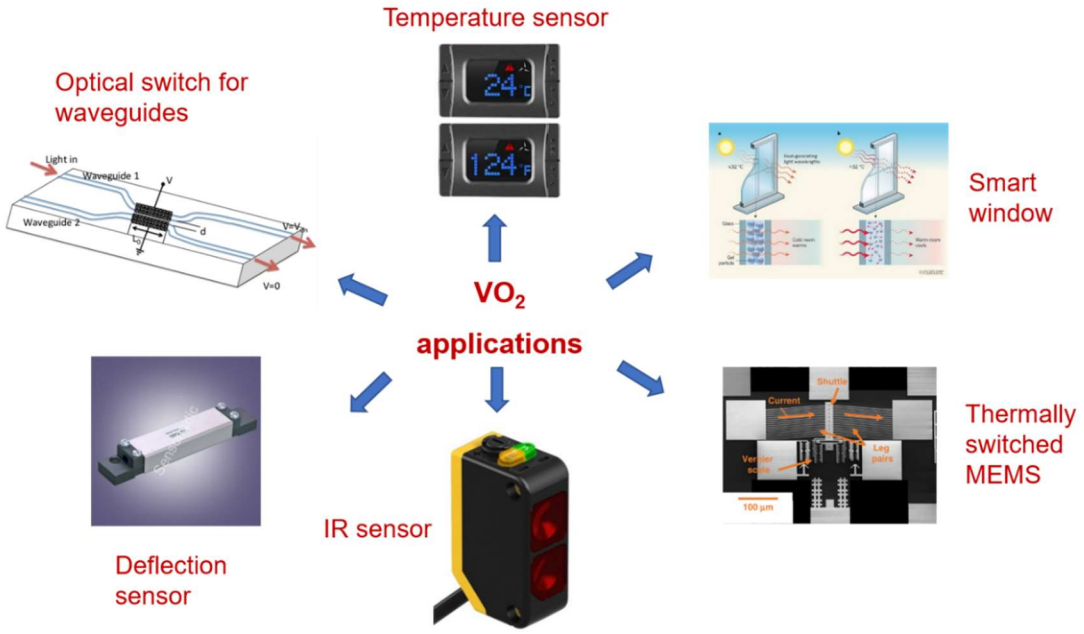

Figure 1.10: Applications of VO_2

SMT materials have a great variety of applications because of their capability to adapt and adjust structurally and electrically at a considerably small time window. We can achieve a system providing switching robustly and inexpensively by implementing these properties. For example, an electric-electronic system can be harmed by a high-speed noise

signal if the acceptable threshold is lower than its voltage amplitude level. For resolving this issue, SMT materials can be used to protect the systems. That is because their phase gets changed when instigated by the additional voltage level allow the noise signal to pass through alternative circuit paths within a small time frame. This threshold voltage control is required; this voltage can be shifted by metal-doping or geometric changes in the VO_2 film surface. This is how we can control the required voltage needed to permit the extra voltage noise to conducted through alternative ways.

At present, widespread use of lithium ion batteries has caused the phase transition materials like VO_2 to have an important great role. Recently, electric vehicles are widely using the Li-ion batteries. However, there is a serious hazard related to them, which is the explosive nature of Li-ion batteries. In order to protect the circuit from being damaged by short-circuit or overcurrent, Positive Temperature Coefficient of Resistance (PTCR) is a device used in batteries to. It can reduce the extra current flow when it detects the the battery being overheated. At this high temperature situation, the impeded electrons become unstable and increases the battery pressure, causing fatal explosion. Therefore, an SMT material like VO_2 can offer protection from battery explosion. If SMT material like VO_2 can be used as a part of the protection system, the material will shift from semiconducting to metallic at high temperature situation. In this state, the battery will undergo fast discharge to prevent explosion.

Thermochromic windows is a notable application of phase transition materials. Optical transmittance through VO_2 film decreases at high temperature for infrared wavelength. Therefore, at cold weather temperature, the VO_2 coating on the window glass stays in semiconducting state, and transmits both light and heat through the glass. During warmer temperature, the VO_2 coating becomes metallic, and reflects off the infrared heat, thus cooling the indoor. The visible light wavelengths can pass through through almost at the similar intensity, continuing the constant flow of sunlight to the indoor.

CHAPTER TWO

SYNTHESIS OF VO_2 THIN FILM

Since the very first discovery of the phase transition behavior of VO_2, researchers have been striving continuously to determine the most feasible and optimized method for synthesizing VO_2 and fabricate functional devices. Some of the synthesis methods explored include aerosol assisted chemical vapor deposition (AACVD) [16], chemical solution deposition process [17], and reactive DC magnetron sputtering [18]. In 2007, Piccirillo et al. deposited VO_2 deposition on glass substrate by implementing AACVD process from vanadium (III) acetylaconate and vanadyl (IV) acetylaconate [19]. Later on, implementation of AACVD method had a consequence of a mixture of V_2O_3, VO_2 and V_2O_5, and presence of the two different oxides can affect the quality of the VO_2 film and its characteristics. In another report [20], VO_2 was prepared from $VOCl_2$ solution, with poly(vinylpyrrolidone), and it displayed decent optical properties, including infrared transmittance decreasing by 45%, whereas the gas-phase methods of VO_2 synthesis results in 41.5%. However, the vanadium precursor which is required for this method, is highly toxic [17]. The DC magnetron sputtering provides VO_2 film with a great uniformity and purity, but it requires a high temperature of 650 °C [18]. In another similar solution-based method of VO_2 synthesis VO_2 nanorods were synthesized through a hydrothermal reaction from V_2O_5 xerogel, poly (vinylpyrrolidone) and lithium perchlorate ($LiClO_4$) [19]. But it takes more than 7 days for this method to be finished, which makes it less cost effective. The atmospheric pressure chemical vapor deposition method has been applied to synthesize VO_2 on substrates like glass, SnO_2, and F-SnO_2 [20]. But the VO_2 thin films yielded from

this method does not exhibit good optical properties, for example, IR transmittance change is less than 10% for lasers with near IR wavelengths. In another report V_2O_5 was prepared by sol-gel method on fused-quartz substrates and pure polycrystalline VO_2 was synthesized by annealing V_2O_5 at 550°C for 10 hours, which performs great, but the method is highly expensive and time consuming [21]. The pulsed laser deposition (PLD) technique has gained popularity more recently due their ease of synthesis of VO_2 on various substrates, including sapphire and Si [22]. However, this method resulted in VO_2 films with weak modulation in transmittance characteristics 2.3%, 5.4%, 4.8%, and 2.2% for different wavelengths 400 nm, 500 nm, 600 nm and 700 nm, respectively [22].

Some good quality VO_2 film synthesized on silicon and quartz substrates using chemical vapor deposition (CVD) technique, with Vanadium acetylacetonate as precursor has also been reported [23]. The problem is the room temperature resistances of the thin films grown from this method at 400 – 450 °C, which are in kilo ohm range only, making the VO_2 less semiconducting than it should be [23]. Reactive high-power impulse magnetron sputtering is also an attractive technique for VO_2 film deposition, where the chamber temperature is only 300 °C only, and it yields good change of electrical resistivity by 350 times and good optical transmission variation [24–27].

For synthesis of VO_2 thin film, a good number of techniques have been developed and implemented such as Pulsed Laser Deposition, Sputtering, Chemical Vapor Deposition, Direct Oxidation and many more. In our laboratory, we have prioritized a

few criteria to select the most feasible growth method. The cost has to be low, and the crystalline quality should be high enough according to laboratory standard. Among the techniques, the following two are quite notable; Pulsed laser Deposition and Direct Oxidation. These two are chosen because of their high probability to synthesize good quality of VO_2 thin film in laboratory environment. These methods have different features. For our research we selected the direct oxidation considering the availability of our budget, equipment and post-synthesis processing of the thin film.

Pulsed laser deposition

One of the notable physical vapor deposition techniques is pulsed laser deposition (PLD). Its applications are quite diverse, and frequently required for optical coating, semiconductor coating and industrial coating, metal sputtering and so on. Also it is required for dielectric coating. Dielectric coatings are non-conducting insulating materials which gets charged. In a plasma region Reactive Sputtering most frequently uses Pulsed Laser Deposition. The chemical reaction takes place between the vaporized target material and oxygen in an ionized form. Silicon oxides and other molecules get structured by this chemical reaction. Some insulating materials like titania, silica and alumina are impossible to deposit with straight DC sputtering. In those situation, pulsed laser deposition comes to rescue with reactive sputtering. Pulsed laser deposition can provide better deposition rates than RF sputtering for thin films at feasible pulsing periods. Consequently, the quality controlled issue is resolved which occurs due to arcing.

Direct oxidation

In addition to the aforementioned techniques, research efforts have been focused on direct oxidation of deposited Vanadium film, which is attractive due to its simplicity and inexpensive process, resulting in large area high quality VO_2 films on a large variety of substrates of varied shape and topography [28, 29]. Additionally, VO_2 patterned growth can be achieved by simply patterning the deposited vanadium metal. The direct oxidation method of VO_2 synthesis has been extensively studied on films grown on sapphire, where high quality films, comparable to those deposited by PLD technique has been observed [28–30].

Direct oxidation involves oxidizing a material previously deposited on a substrate. Direct oxidation combines oxygen with other gases in a process chamber made from quartz at an optimum temperature and pressure. The oxygen mixed gaseous reactants flows inside the chamber in a laminar way, and reacts with the heated substrate placed inside the chamber. A material film is created on the substrate surface by the mixture of oxygen and other gases. At the same time, a vacuum pump pulls out the waste gases from the quartz chamber. For the reaction to take place, the substrate has to be heated up to the crucial temperature and the temperature has to maintained consistently throughout the oxidation process. Therefore, for a decent quality of direct oxidation, the correct temperature has to be chosen, because it is directly related with the material quality. The direct oxidation process creates a thin film coating of oxide on the substrate at a medium

rate. Direct oxidation and physical vapor deposition (PVD) are almost similar in some ways. In PVD, solid materials are vaporized and reacts and creates the coating on substrate, and direct oxidation involves reactants which are gaseous and solid in the first place and never vaporized. Direct oxidation is advantageous in the sense that it can synthesize high quality pure and water-resistant material on the substrate. It, through these advantages and cost effectiveness (for the film quality deposited) over other methods, is one of the most sought-after thin film deposition method in the semiconductor industry and optoelectronics. After the direct oxidation, the final product can be a bulk or thin film or thick coating, any of them can be of monocrystalline, polycrystalline and amorphous structure. The synthesis and structure of the ultimate oxidized product are dependent upon the physical parameters and chemical ingredients selected for the reaction. In the field of solid-state electronics, this method has become one of the most crucial growth techniques of depositing thin films and coatings. Direct oxidation technique is one of the branch methods of the umbrella technique chemical vapor deposition (CVD), which also involves reduction, nitride formation, carbide formation and hydrolysis. A sequence of various reactions is customarily involved in creating a unique product. The reactions might be heterogeneous, or homogeneous reaction. Reactions of heterogeneous type are a preferable because of slower rate of reaction between gaseous components and solid substrate, ensuring uniformity of the deposited film. Homogeneous reactions cause outliers and unwanted clusters in the deposited film, making it non-uniform, that is why it is not preferable.

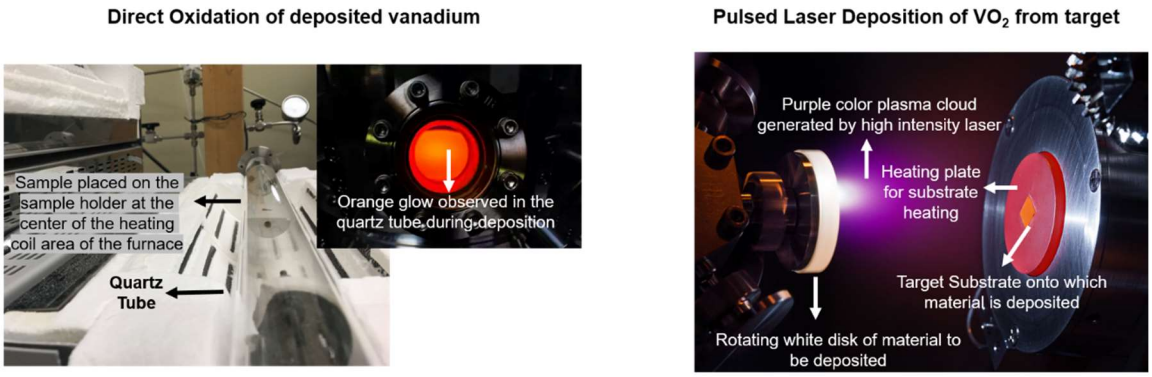

Figure 2.1: Comparison of VO_2 synthesis techniques

In this chapter, we have discussed our direct oxidation method of VO_2 thin films synthesized on two piezoelectric substrates, AT-cut quartz and GaN (2 nm)/AlGaN (18 nm, 25% Al)/GaN (1.8 µm)/Si, and compared with those grown on two traditional substrates sapphire and SiO_2 (100 nm)/Si. The properties of the films grown on piezoelectric substrates were found to be quite comparable, and sometimes superior to those grown on the traditional substrates, which is highly promising for various sensing, actuating and optical modulation applications and synthesis parameters.

Synthesis of VO_2 on regular substrates

VO_2 films were investigated in this work were synthesized using a homemade low pressure furnace (Figure 2.2) through controlled oxidation of vanadium thin films of desired thicknesses deposited on the substrate of choice (c-plane sapphire and SiO_2/Si (100), shown in Figure 2.3 using electron-beam evaporation with a deposition rate of 1.5 A°/s.

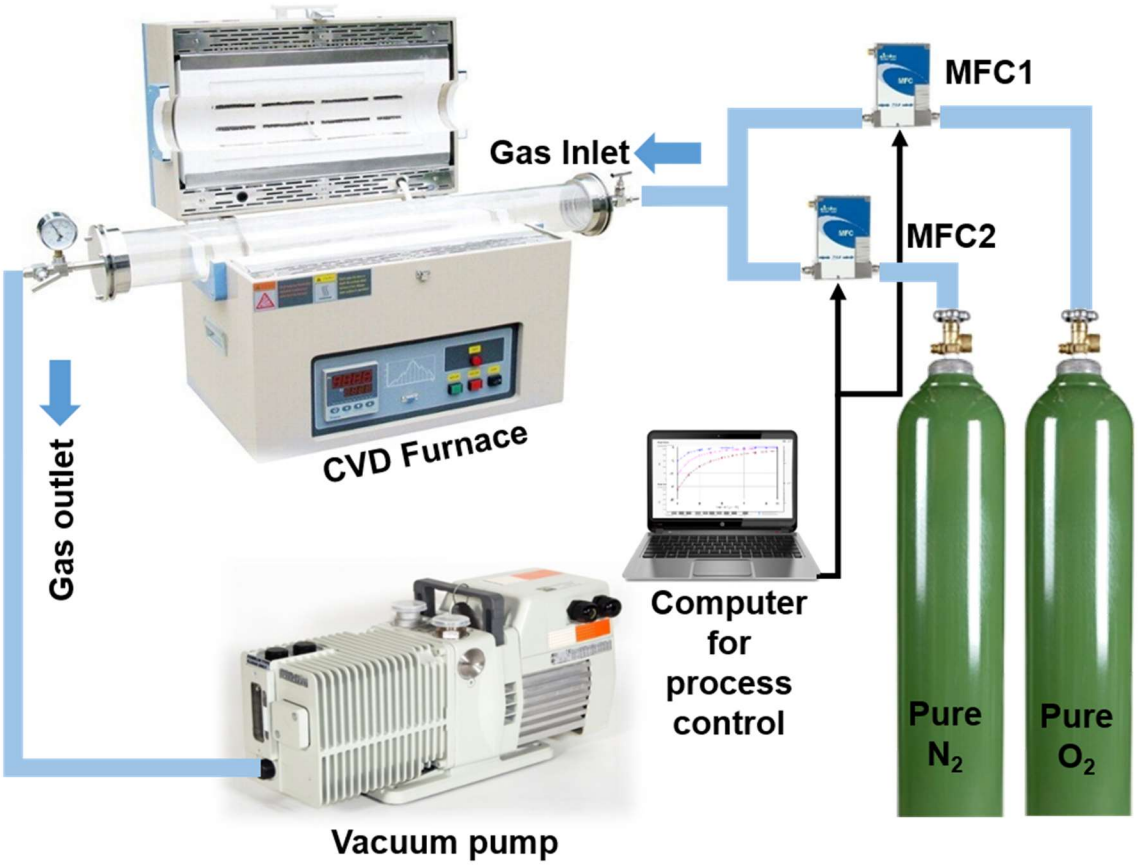

Figure 2.1: The experimental set up for direct oxidation based VO_2 synthesis used in this study

Prior to growth diced substrates with nominal dimensions of 1 × 1 cm, pre-deposited with a thin film of vanadium (using vanadium pellets from Kurt J. Lesker Inc. with 99.7% purity), were thoroughly cleaned using standard cleaning procedure to remove the grease and unwanted debris from the surface, before loading into the furnace chamber. Once the chamber pressure may reach 4.53 Pa under pump down, N_2 gas (purity 99.999% from Airgas) flow was started at a constant rate of 400 sccm until the chamber pressure stabilized at ~2666 Pa. The temperature of the furnace was then increased to 475

°C, and O_2 flow started at the rate of 100 sccm. The optimized growth conditions for VO_2 films (starting with 70 nm Vanadium deposition, nominally targeting 140 nm VO_2 thickness, following the Deal-Grove model) on the various substrates are summarized in Table 2.1. The oxidation durations were optimized over several growth iterations to ensure high quality of the VO_2 films, carefully avoiding under-oxidation and over-oxidation.

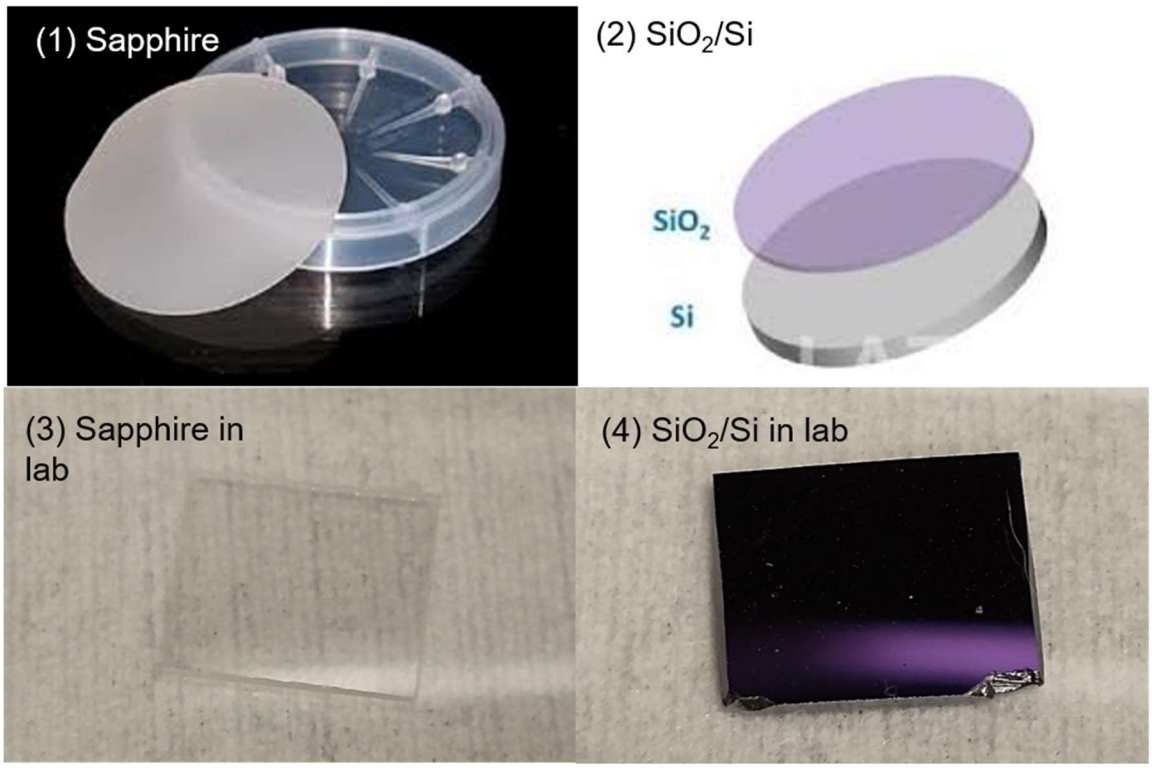

Figure 2.3: (a) Sapphire and (b) SiO_2/Si substrates available commercially, (c) Sapphire and (d) SiO_2/Si substrates in this research

Table 2.1: Summary of the optimized material synthesis parameters for VO_2 samples grown on different regular substrates Sapphire and SiO_2/Si

Substrate	**Optimized VO_2 Growth Parameters**			
	Temperature (°C)	**Pressure (Pa)**	**Oxidation time (min)**	**Vanadium thickness (nm)**
c-plane Sapphire	475°	5.2	50	70
SiO_2/Si	475°	6	40	70

Synthesis of VO_2 on piezoelectric substrates

Explaining VO_2 behavior on very dissimilar substrates such as these is not straight-forward; however, we did manage to optimize the film quality, especially focusing on the resistance transition ratio, optical transmittance change, and transition temperature. We utilized sapphire and SiO_2/Si substrates for validation and benchmarking the quality of the VO_2 thin films by comparing them with the existing literature (where these substrates are most commonly used for VO_2 synthesis). On the other hand, AT-cut quartz and GaN/AlGaN/GaN/Si substrates (displayed in Figure 2.4) were selected because of their piezoelectric properties, which can enable the VO_2 films to change phase based on strain changes, as well as offer potential for integration with versatile and significant device applications utilizing these substrates. Finally, muscovite was selected for its flexibility and corresponding utility as a test platform for enabling phase change in VO_2 through strain.

However, there are only a few existing reports on the investigation of phase transition behavior of VO_2 on piezoelectric substrates such as AT-cut quartz, or technologically interesting GaN/AlGaN/GaN/Si substrates. These substrates possess excellent piezoelectric properties, and VO_2 layers incorporated on them can be subjected to high strain through externally applied electric field or in a MEMS structure, such as a cantilever, where a VO_2 sensing element integrated at the base of the cantilever can be subjected to large deflection induced strain [31].

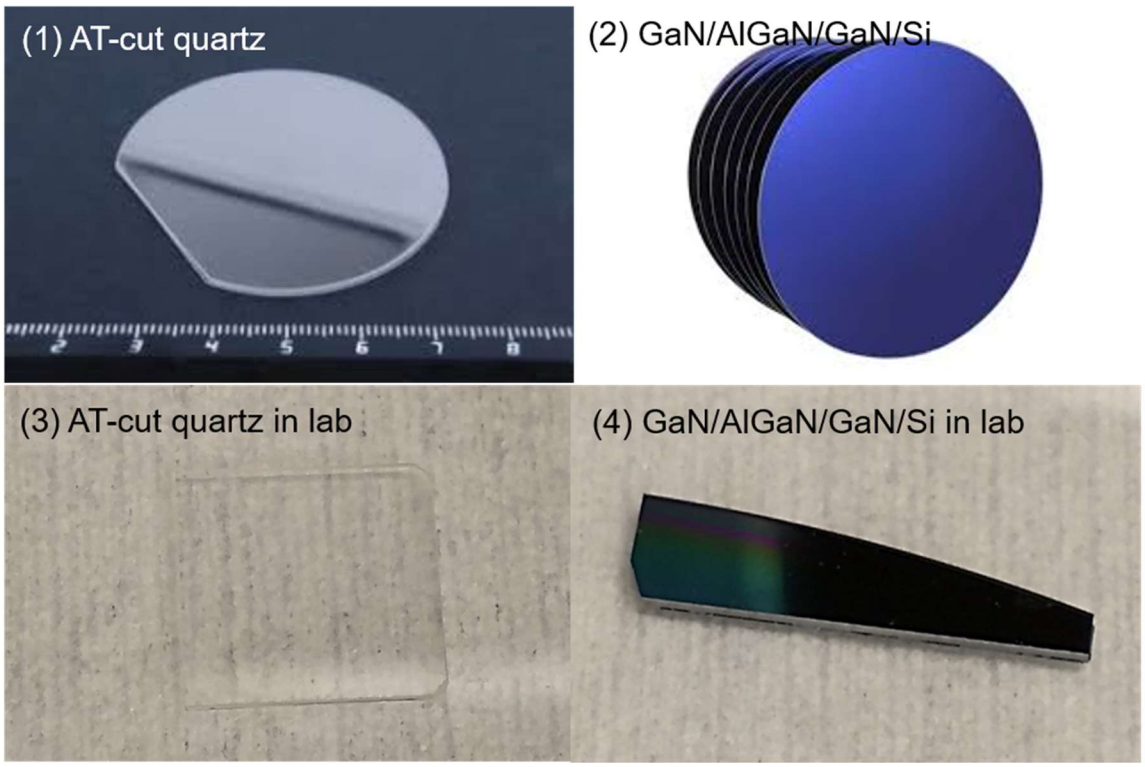

Figure 2.4: (a) AT-cut quartz and (b) GaN/AlGaN/GaN/Si available commercially, (c) AT-cut quartz and (d) GaN/AlGaN/GaN/Si substrates in this research

VO_2 films on AT-cut quartz and GaN/AlGaN/GaN/Si were synthesized using the same homemade low pressure furnace used for controlled oxidation of vanadium thin films of desired thicknesses deposited on the regular substrates sapphire, SiO_2/Si (100), as described before. The only differences with the VO_2 synthesis on regular substrates are the chamber pressure and the duration of oxidation. It can be seen from Table 2.2 that the growth duration for optimized VO_2 growth on AT-cut quartz substrate was slightly longer than for other substrates (inadequate growth duration resulted in incomplete oxidation of the Vanadium film). We are not sure of the cause for such a long growth duration, but it clearly indicates the strong role of substrate on the synthesis process.

Table 2.1: Summary of the optimized material synthesis parameters for VO_2 samples grown on different piezoelectric substrates AT-cut quartz, and GaN/AlGaN/GaN/Si

Substrate	**Optimized VO_2 Growth Parameters**			
	Temperature (°C)	**Pressure (Pa)**	**Oxidation time (min)**	**Vanadium thickness (nm)**
AT-cut Quartz	475°	7.5	70	70
GaN/AlGaN/GaN/Si	475°	4.5	60	70

Synthesis of VO_2 on flexible substrates:

VO_2 thin film was synthesized on 70 nm vanadium coated muscovite disks $KAl_2(AlSi_3O_{10})(F,OH)_2$, (shown in Figure 2.5) utilizing the similar direct oxidation-based

technique we have applied for regular substrates and piezoelectric substrates [10]. The synthesis of the VO_2 films on muscovite were achieved by using the same homemade low-pressure furnace (Figure 1 (a)) as we did for the controlled oxidation of vanadium thin films of desired thicknesses deposited on the regular substrates (c-plane sapphire and SiO_2/Si (100)) and piezoelectric substrates (AT-cut quartz, or GaN/AlGaN/GaN [c-plane or (0001) plane])/Si (111)) [32]. After optimization, synthesis parameters for VO_2 thin films (starting with 70 nm vanadium deposition on the flexible substrates are summarized in Table 2.3.

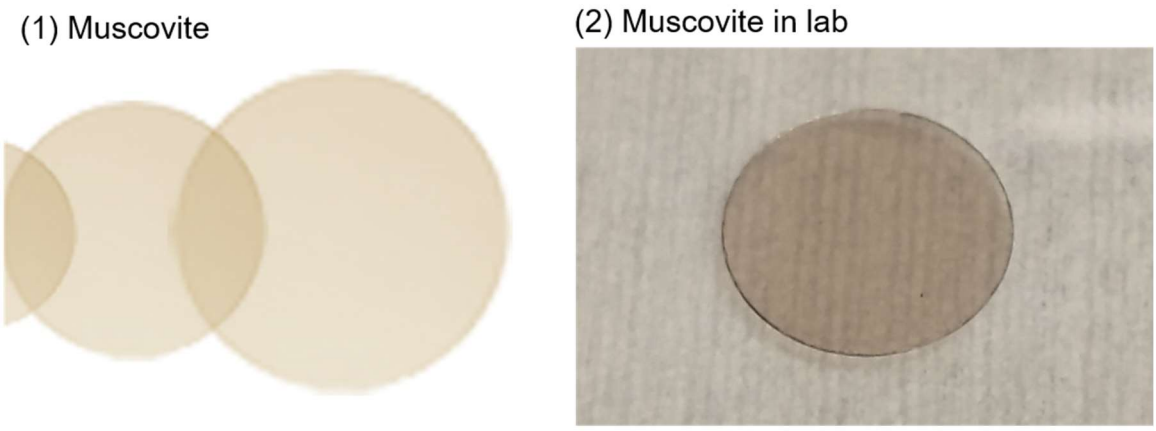

Figure 2.5: (a) muscovite available commercially, (b) muscovite substrates in this research

The optimization was decided based on the VO_2 thin films attaining specific benchmarks in terms of quality, which includes the resistance transition ratio, optical transmittance change, and transition temperature. The typical target transition resistance ratio is > 400, it has an optical transmittance of > 80%, and transition temperature in the range of 60–75 °C. We would like to mention here that although the nature of the substrate can

significantly affect the film quality, our synthesis method, with proper optimization, was able to produce VO_2 thin films of high quality as manifested by the transition resistance ratio, transmission percentage change, and transition temperature, which clearly underlines the utility and potential of this technique. The pressure and duration of oxidation were found to be the most significant parameters as before, optimized over several growth iterations, to ensure high quality of the VO_2 films for flexible substrate muscovite mentioned above, carefully avoiding under-oxidation and over-oxidation.

Table 2.3: Summary of the optimized material synthesis parameters for VO_2 samples grown on different piezoelectric substrates AT-cut quartz, and GaN/AlGaN/GaN/Si

	Optimized VO_2 Growth Parameters			
Substrate	**Temperature (°C)**	**Pressure (Pa)**	**Oxidation Time (min)**	**Vanadium Thickness (nm)**
Muscovite	475 °C	4.6	60	70

Synthesis of metal doped VO_2 thin films

While traditionally VO_2 is grown on sapphire, Si or quartz substrates, its synthesis on muscovite substrate has attracted special attention due to the optical transparency and flexibility of muscovite, which not only offers the possibility of modulating the optical properties of the transmitted light through phase transition but can enable the phase transition by application of mechanical strain. However, the typical transition temperature

of 67 C is not low enough to induce phase change by application of strain, in unheated substrates, which can enable a host of applications requiring high sensitivity associated with the phase change region. Therefore, reduction in the transition temperature of the VO_2 is very much desired, which will make the VO_2 thin film will be more sensitive to physical parameters such as temperature, strain or electric field even at room temperature without any need for heating, enabling it to be used as a thermal sensor with great sensitivity. This can be achieved by doping the vanadium with metallic do-pants such as W, Ti and Cr, which can reduce the transition temperature of VO_2 thin films [33] - [34]. In our reports [34] - [35] we have demonstrated the synthesis and properties of VO_2 synthesized on various substrates, including piezoelectric and flexible ones.

The synthesis of the VO_2 film based sensors were achieved by using the same homemade low-pressure furnace through the controlled oxidation of vanadium thin films of desired thicknesses deposited on AT-cut quartz and muscovite. Prior to growth, the substrates were coated with high purity vanadium thin films. The doped VO_2 film was synthesized by first depositing a 35 nm layer of Ti, which was followed by a deposition of 35 nm V. The oxidation durations were optimized over several growth iterations to ensure high quality of the VO_2 films, carefully avoiding under-oxidation and over-oxidation. Also, it was ensured that the VO_2 film has uniformity all over the substrate, through detailed characterization.

CHAPTER THREE

CHARACTERIZATION TECHNIQUES OF VO_2 THIN FILM

Following synthesis, the VO_2 thin films were characterized using a number of different techniques such as material characterization, electrical characterization and optical characterization. These techniques provide a clear picture of the surface and structural quality of the VO_2 thin films, their crystalline nature and an estimation of their response for being the prime material for VO_2 film based diaphragms. Also the characterization techniques allow us to determine the necessary parameters required to subject the diaphragms to be used as optical modulators later on.

Material characterization of VO_2

a) Optical microscopy and atomic force microscopy

Optical microscopy captured using microscope Olympus BX41M-LED at 50× magnification and atomic force microscopy (AFM, Veeco Dimension 3100) operated in tapping mode and processing the data using the AFM software application of the apparatus. To acquire an image, the AFM perfoRMS raster-scanning of the probe over a small area of the sample, measuring the local property (force between the probe and the sample) simultaneously [36]. The AFM acquires the image resolution by measuring the vertical and lateral deflections of a cantilever by using the optical lever. A laser beam is reflected off the cantilever, operating the optical lever. The reflected laser beam strikes a position-sensitive photo-detector consisting of four-segment photo-detector.

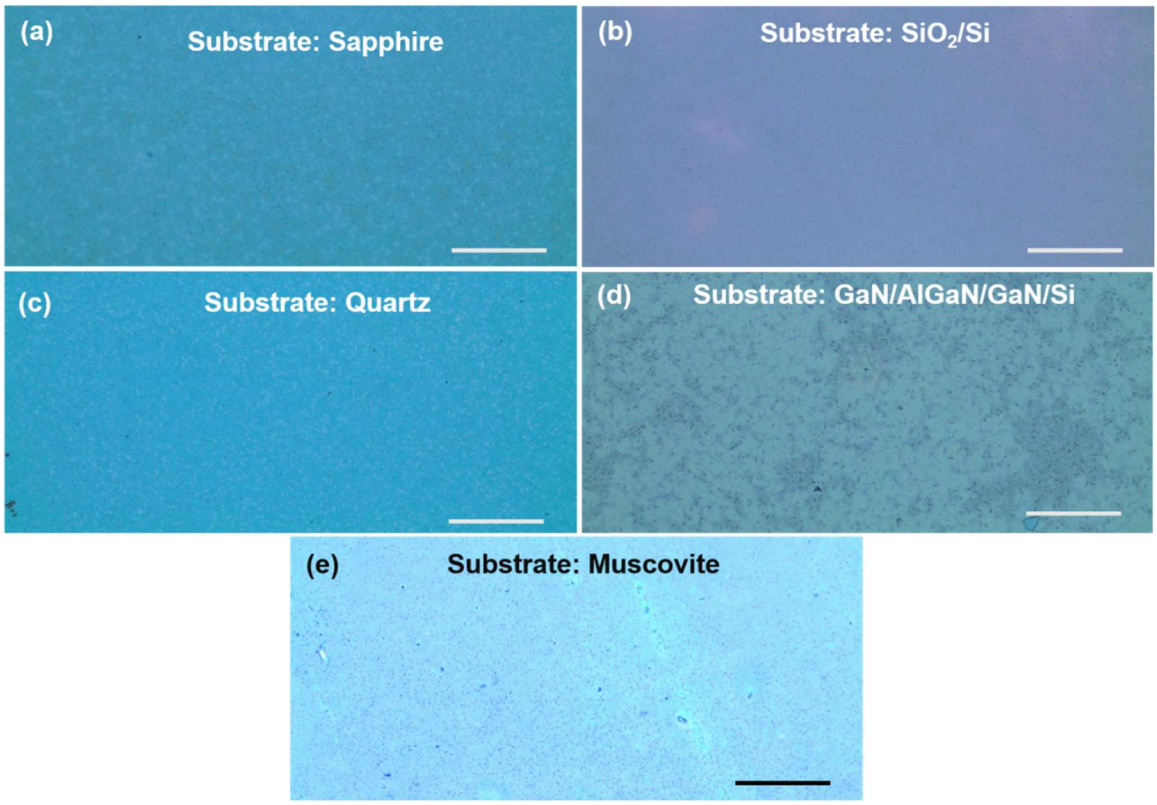

Figure 3.1: Optical images (50× magnification) of VO_2 thin films (5 mm × 3 mm) synthesized from 70 nm vanadium deposited on a (a) c-plane sapphire, (b) SiO2/Si, (c) AT-cut quartz, (d) GaN/AlGaN/GaN/Si, and (e) Muscovite substrates. The scale bar is 500 μm for all substrates.

The differences between the segments of photo-detector of signals indicate the position of the laser spot on the detector and thus the angular deflections of the cantilever [37]. An image processing software known as NanoScope Analysis has been used to determine the RMS roughness of the AFM images.

Figure 3.1 shows the optical microscopic images of the VO_2 samples grown on the four substrates, i.e., sapphire, SiO2/Si, quartz and GaN/AlGaN/GaN/Si while surface morphology images (5 × 2.5 μm) and the root-mean-square (RMS) surface roughness of

the polycrystalline VO_2 samples synthesized on the various substrates are shown in Figure 3.2. From Fig. 3.2, we find the films to be mostly uniform with some granularity, as expected for the polycrystalline thin film layers. The bluish-green and purple color of VO_2, in comparison with what mentioned in literature [33], is also clearly noticeable in all four images shown in Fig. 3. In Fig. 4, the AFM images are displayed. The RMS roughness values were calculated as 8.19, 7.37, 10.3 and 9.75 nm for VO_2 samples grown on sapphire, SiO2/Si, quartz, and GaN/AlGaN/GaN/Si, respectively (Table 2). The uniformity of the roughness numbers indicates consistent morphological quality of the VO_2 thin films, which compare favorably with the surface roughness values reported in the literature, as expected from a polycrystalline film of monoclinic grain structure [38], typically, an increase in surface roughness in films is observed with an increase in oxidation time, as reported by Lindstrom et al., where the VO_2 surface roughness was found to increase from 35 nm to 60 nm when the oxidation time was increased from 5 to 90 minutes [39].

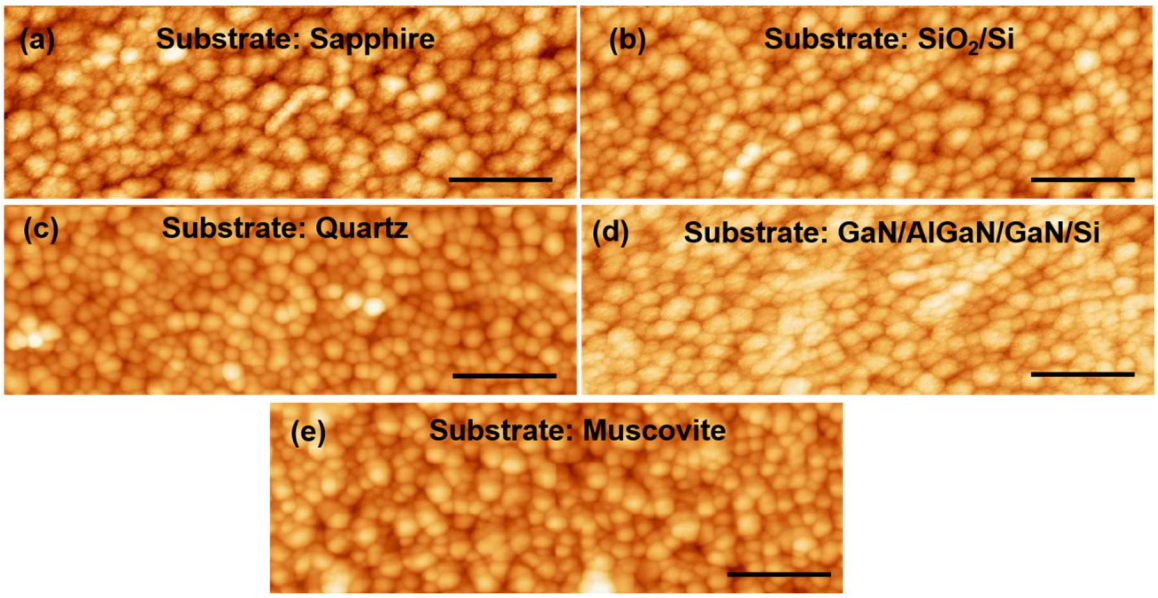

Figure 3.2: Surface morphology images (5 µm × 2.5 µm) of thin films synthesized from 70 nm vanadium deposited on (a) c-plane sapphire (z-scale bar 58.1 nm), (b) SiO2/Si (z-scale bar 50.4 nm), (c) AT-cut quartz (z-scale bar 75.4 nm), (d) GaN/AlGaN/GaN/Si (z-scale bar 68.1 nm), and (e) muscovite (z-scale bar 88.5 nm) substrates. The scale bar: 200 nm for all substrates.

b) X-ray Diffraction Patterns and Raman spectroscopy

To determine the lattice structure and purity of the VO_2 film, X-ray diffraction (XRD) measurements (Rigaku Ultima IV system) were made on the VO_2 samples grown on the four substrates, using Cu Kα radiation (wavelength 15.406 nm) where the diffracted beam was recorded from 5° to 90° with a step size of 0.02°. X-ray diffraction is a robust and excellent method to characterize solids of different types of crystalline structure, which has an infinite length of series of unit cells. Incident light gets diffracted by a series of 3D arrangement of particles, according to Bragg.

The phenomenon can be explained by the equation, $n\lambda = 2d \sin\theta$ (Bragg's Law) where λ = light wavelength, Cu Kα radiation (wavelength 15.406 nm) here, d = spacing between the planes of the 3D crystal, θ stands for the angle between incident light and the planes of the crystal (parallel). Constructive interference takes place when the atoms and their electrons scatter the incident x-ray and we plot the data as peak intensity vs. 2θ. Patterns show peaks of different intensities at certain angles of 2θ, which are like 'signatures' of particular phases in a plane of the crystal. Lattice size and centering determines the values of inter-planar distance d. X-ray absorption and diffraction by the atoms in the crystal determine the intensities of the characteristic peaks. The solid sample, it may be crystalline or amorphous, is placed as a target for the source of x-ray. The d-spacing and the lattice of the crystal play the role for diffracting the x-ray beam incident from the source. The intensities are determined from the diffracted beam, providing the powder pattern These diffracted rays are measured at certain angles to view intensity. Ultimately the XRD pattern is plotted with peak intensity vs. 2θ. In order to recognize an existing phase, the XRD pattern and the inter-planar distances are used to search through the XRD database.

Fig. 3.3 show the typical X-ray scans, in which the characteristic peaks for VO_2 films synthesized on c-plane sapphire are found at 38.36° for VO_2 (020), and 44.6° for (012), with VO_2 (020) being the prominent peak [40]. For SiO2/Si, obvious VO_2 peaks are found at 38.42° for (020) plane, 44.66° for (012) plane, and 69.28° for (202), the most prominent one. For VO_2 on quartz, conspicuous peaks are exhibited at 38.5° (the

prominent peak, 020 plane), and 44.74°, for (012) plane. For GaN/AlGaN/GaN/Si (111), we see VO_2 intense diffraction peaks at 38.52° for (020) and 44.76° for (012) plane, which are quite comparable to those reported in the literature (JCPDS card no. 44-0252) on various substrates [40–41]. For all four substrates, the common intense diffraction peak exists for VO_2 (020), prominent in all four except for SiO2/Si substrate. For sapphire, SiO2/Si, quartz and GaN/AlGaN/GaN/Si, VO_2 (020) is found at 38.36°, 38.42°, 38.5° and 38.52°. A summary of the 2θ peak position and the full width at half maximum (FWHM) values for the prominent peaks are presented are summarized in Table 2.1, where the tight range of the FWHM (0.06° – 0.20°) indicate high directionality of the polycrystalline domains in the VO_2 films.

For identification of the phase and the Raman modes, we collected Raman spectra using a Renishaw InVia micro-Raman spectrometer (10× objective) with a 532 nm diode laser (Crystalaser), at 50% of the maximum laser power. We vary the Raman shift from 100 to 1000 cm^{-1} for three different spots on each of the sample [40, 41].

Raman spectroscopy performed on the VO_2 samples are shown in Figure 5. The Raman spectra on all the substrates displayed intensity peaks at Raman shifts ~195, 223, 395, and 614 cm^{-1}, which correspond to VO_2, and indicate the dominating presence of VO_2 in the thin films synthesized on these substrates [42, 43]. For the SiO2/Si and GaN/AlGaN/GaN/Si substrates, we find an additional intense peak at 520.18 cm^{-1}, due to the Si substrate.

The surface and structural characterization were performed on VO_2/muscovite samples by AFM, XRD, and Raman spectroscopy (Figures 2e–5e). All the characterization results indicate the presence of uniform and high quality VO_2 in the sample, which predicts the high reliability of the characterization results after applying strain on the VO_2/muscovite thin films [44].

Electrical characterization

Electrical resistivity changes over the range of semiconductor metal transition (SMT) in the VO_2 thin films (effected by varying the sample temperature from 20 to 120 °C) were measured using a setup as shown in Fig. 2.5. The inset shows two probes contacting the surface of the VO_2 thin film for resistance measurement, which were connected to a Datalogger (Keysight 34972A LXI Data Acquisition Unit). An annular ceramic heater (positioned below the sample in direct contact with it) is also shown in the inset, which was used to heat the sample over the desired measurement temperature range. A thermocouple was also placed on the VO_2 sample, to ensure accurate measurement of sample temperature simultaneously with the measurement of the substrate resistivity changes.

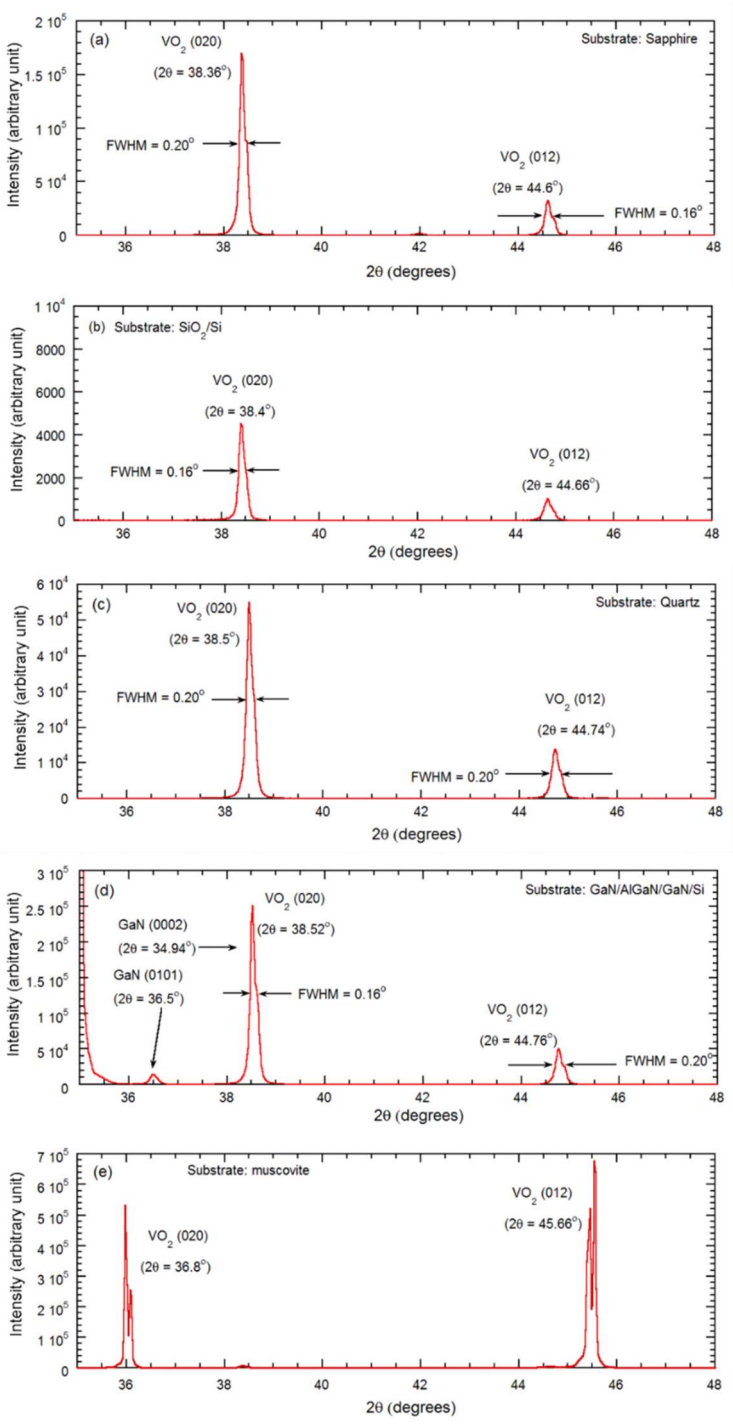

Figure 3.3: X-ray diffraction peaks are presented for the VO_2 thin films synthesized on (**a**) c-plane sapphire, (**b**) SiO_2/Si, (**c**) AT-cut quartz, (**d**) GaN/AlGaN/GaN/Si, and (**e**) muscovite substrates. The VO_2 (020) and VO_2 (012) peaks, along with their respective full width at half maxima (FWHM), are pointed out with arrows.

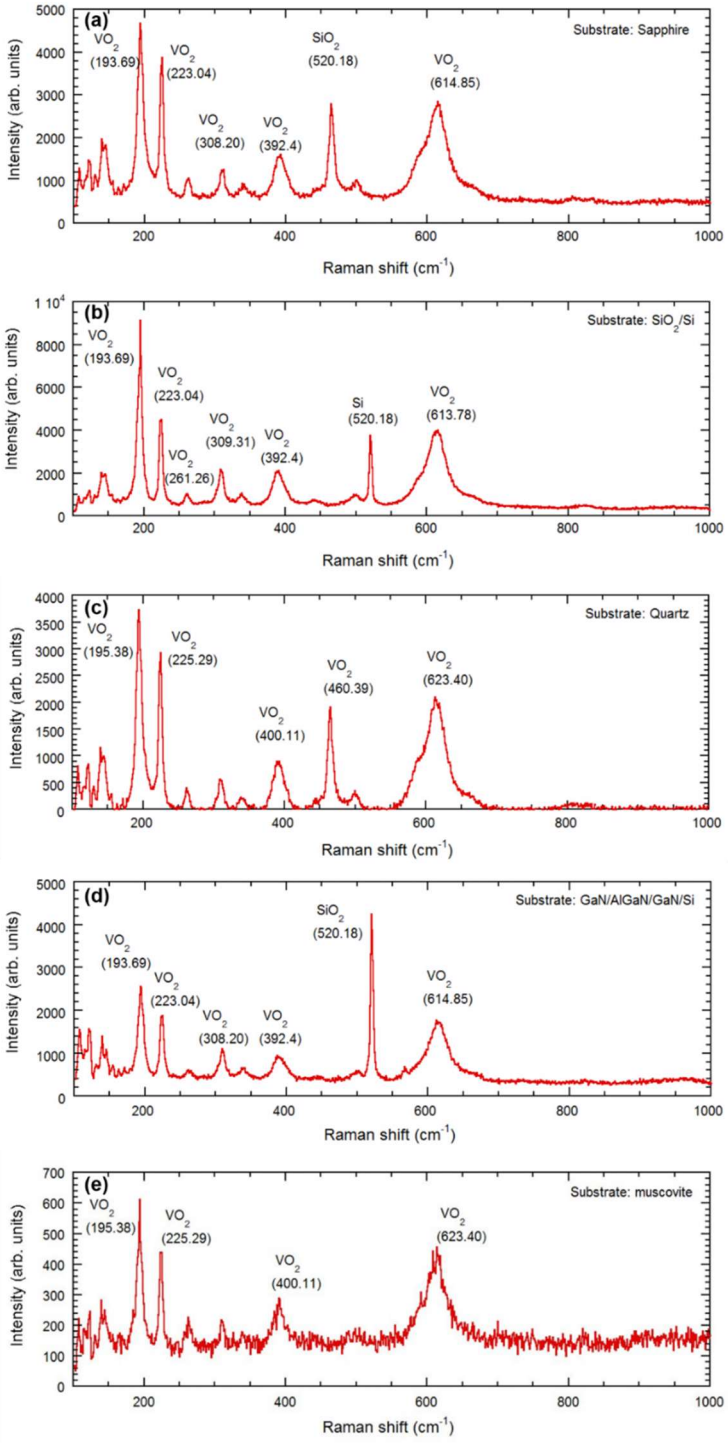

Figure 3.4: Raman peaks are presented for the VO_2 thin films synthesized on (**a**) c-plane sapphire, (**b**) SiO_2/Si, (**c**) AT-cut quartz, (**d**) GaN/AlGaN/GaN/Si, and (**e**) muscovite substrates. The VO_2 (at 193 cm^{-1}, at 223 cm^{-1}, and 614 cm^{-1}) common peaks.

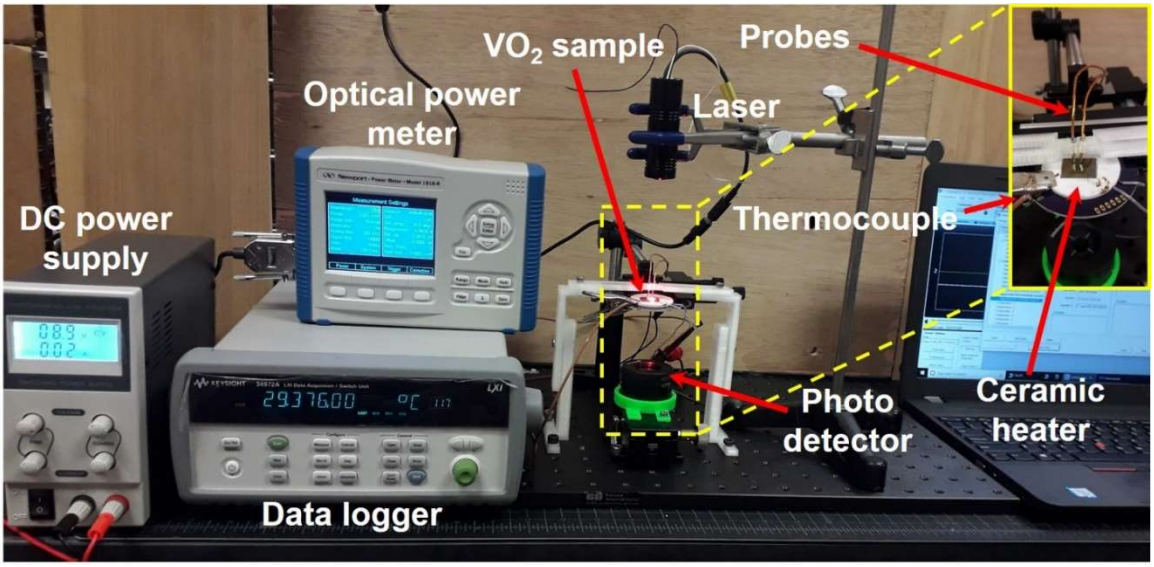

Figure 3.5: Experimental setup for electrical and optical characterizations of the VO_2 thin films. The laser is shone from the top, while a photodetector at the bottom (along with a power meter) measures the transmitted laser power as phase transition occurs. Inset shows magnified image of the white annular ceramic heater with the sample on top contacted by two current measurement probes.

Figure 3.6 shows the change in resistivity, both in forward and reverse directions, of typical VO_2 films on all four substrates when their temperature was varied from 20 to 120 °C. The average transition temperature (from the forward and reverse characteristics), determined to be the point of maximum slope of the respective transition curves, were found to vary within a narrow range among the substrates, with the maximum T_c of 72 °C recorded for VO_2 on SiO_2/Si substrate, and the minimum of 61 °C for VO_2 on quartz substrate. The T_c values, temperature ranges of transition (taken as $T_c \pm 20$ °C), and resistivity ratios (corresponding to the lower and upper SMT of the temperature range) for all four substrates are summarized in Table 3.1. The highest transition ratio of 1094 was recorded for VO_2 on sapphire, while the lowest of 665 was

observed for the film grown on GaN/AlGaN/GaN/Si substrate. Although the VO_2 films on piezoelectric substrates, GaN/AlGaN/GaN/Si and AT-cut quartz, exhibited somewhat lower transition resistivity ratios compared to those of the traditional substrates, sapphire and SiO_2, still those ratios are quite significant for practical usage of those films.

The slope in the electrical resistivity curve before and after SMT are typically attributed to hopping transport of the carriers through Frenkel-Poole mechanism [46]. The activation energy of the carriers can be determined from the Arrhenius plots corresponding to the relevant sections [47–48]. The Arrhenius equation correlating the VO_2 film resistance R (for relevant sections) and the activation energy E_a is given as: $R = Ce^{-\frac{E_a}{kT}}$, where k is Boltzmann constant, and T is the absolute temperature. By taking natural logarithm of both sides, the equation can be written as: $\ln(R) = -\frac{E_a}{kT} + \ln(C)$, which allows the activation to be determined directly from the slope. Figures 7(a) – (d) shows plots of ln(R) vs. (-1/kT) for the VO_2 films on all the substrates, utilizing the electrical characterization results shown in Fig. 3.6.

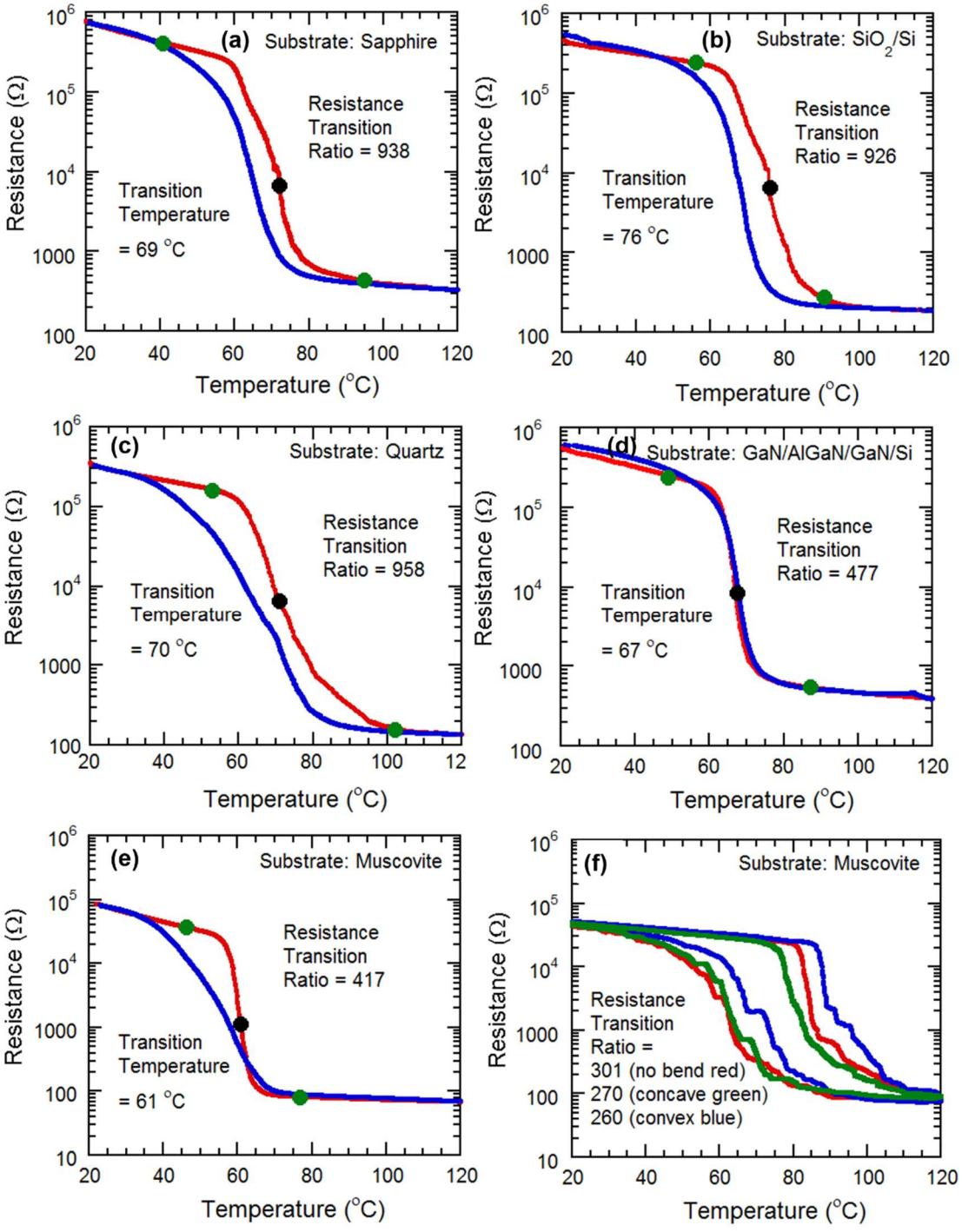

Figure 3.6: Semi-log plots of resistance variation as a function of temperature for the VO_2 thin films grown on various substrates (a) c-plane sapphire, (b) SiO_2/Si, (c) AT-cut quartz, (d) GaN/AlGaN/GaN/Si, and (e) muscovite substrates, muscovite substrate as they undergo a semiconductor–metal transition (SMT) during no mechanical strain (red), tensile strain (blue), and compressive strain (green)

Table 3.1: Summary of the material, electrical and optical properties of the films synthesized on the five different substrates: sapphire, SiO_2/Si, AT-cut quartz, GaN/AlGaN/GaN/Si and muscovite.

Parameters	c-Plane Sapphire	SiO_2/Si	AT-Cut Quartz	GaN/AlGaN/GaN/Si	Muscovite
RMS roughness of AFM image (nm)	8.19	7.37	10.3	9.75	12.2
2θ angles of prominent XRD peaks (FWHM)	38.36° (020) (0.14°)	69.28° (202) (0.06°)	38.5° (020) (0.20°)	38.52° (020) (0.16°)	36.8°
2θ angles of common XRD peaks (FWHM)	38.36° (020) (0.14°)	38.42° (202) (0.16°)	38.5° (020) (0.20°)	38.52° (020) (0.16°)	36.8°
Electrical Transition temperature (forward)	69 °C	76 °C	70 °C	67 °C	61 °C
Optical Transition temperature at λ = 1550 nm	64 °C	69 °C	59 °C	64 °C	79 °C
Resistance transition ratio	938	926	958	477	417

For each film, the semiconducting and the metallic sections (before and after SMT, respectively) of the plots have been fitted with straight lines, and the corresponding slopes have been noted to determine the activation energies. The activation energies for the VO_2 thin films on all four substrates have been recorded in Table 3.1, for both semiconducting phase and metallic phases. The activation energies found from the Arrhenius plots were found to vary from 0.06 – 0.3 eV), which is consistent with the values reported in the literature [48–49]. As we can see from Table 3.1, the activation energies are found to be significantly lower (by a factor of ~5) for metallic phases (at higher temperature), which is expected and indicates that less energy is required by the carriers to overcome the threshold energy barrier for conduction.

We would like to point out here that the synthesis of VO_2 on III-Nitride epitaxial layers was only once reported earlier, by our group [31]. In the previous report from our group a transition ratio of ~300 was recorded on GaN/AlGaN/GaN/Si substrate with a T_C of 65 °C. The transition ratio of ~ 665, reported here in this paper is clearly a significant improvement over that, and the transition temperature is also found to be 64 °C, which is comparable to that reported earlier [31]. While further investigation is necessary for further understanding of the impact of strain and substrate in the VO_2 films, our results clearly indicate a great promise for developing highly sensitive MEMS devices using these films, when used in conjunction with the piezoelectric III-Nitride films [16, 50–51] and quartz [52]. Comparison with other reports are shown in Table 3.2.

Table 3.2: Summary of the transition temperature and resistance ratio reported for VO_2 films on various substrates synthesized by multiple methods.

Substrate	Reference	Synthesis process	Film thickness (nm)	Transition temperature (°C)	Resistance ratio	Crystal type
Sapphire	Zhao et al. [26]	DC reactive spluttering	120	65	48000	Monocrystalline
	Yu et al. [42]	DC magnetron sputtering	120	80	1300	Amorphous
	Jian et al. [43]	Pulsed laser deposition	30	48	7200	Monocrystalline
	Bian et al. [44]	Pulsed laser deposition	200	46		Polycrystalline

	Kovacs et al. [45]	Pulsed laser deposition	28		2000	Polycrystalline
	Yang et al. [46]	Pulsed laser deposition	200	75	15000	Dual orientation
	Chae et al. [47]	Laser ablation	-	65	18000	Monocrystalline
	This paper	**Direct oxidation**	**140**	**68**	**1094**	**Polycrystalline**
SiO_2/Si	Kovacs et al. [45]	Pulsed laser deposition	36	55	100	Polycrystalline
	Chae et al. [47]	Laser ablation	-	65	10	Polycrystalline
	Bhardwaj et al. [48]	Reactive pulsed laser deposition	-	55	100	Polycrystalline
	Youn et al. [49]	Pulsed laser ablation	90	68	50	Polycrystalline
	This paper	**Direct oxidation**	**140**	**72**	**1065**	**Polycrystalline**
Quartz	Liu et al. [12]	Aqueous sol-gel process	400	68	500	Polycrystalline
	Zhang et al. [40]	RF plasma assisted O-MBE	60	85	400	Polycrystalline
	Dejene et al. [50]	Reactive Pulsed laser ablation	500	50	1000	Polycrystalline
	Kizuka et al. [51]	Reactive RF magnetron sputtering	300	59	1188	Polycrystalline
	Dang et al. [52]	Reactive RF magnetron sputtering	300	67	105	Polycrystalline
	Taha et al. [53]	Pulsed DC magnetron sputtering	150	73	300	Crystalline
	Liu et al. [54]	Reactive Pulsed		59	2000	Amorphous

	This paper	laser ablation **Direct oxidation**	**140**	**61**	**1017**	**Polycrystalline**
III-Nitrides	Singh et al. [35]	Low pressure CVD		65	300	Polycrystalline
	Slusar et al. [38]	Pulsed laser deposition	130	77	1000	Monocrystalline
	This paper	**Direct oxidation**	**140**	**64**	**665**	**Polycrystalline**

Electrical characterization of VO_2 on flexible substrates

(a) Substrate heating without mechanical strain applied

The procedure and experimental setup are similar to the ones we used for the four other substrates beforehand. Silver conductive paste is used to form two stable terminals on the VO_2 surface. The terminals are connected to the data acquisition unit which is used for measurements of resistance and temperature. The VO_2 was placed on top of a ceramic heater, which is used for varying the temperature of the sample by heating or cooling it.

The resistance of the VO_2 thin film was measured with respect to the change of temperature from 20 °C to 140 °C, with an attached thermocouple to record the temperature. With an increase in heat, the VO_2 starts changing its phase and conductivity, from semi-conductor to metallic (see Figures 3.6 (e) and (f)). The transition ratio is observed to be 301 in Figure 3.6 (f), which is slightly lower than that observed in Figure 3.6 (e).

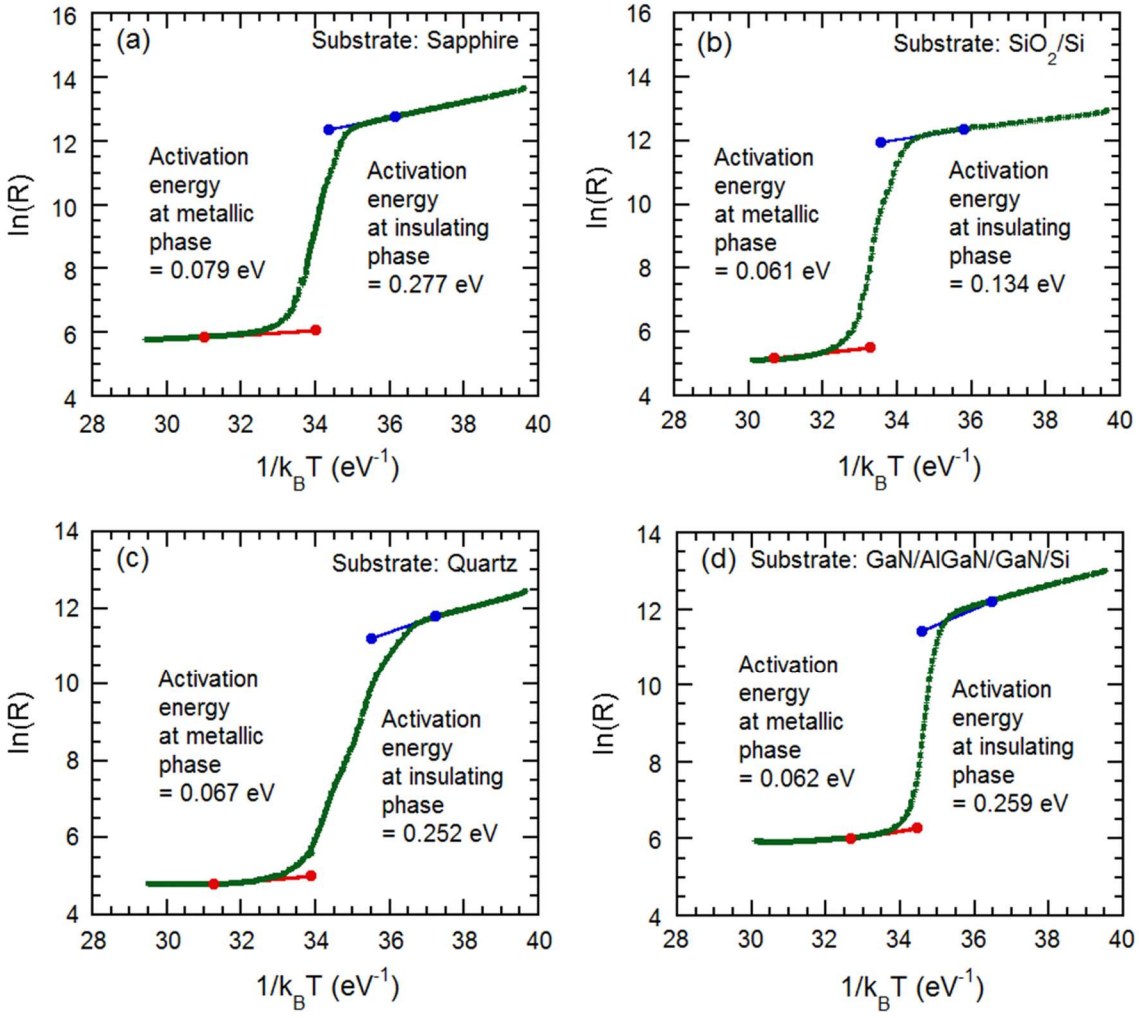

Figure 3.7: Arrhenius plots (green curves) for the VO_2 films synthesized on the different substrates. The blue and red lines are linear fits to the relevant sections of the semiconducting (pre-SMT) and metallic (post-SMT) phase plots, respectively. From the slopes of the linear fits, the activation energies corresponding to the particular phases have been determined and include in the figures.

(b) Substrate heating with tensile strain applied to the sample

For this we used a setup where, at the edge of the ceramic heater, the VO_2 sample is attached to a clamp. The other portion of the sample is kept freely suspended. The suspended part of the VO_2 thin film is bent in a convex way, by pressing down the sample with a screw-and-wedge as before. The strain was enough to ensure the convex

bending of the VO_2 is visible. The heater was used to apply heat on the convexly bent VO_2 thin film, and the temperature was varied from 20 °C to 140 °C.

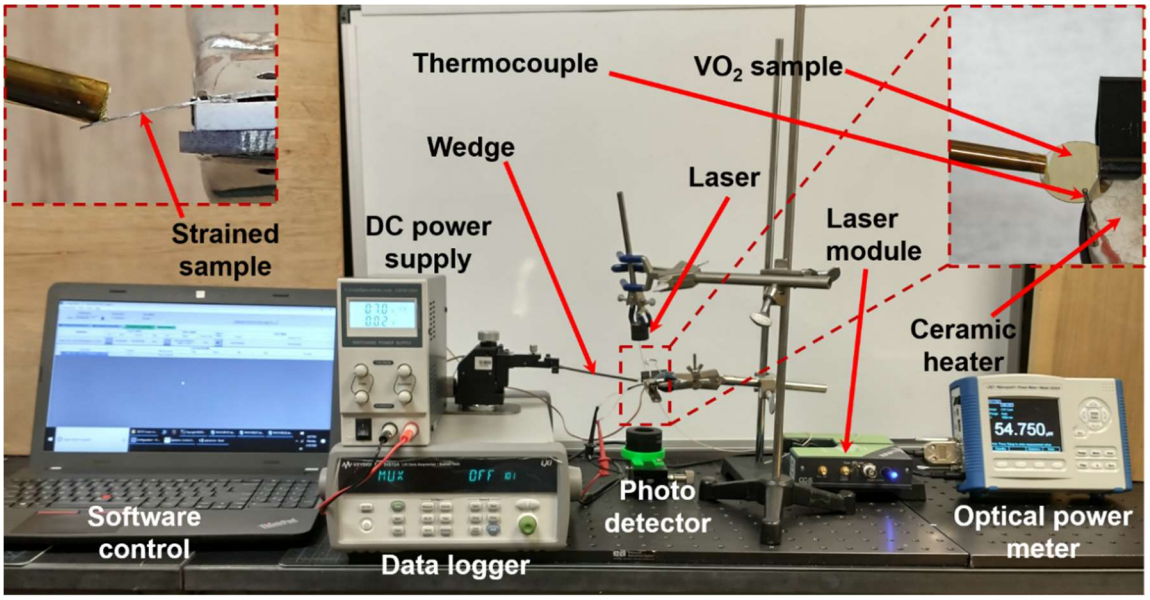

Figure 3.8: Experimental setup for electrical and optical characterizations of the VO_2 thin films on flexible substrates. The laser is shone from the top, while a photodetector at the bottom (along with a power meter) measures the transmitted laser power as phase transition occurs. Inset shows a magnified image of the white annular ceramic heater with the sample on edge pressed and bent with a wedge.

As with the previous setup, the resistance is measured by the data acquisition unit. As the VO_2 undergoes the SMT transition, the resistance decreases sharply. The effect of convex bending is observed after plotting the transmitted optical power data, we see that the ratio of change has decreased slightly to ~270 (Figure 3.6 (f)). In addition, the transition region has shifted to the right, indicating that under tensile strain, the SMT for VO_2 occurs at a higher transition temperature compared with the unstrained case.

(c) Substrate heating with compressive strain applied to the sample

This characterization setup is similar to the one for the tensile strain study, but this time the sample is pressed upwards in the free edge, to ensure the concave bending of the sample. Again, the resistance varied with change in temperature, experiencing the steepest change at the SMT transition region of the VO_2. After plotting the data, it is observed that ratio of change is ~260, but this time the transition region has shifted to the left, which means, while the VO_2 is bent concavely, the SMT occurs at a lower transition temperature (Figure 3.6 (f)).

Electrical Characterization of metal-doped VO_2

The experimental setup in Figure 3.8 was utilized to measure the electrical resistance variation. A two-point probe measurement setup was implemented to observe the effect of substrate heating on the electrical resistance of VO_2 following previously reported [53]. A ceramic heater is used to vary the temperature of the VO_2 film, assisted by a thermocouple for recording the temperature, and tungsten probes connected to a data acquisition unit for measuring the surface resistance. The results are plotted in Figure 3.8.

As seen from Figs. 3.9, the Ti-doped VO_2 shows a significant reduction in transition temperature from 70 °C to 35 °C. However, this is also associated with a reduction in the transition resistance ratio from 958 to 36. On the other hand, the transition temperature for the VO_2 synthesized on muscovite changed from 61 °C to 47 °C, while the transition resistance ratio reduced from 417 to 99.

The effect of strain on VO_2 based sensing films deposited on the muscovite substrate was studied using an experimental set up as shown in Figure 3.8. A thermocouple is also shown touching the VO_2 substrate to measure the film temperature. We studied both tensile and compressive strain by bending the edge of the film using a micropositioner extended arm. The arm is pressed downwards on the top of the sample to create tensile strain, and it can be pressed upwards from the bottom of the sample to produce compressive strain. The tensile strain causes the surface resistance to increase while compressive strain results in a decrease in surface resistance in agreement with previous reports [54].

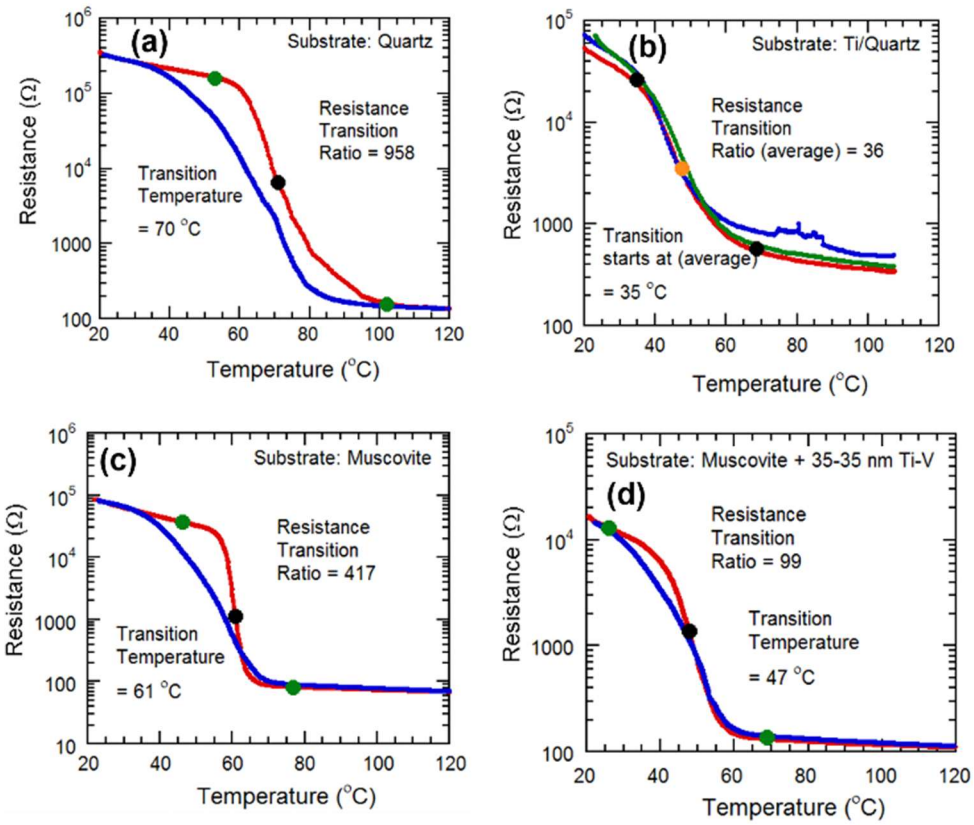

Figure 3.10: Phase transitioning plots of VO_2 thin films synthesized on (a) AT-cut quartz, (b) Ti (35 nm, doping layer) coated AT-cut quartz, (c) muscovite, (d) Ti (35 nm, doping layer) coated muscovite.

In Figure 3.10, the variation of surface resistance is plotted with respect to variation of deflection due to applied strain. The change of resistance is recorded with change of tensile strain at room temperature, compressive strain at room temperature and compressive strain around transition temperature at phase transitioning region. For tensile strain the change in resistance per °C comes out to be 3.55 %. The slope of resistance change is significantly more at the phase transition region compared to room temperature. At room temperature due to compressive strain, rate of change of resistance per °C is 5.95 % and for around transition temperature, it is 9.09 %. The VO_2/Ti/muscovite thin film sample shown in Figure 3.7 can be approximated as a square cantilever with thickness t = 150 μm, and beam length L = 11 mm (1.1×10^4 μm), one end attached and the other end as freely suspended. From Figs. 3.10 (a)-(c), we see that the maximum deflection of the free end of the cantilever Y_{max} = 127 μm.

The length to thickness ratio of the approximated cantilever is 73:1, which is more than 10:1. Therefore, the average strain ε due to deflection of the free end of the cantilever can be calculated from the formula stated below [55]:

$$\varepsilon = 1.5 \left(\frac{t}{L^2}\right) Y \qquad (1)$$

Here t is the cantilever beam thickness, L is the cantilever beam length, and Y is the cantilever deflection at the free end.

Plugging in the values of the parameters of the right hand side of the equation (1), we can calculate the strain as $\varepsilon = 2.36 \times 10^{-4}$. From Figure 3.10 (a), the fractional resistance change (over the entire deflection range) can calculated as $\Delta R/R = 0.032$ for

tensile strain at 22 °C. From the maximum deflection Y_{max} = 127 μm, the gauge factor GF is calculated from the formula [56]:

$$GF = \frac{\Delta R/R}{\varepsilon} \qquad (2)$$

Plugging in the values of the right hand side of the equation (2), the calculated gauge factor = 136. Following the same procedure the relative resistance change for 127 μm deflection in Figure 3.10 (b) comes out to be the ΔR/R = 0.038, which yields a GF value for the compressive strain at 22 °C as 161. Similarly, from the plot in Fig. 3.10 (c), we find ΔR/R = 0.086, and for the compressive strain of $\varepsilon = 2.36 \times 10^{-4}$, the GF turns out to be 364 at 50 °C. Comparing the GF values in all three cases we find that the gauge factor is maximum when the relative variation of resistance is maximum during compressive strain, which happens at the phase transition region (50 °C).

Comparing the GF values with those of common semiconductors, we find that these values are significantly higher than the best values reported for Si piezoresistors, which have the maximum gauge factor 95 [56]. They are also comparable to the GF values reported for III-nitride based piezoresistors, although they are lower than that is possible with the III-Nitride piezotransistor technology. For III-V based piezoresistive microcantilevers, the gauge factor reported previously for tensile strain was 75 [57]. The GF of 136 determined for tensile strian in this work, is higher than the GF calculated for tensile strain on III-V based piezoresistive microcantilevers [57].

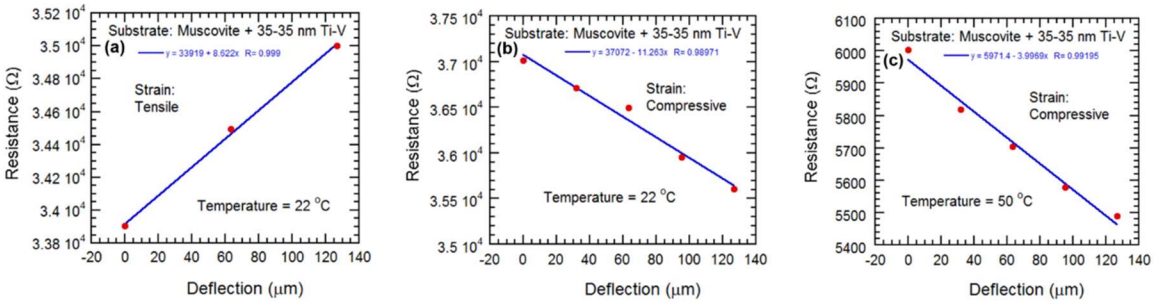

Figure 3.9: (a) Effect of tensile train on the resistance between two contacts on Ti-doped VO_2 at 22 C (room temperature). Effect of compressive strain on the resistance of Ti-doped VO_2 on muscovite (b) at 22 C (room temperature) and (c) at 50 C (transition region).

For III-V nitride based pressure sensors with integrated transistors [58], the maximum gauge factor reported be 260 for operation in the sub-threshold region, which is still less than the maximum gauge factor 364 found for our flexible VO_2/Ti/muscovite thin films at phase transition temperature. However, piezotransistors formed by GaN microcantilever with embedded AlGaN/GaN HFET provides gauge factor ~8700 for gate bias voltage -3V, caused by a deflection of only 1 μm [59], and 3200 due to gate bias voltage of -3.1V [60], which are still much superior compared to the values reported here for our macroscopic devices. Nonetheless, the presented VO_2 based sensing devices required no specialized and expensive layer structures like the III-Nitrides or complicated fabrication methodology. Thus, they can be promising for applications requiring near room temperature strain sensing requiring high sensitivity.

Effect of vanadium thickness on properties of VO_2/quartz:

In the system of VO_2 synthesis by direct oxidation, a vital step is deposition of vanadium metal on the substrate by electron beam evaporation. We can select the

thickness of vanadium metal film prior to deposition. We wanted to observe if different thicknesses of vanadium have any significant effect on the substrate. Resistance change of VO_2 due to semiconductor to metal transition VO_2 characteristics later on. We found out that the effect is quite significant and drastic. The variation of metal thickness plays a highly important role not only on the VO_2 characteristics, but also the synthesis parameters

Table 3.3: Comparison of the synthesis parameters for samples grown on Quartz substrates (Deposited Vanadium of three different thicknesses)

V thickness	**35 nm**	**55 nm**	**70 nm**
Chamber pressure	164 mTorrs	224 mTorrs	227 mTorrs
Reaction Temperature	485°C	485°C	485°C
Gas Flow ratio N_2 : O_2	300 sccm : 75 sccm	300 sccm : 75 sccm	300 sccm : 75 sccm
Oxidation duration	8 minutes	15 minutes	25 minutes

For the AT-cut quartz substrate, we have optimized the synthesis parameters for three different thicknesses of vanadium metal film (35 nm, 55 nm and 70 nm). It should be noted that deviation from these optimized parameters will cause the vanadium metal to be over-oxidized or under-oxidized, which is not desirable for growing a good quality of vanadium thin film. Usually, the higher thickness of vanadium film requires higher amount of duration of oxidation.

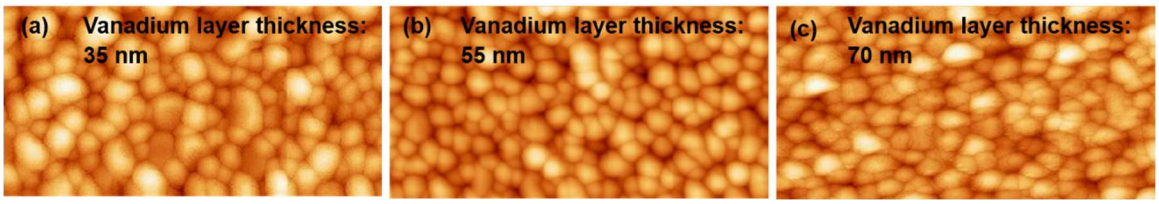

Figure 3.11: Surface morphology images (5 × 2.5 μm) of thin films synthesized from (a) 35 nm Vanadium (b) 55 nm Vanadium (c) 70 nm Vanadium deposited on AT-cut quartz

For the analyzing the surface morphology, we performed atomic force microscopy (AFM) in tapping mode on all three thickness variations of VO_2/quartz and determine the RMS roughness. The lattice structure of the VO_2 films were analyzed by x-ray diffraction patterns as before, using Cu Kα radiation, recording the diffracted beam from 5° to 90° with a step size of 0.02°. All the thin films show common XRD peak at VO_2 (011) plane, with FWHM ranging from 0.10° to 0.14°, as we see in Figure 3.11. The XRD pattern validates the significance presence of decent quality polycrystalline VO_2 (011) thin film by analyzing its diffraction beam angle, peak intensity and full width half max.

The optimization of synthesis parameters has ensured good quality of polycrystalline VO_2 thin film with different thicknesses (35 nm, 55 nm and 70 nm), as we saw from the AFM images and RMS roughness, and XRD patterns. Using the experimental setup shown in Fig. 3.5, we observe the resistance changes with temperature variation when heat is applied, due to the semiconductor to metal transition, and plotted in a semi-logarithmic scale. The ratio of resistance at semiconductor phase

and metallic phase is calculated for all three types samples, and we find them in same order and range (821, 860 and 846), as shown in Fig. 3.12.

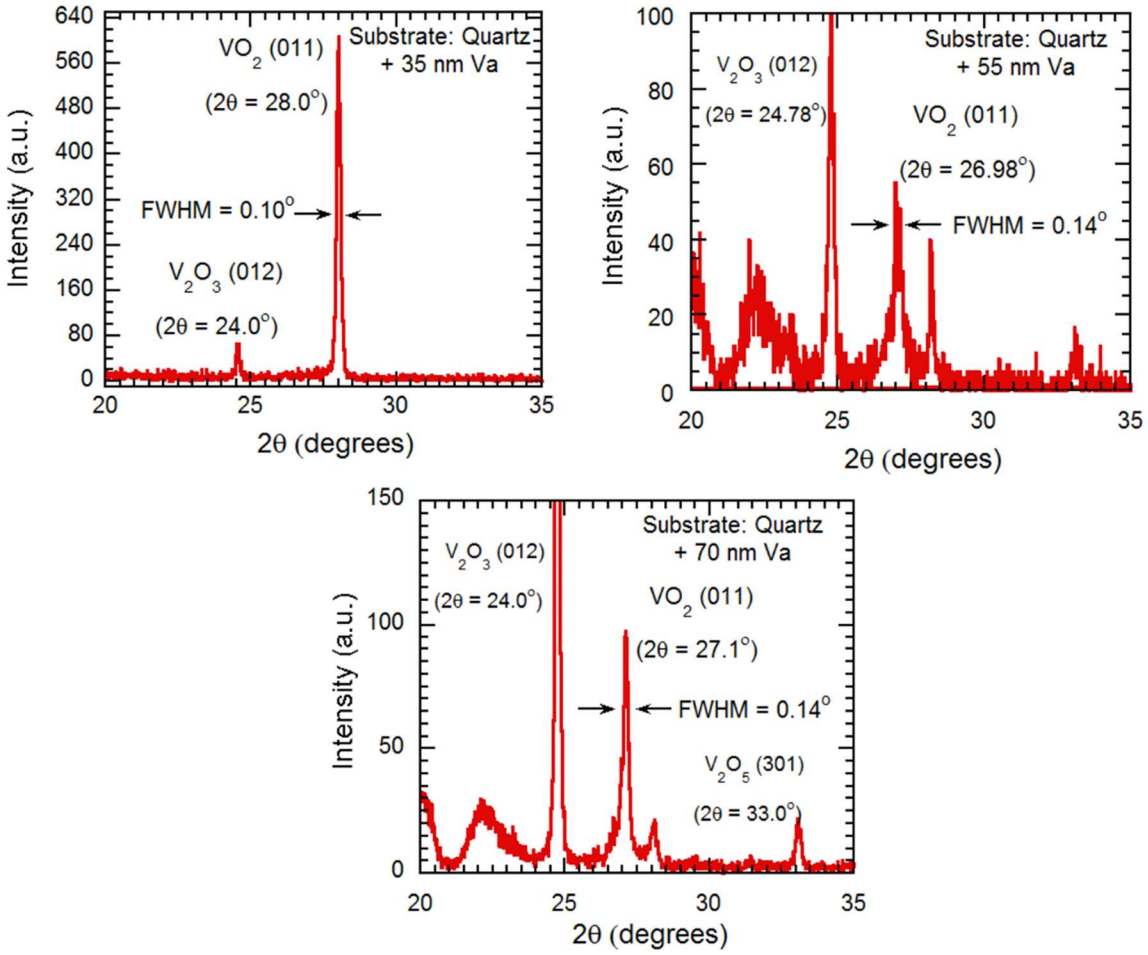

Figure 3.12: X-ray diffraction peaks are presented for the VO_2 thin films synthesized on AT-cut quartz with deposited vanadium thickness (a) 35 nm, (b) 55 nm, (c) 70 nm. The VO_2 (011) along with their respective full width at half maxima (FWHM), are pointed out with arrows.

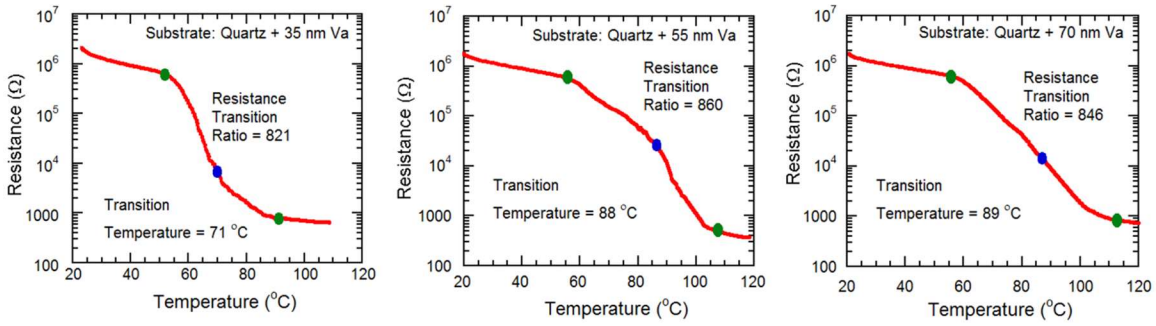

Figure 3.13: Semi-log plots of resistivity variation as a function of temperature for the VO_2 thin films grown on AT-cut quartz with deposited vanadium thickness (a) 35 nm, (b) 55 nm, (c) 70 nm as they undergo semiconductor-metal transition (SMT). The transition resistance ratios, along with the beginning (green dots), mid (blue dots, corresponding to maximum slope points in the curves), and end transition temperatures (green dots) are shown for all the samples

Table 3.4: Comparison of the results of electrical and optical characterization for samples grown on Quartz substrates (Deposited Vanadium of three different thicknesses)

V thickness	**35 nm**	**55 nm**	**70 nm**
Resistance transition ratio	821	872	846
RMS roughness (nm)	15.7	7.6	12.5
2θ angles of common XRD peaks (FWHM)	28° (011) (0.10°)	26.98° (011) (0.14°)	27.1 (011) (0.14°)

CHAPTER FOUR

INFRARED TRANSMISSION CHARACTERISTICS OF PHASE TRANSITIONING VO_2 ON VARIOUS SUBSTRATES

Apart from the transition of electrical properties of VO_2 during phase transition as described in the previous chapter, the reversible change of optical properties of VO_2 is becoming a point of interest recently, because of the sharp and abrupt change of optical power transmitted through VO_2 or reflected by VO_2 during phase transition [61]. When a VO_2 thin film is subject to being exposed to electromagnetic waves (UV, visible light, near-IR, IR, mid-IR), some of the optical power carried by the beam transmits through the VO_2 film, a portion of it is reflected, and the rest of the power is absorbed by the VO_2 film 62]. When the semiconductor to metal transition (SMT) initiates, the percentage of the transmitted optical power undergoes a sharp change to another level. The direction of the change depends on whether the VO_2 is transitioning its state to semiconductor or to metal. It also depends on the wavelength of the light transmitted through it. At visible wavelengths, the transmission of light increases through VO_2 when the film is transitioning from semiconductor to metal [63], and vice versa. After crossing a wavelength threshold, when the wavelength is near IR or IR, the transmission of light through VO_2 starts to decrease when the film is transitioning from semiconductor to metal, and vice versa. Taha et al. 64] reports the percentage of the decrease of optical power as 42% for a wavelength at 1550 nm, and 60% for a wavelength at 2000 nm. Moreover, VO_2 on quartz shows similar characteristics which have been observed by other researchers (i.e., 40.9% at 1550 nm

[65]). They also report 48.8% of change when the laser is of a wavelength of 1800 nm. At 1550 nm, the transmission loss through the optical fiber (glass) is minimal, which makes this wavelength very attractive for optical communication, as widely reported [66]. The results from the literature provides an estimate of what type of results we should expect if we use the telecommunication wavelength 1550 nm laser beam to transmit through the VO_2 thin film. In order to observe the phenomenon, first we synthesize VO_2 thin films on five types of substrates (sapphire, SiO_2/Si, AT-cut quartz, GaN/AlGaN/GaN/Si, and muscovite) using a low-pressure direct oxidation method [31]. In our research we have utilized the 1550 nm telecom wavelength laser to determine the variation in optical transmissivity of VO_2, induced by phase transition. The flexibility of the muscovite substrates enabled us to apply both a compressive and tensile strain on it [66] and study their effect on the transition temperature [67].

Optical Characterization of VO_2 for near-IR wavelengths 980 nm and 1064 nm

In addition to the electrical characterization, variation in transmitted optical power (for transparent films) with temperature is often investigated to determine optical property changes associated with SMT. Transmitted optical power through VO_2 thin films undergoes a sharp transition during SMT, which is significantly higher for infrared light compared to visible light. Like the resistivity change, the transmitted optical power was also measured spanning across the SMT for the VO_2 thin films as a function of temperature, using the same characterization setup as shown in Fig. 3.5. An IR laser was held with a clamper above the sample at an optimal height so that the laser is focused on the sample,

while a photodetector (Newport 918D-IR-003R, range 780 to 1800 nm) was placed beneath the central hole of the annular ceramic heater to measure the transmitted light power, with the help of a Newport 1918-R power meter.

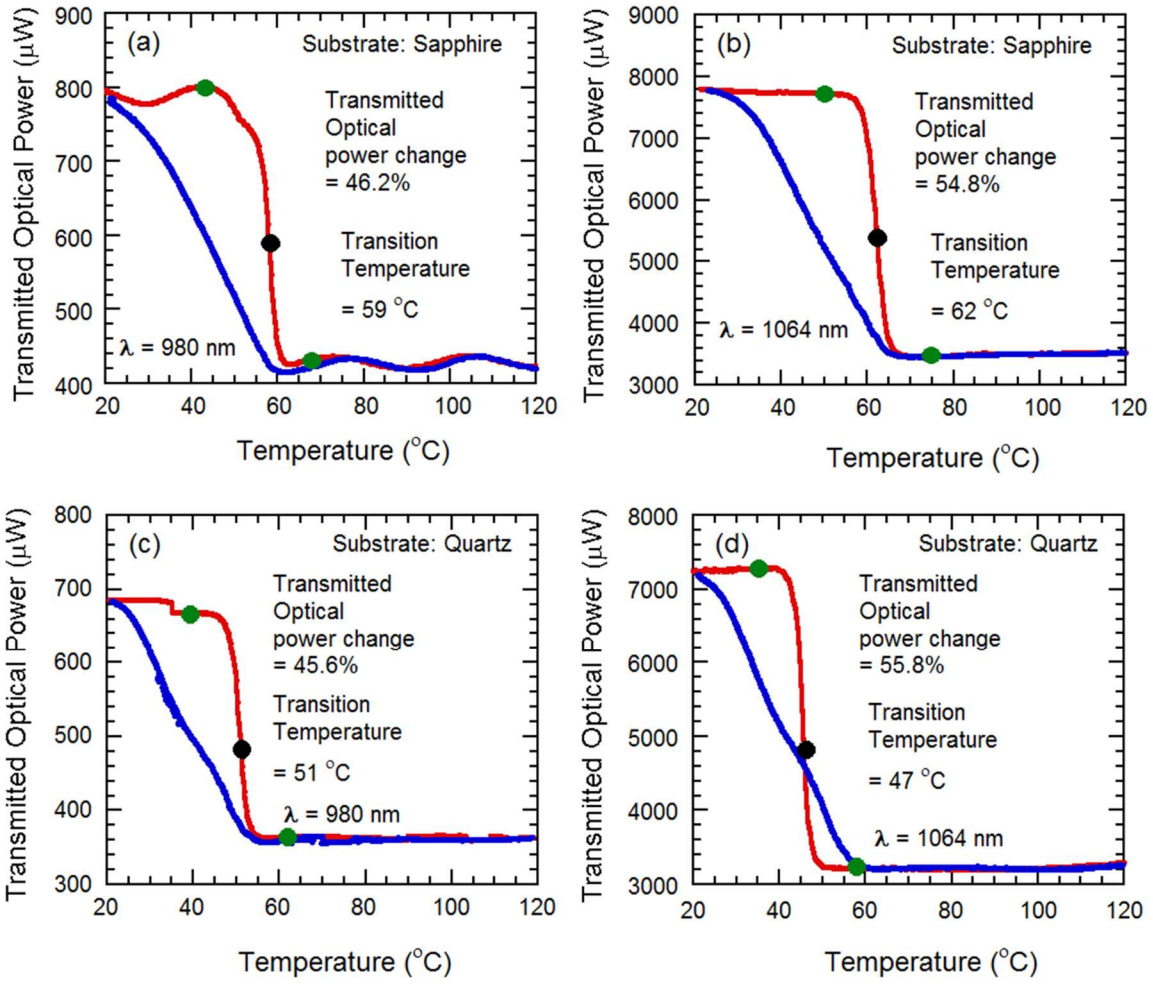

Figure 4.1: Transmitted optical power for two laser wavelengths (980 and 1064 nm), plotted against temperature, for the VO_2 thin films grown on c-plane sapphire (a, b), and AT-cut quartz (c, d), as they undergo metal-insulator transition (SMT). The transmitted optical power change, along with the beginning (green dots), mid (black dots, corresponding to maximum slope points in the curves), and end transition temperatures (green dots) are shown for all the samples.

Figures 4.1 (a)–(d) show the experimental results on the variation of transmitted optical power through the VO_2 films grown on AT-cut quartz and c-plane sapphire for two IR lasers wavelengths 980 and 1064 nm. A sharp change in transmitted laser power through the VO_2 thin film is observed at SMT, as expected, since semiconducting VO_2 allows IR light to transmit through it before SMT, while "metallic" VO_2 film resulting after SMT, acts as a lossy medium for the electromagnetic (EM) waves [68], and causes a sharp drop in the transmitted power. A reduction in transmitted laser power by 46.2% at 980 nm, and 54.8 % at 1064 nm, was observed for the VO_2 film on sapphire substrate, whereas for the film on AT-cut quartz substrate, the transmitted laser power decreased by 45.6% at 980 nm, and 55.8% at 1064 nm. A summary of the optical properties of the films are presented in Table 4.1. We note that the change in transmitted optical for sapphire and quartz are one of the highest reported so far at 1064 nm. We also note that the actual magnitude of the transmitted power for both the substrates is much lower for 980 nm compared to 1064 nm, since the optical transmittance changes much more drastically as the wavelength increases [69]. We also note here that the forward optical transitions are much sharper compared to the reverse transitions. This has been observed to some extent for the electrical characteristics as well, but not as prominently as seen for the optical ones. This "lag" may be due to the slower rate of cooling of the region exposed to the laser, when the substrate is cooled, as the optical absorption in the highly conductive material (the area where laser is focused) is high, preventing quick changes in temperature.

Comparing the electrical and the optical transition plots in Figs. 3.6 and 4.1 for AT-cut quartz and c-plane sapphire substrates, we find that the forward optical transitions are much sharper, with significantly lower transition temperatures, compared to those of the electrical transitions. This is likely due to the fact that the electrical transition plots are influenced by the resistance of almost the entire VO_2 film, which changes temperature due to the thermal energy provided by the heater through a comparatively slow process. On the other hand, during optical transition, the transmitted optical power is influenced only by the small area of the VO_2 film on which the laser is focused. Since the transition of that small area is affected both by the thermal energy provided by the heater and the energy absorbed from the laser power focused on it, the transition happens much quicker, which is manifested as a much steeper transition slope and significantly reduced transition temperature.

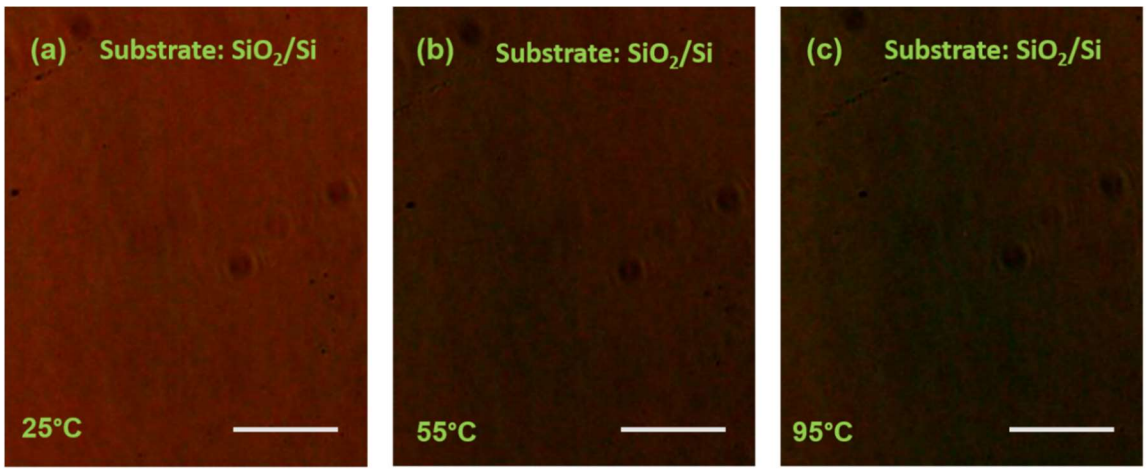

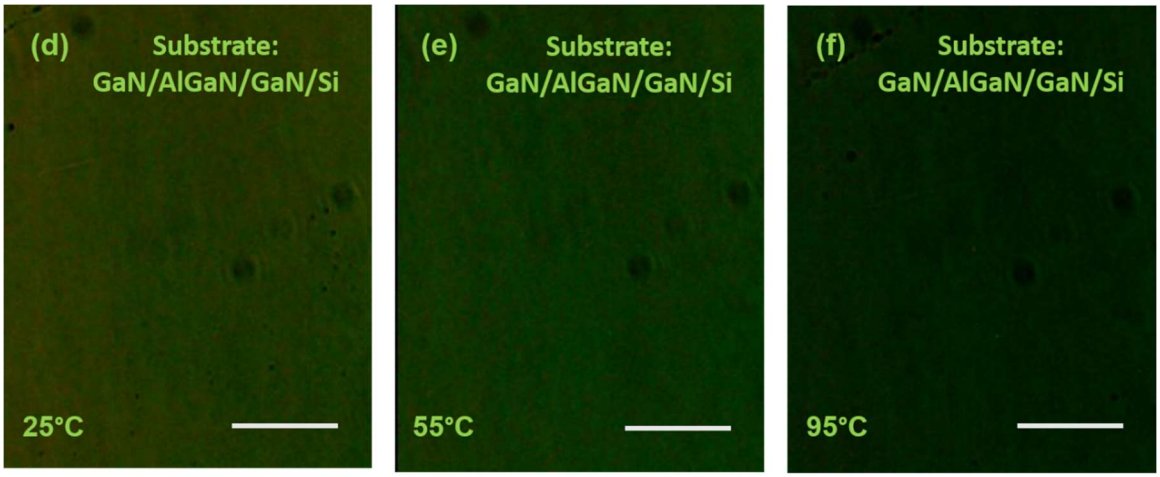

Figure 4.2: Optical microscopy images (20 × magnification) of VO_2 thin films (5 × 3 mm) grown on SiO_2/Si substrate (a, b, c) and GaN/AlGaN/GaN/Si substrate (d, e, f) taken near the beginning (25°C), at the middle (55°C), and toward the end (95°C) of the metal-insulator transition (SMT). As the samples undergo phase transition, their color changes significantly from lighter to darker. The scale bar: 200 μm for all substrates.

The VO_2 on SiO_2/Si and GaN/AlGaN/GaN/Si did not allow any transmission of laser power in the near IR region, as the silicon substrate absorbed all the light from the laser (VO_2 on Si only partially allows transmission of laser at mid IR wavelengths i.e. ~2500 nm, still significantly reducing the optical transmitted power by 55%) [70]. However, we recorded the significant color change (from optical microscopy images) of the VO_2 thin films (from lighter to darker) while undergoing the SMT, which is consistent with earlier reports [31]. Optical images of the VO_2 thin films, (a) near the beginning (25°C), (b) middle (55°C), and (c) toward the end (95°C) of the SMT, are shown in Figure 4.2, which indicates significant darkening of the film as higher temperatures. This can be attributed to lower reflection of light as more of it absorbed in the material, which behaves like a lossy medium for the EM waves [66]. Comparison with other reports are shown in Table 4.2.

Optical Characterization of VO_2 at telecommunication wavelength 1550 nm

a) Substrate heating by ceramic heater

Variation in transmitted optical power vs. temperature is often observed to identify and measure optical property changes due to SMT at telecom wavelength 1550 nm. The transmitted optical power was measured during the SMT for the VO_2 thin films as a function of temperature, using the same characterization setup as shown in Figure 3.5.

In Figure 4.3, we observed the experimental results on the transmitted optical power variation through the VO_2 films grown on c-plane sapphire, SiO_2/Si, AT-cut quartz, GaN/AlGaN/GaN/Si, and muscovite for the IR laser's wavelength at 1550 nm. Just like the phenomenon for 980 nm and 1064 nm, the transmitted laser power through the VO_2 thin film undergoes a sharp change, and causes a sharp drop in the transmitted power. A reduction in transmitted laser power by approximately 80% for 1550 nm, was observed for the VO_2 film on all the substrates. A summary of the optical properties of the films are presented in Table 4.1. We note that the transition in transmitted optical power is the highest reported so far at wavelength 1550 nm.

Table 4.1: Summary of the optical properties of the VO_2 films synthesized on the five different substrates: sapphire, SiO2/Si, AT-cut quartz, GaN/AlGaN/GaN/Si and muscovite.

Parameters	c-plane Sapphire	SiO_2/Si	AT-cut Quartz	GaN/AlGaN/GaN/Si	Muscovite

Optical Transition temperature at λ = 980 nm	59 °C	-	51 °C	-	
Optical Transition temperature at λ = 1064 nm	62 °C	-	47 °C	-	
Optical Transition temperature at λ = 1550 nm	64 °C	69 °C	59 °C	64 °C	79 °C
Change of Transmitted laser power or color at λ = 980 nm (%)	46.2	Brown to brownish-green	45.6	Lighter to darker green	
Change of Transmitted laser power or color at λ = 1064 nm (%)	54.8	Brown to brownish-green	55.8	Lighter to darker green	
Change of Transmitted laser power or color at λ = 1550 nm (%)	80.84	82.8	81.86	85.33	80

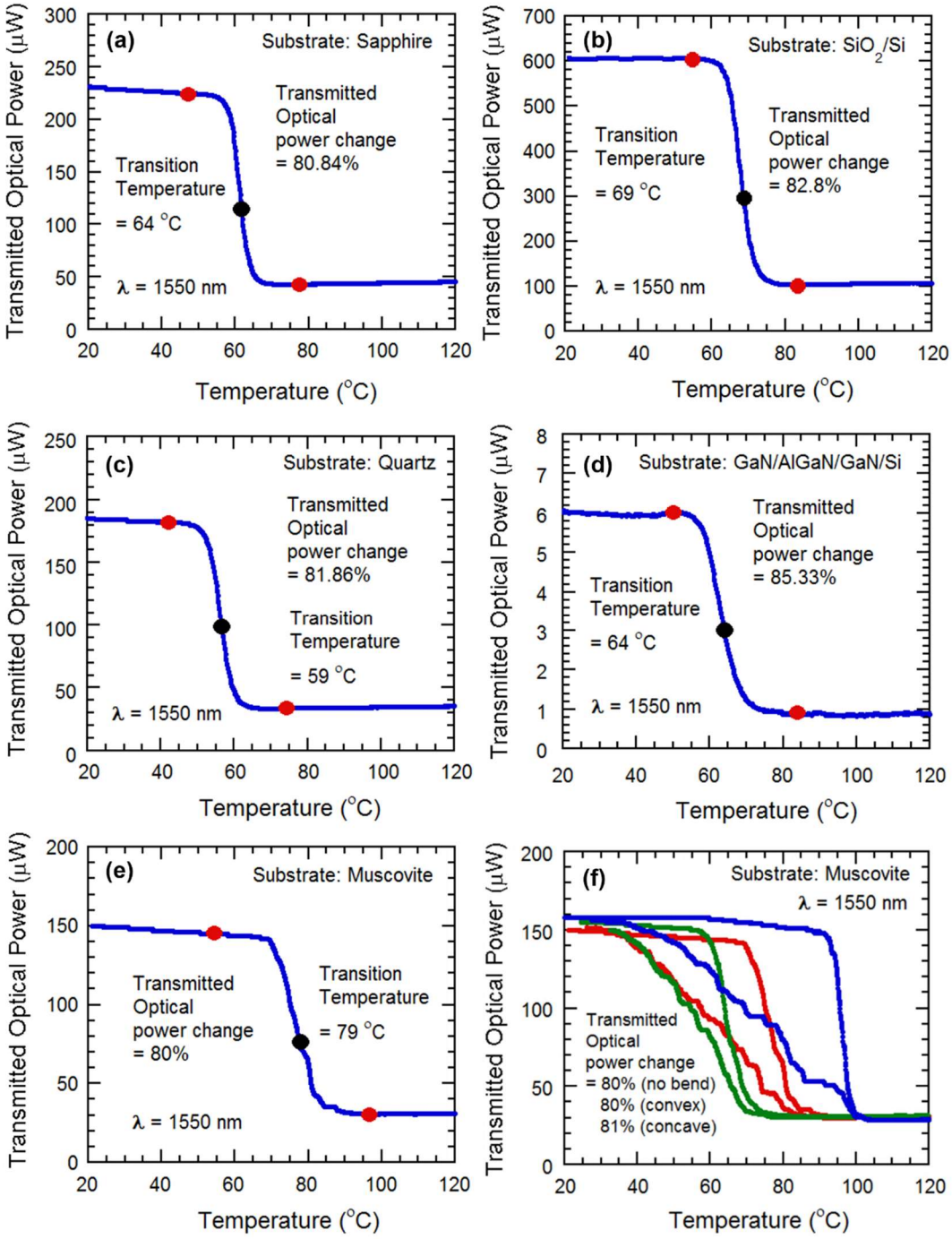

Figure 4.3: Transmitted optical power for IR laser wavelengths (1550 nm) plotted against temperature. Thin films grown on c-plane sapphire (a), SiO_2/Si (b), AT-cut quartz (c), GaN/AlGaN/GaN/Si (d) and muscovite (e) as they undergo metal-insulator transition (SMT). The transmitted optical power change, along with the beginning (red dots), mid (black dots, corresponding to maximum slope points in the curves), and end transition temperatures (red dots) are shown for all the samples.

We observe that optical transitions are sharper in Figure 4.3, and compared with the transition temperatures of electrical transitions (Figure 3.6), here, the transition temperatures are significantly lower. The reason is likely to be the fact that resistance of almost the entire VO_2 film influences the electrical transition plots, and the thermal energy from the heater changes the temperature in a slower process. During optical transition, only the small area of the VO_2 film with a focused laser beam influences the transmitted optical power. Since the transition of that small area is affected both by the thermal energy provided by the heater and the energy absorbed from the laser power focused on it, the transition happens much quicker, which is manifested as a much steeper transition slope and significantly reduced transition temperature.

b) Substrate heating assisted by high powered laser

Instead of realizing SMT using heating, an electric field, or strain, here, we have used a high-powered laser (124 mW, 635 nm) to induce the semiconductor to metal transition. The IR beam of 1550 nm probe laser was transmitted through the same high-power laser illuminated spot of the VO_2 sample and detected using a photodetector underneath. The details of the characterization setup and the results are discussed later.

Optical characterization of VO_2 on flexible substrate

a) Substrate heating without mechanical strain applied

The procedure and experimental setup is similar to that used for the five other substrates beforehand. The photodetector and the IR laser were the same as before as well. The 1550 nm IR beam was transmitted through the VO_2 sample placed in between the laser and the photodetector. The transmitted IR power through the VO_2 thin film is varied and measured with respect to the change in temperature from 20 °C to 140 °C. The heating induces semiconductor to metal transition in the VO_2 thin film, which initiates changing its phase and conductivity, from semiconductor to metallic. At the transition region, the photodetector detects a sharp decrease of transmitted power, decreasing by ~85%, and return to initial level after being cooled down.

b) Substrate heating with tensile strain applied to the sample

For this we used a setup similar to that used for electrical characterization during tensile strain. At the edge of the ceramic heater, the VO_2 sample is attached to a clamp. The suspended part of the VO_2 thin film is bent in a convex way, by pressing down the sample with a screw-and-wedge. The tensile strain was enough to ensure that the convex bending of the VO_2 was visible from Figure 3.7. The heater was used to apply heat on the convexly bent VO_2 thin film. As with the previous setup, the IR beam is focused on the VO_2 surface, and a portion of the IR laser power is transmitted though the sample and measured by the photodetector. By applying heat, the temperature is varied from 20 °C to 140 °C. The VO_2 undergoes the SMT transition, causing the sharp decrease of transmitted optical power in the transition region. The effect of convex bending is observed after plotting the transmitted optical power data, and we see that the percentage of change has

decreased slightly, but is still around ~80%. Moreover, we notice the transition plot has shifted to the right, indicating the increase in transition temperature due to tensile strain (Figure 4.3 (f)).

c) Substrate heating with compressive strain applied to the sample

The setup is similar to the one used for tensile strain, but this time, the sample is pressed upwards in the free edge, to ensure the concave bending of the sample by compressive strain. Again, the IR power is transmitted through the thin film, and the power is varied due to the variation of the temperature, experiencing the highest percentage of variation at transition region of the VO_2. After plotting the data, it is observed that percentage of change is still close to ~80%, but this time, the transition region has shifted to the left, indicating the decrease in transition temperature due to compressive strain. (Figure 4.3 (f))

d) Substrate heating assisted by high powered laser

Finally, we utilized a high-power laser (124 mW, 635 nm) pulsed at 0.125 Hz (39% duty cycle) frequency to induce SMT in the VO_2/muscovite sample, and plotted the response of the transmitted IR laser power, with the goal of studying the modulation of a probe laser power at the observed telecom wavelength of 1550 nm. A schematic diagram for the experiment is shown in Figure 4.4. We also performed a similar study on VO_2/quartz film, in order to compare the characteristics of VO_2/muscovite film. We used the ceramic heater to maintain a constant temperature closer to the transition temperature (50 °C for

quartz and 45 °C for muscovite) to make it easier for the high-power laser to induce SMT. At each cycle of the red laser being pulsed, we observe that the IR power is pulsing from a high to low level of transmitted power. The higher level of power is transmitted when the VO_2 is in semiconductor phase, whereas the reverse was observed in the metallic phase The experimental results are shown for VO_2 grown on quartz and muscovite substrates in Figure 4.5 (a) and (b), respectively. We find that although the change in transmitted IR power due to high power pulsing was ~25% for the VO_2 on quartz substrate, it was ~40% for VO_2 on muscovite. The fall time constants were found to be ~2.92 s and 3.14 s for the VO_2 on quartz and muscovite substrates, respectively. Inset of Figure 4.5 (a) shows determination of the fall time constant by least square fit of an exponential curve to the fall transient of the transmitted laser power. We would like to mention here that the need for an external heater can be eliminated using a higher-powered laser which can also reduce the switching time constant.

Effect of vanadium thickness on optical properties of VO_2/quartz:

Previously we observed the effect of thickness of vanadium metal layer on the electrical properties of VO_2. Now we are going to check the effect of vanadium thickness on the optical properties of VO_2/quartz. Two wavelengths of IR laser (980 nm and 1064 nm) are transmitted through the three thicknesses of VO_2/quartz thin films. The transmitted optical power is measured with a photodetector and power meter similar to the Figure 3.5. The temperature is varied by applying heat and the transmitted optical power exhibits a sharp decrease during the semiconductor to metal transition of the VO_2 film. At each

wavelength, we observe the change of transmitted power increases due to the increase of vanadium thickness prior to the VO_2 synthesis as summarized in Table 4.2.

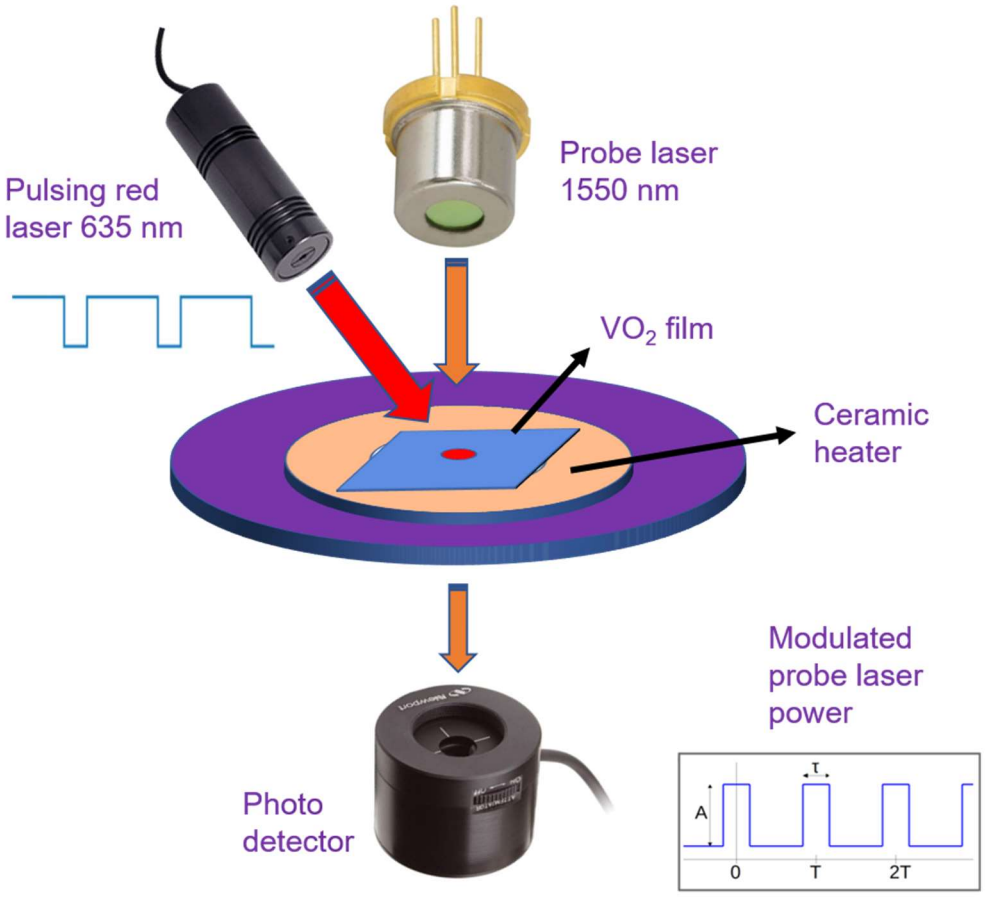

Figure 4.4: Schematic for inducing SMT in VO_2 with a high-powered pulsed laser (124 mW, 635 nm) for modulating the probe laser power (1550 nm) transmitted through the VO_2 thin film.

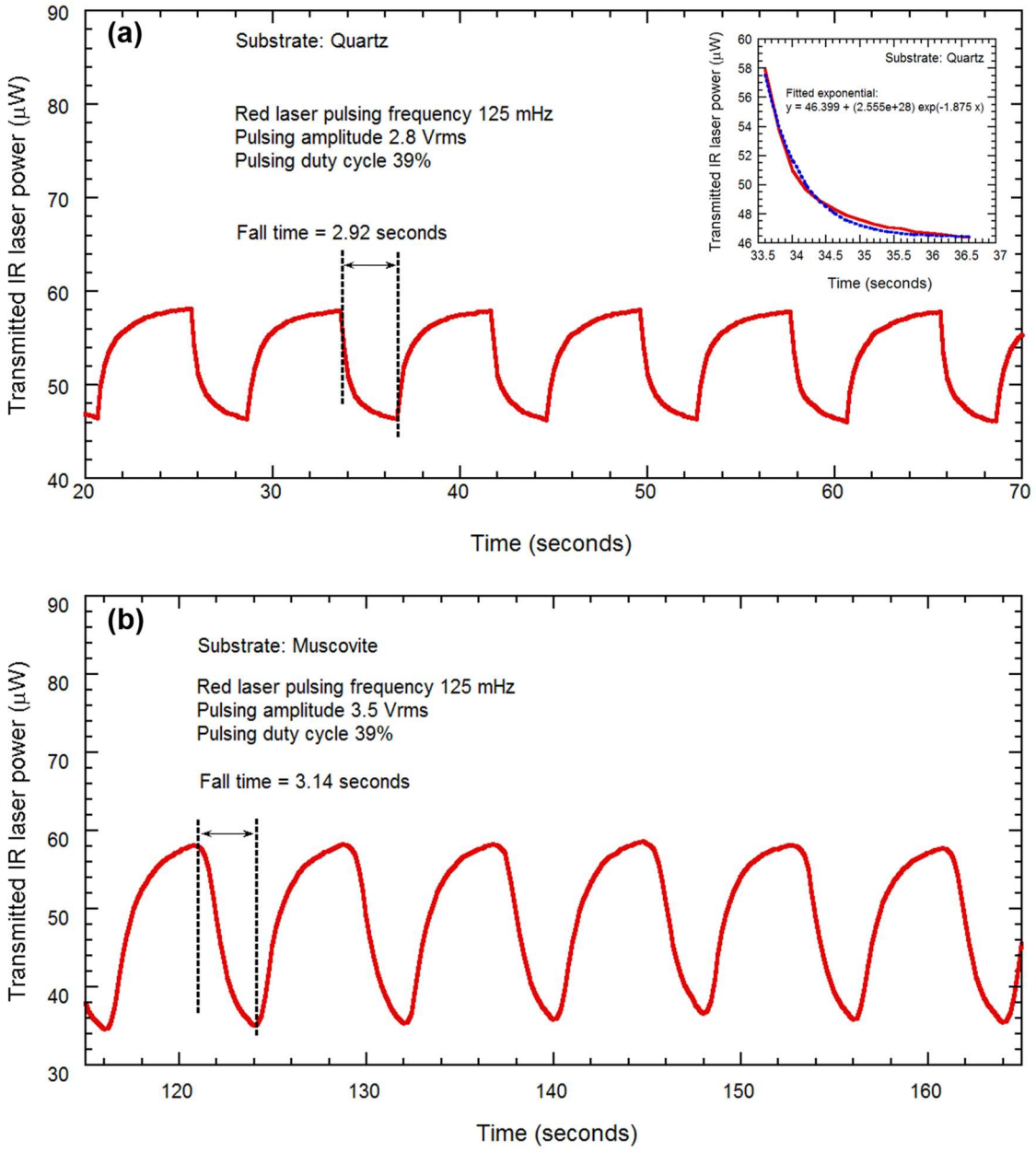

Figure 4.5: Modulation of transmitted optical power for IR probe laser wavelengths (1550 nm), plotted with respect to time, for the VO_2 thin films grown on (a) quartz, falling time 2.92 s and (b) muscovite, falling time 3.14 s, undergo semiconductor to metal transition (SMT) due to pulsing of red laser (635 nm, 124 mW, 0.125 Hz and 39% duty cycle).

Table 4.2: Comparison of the results of optical characterization for samples grown on Quartz substrates (Deposited Vanadium of three different thicknesses)

V thickness		**35 nm**	**55 nm**	**70 nm**
Transmitted power change	λ = 980 nm	34.6 %	42.1 %	47.7 %
	λ = 1064 nm	39.4 %	54.5 %	60.2 %

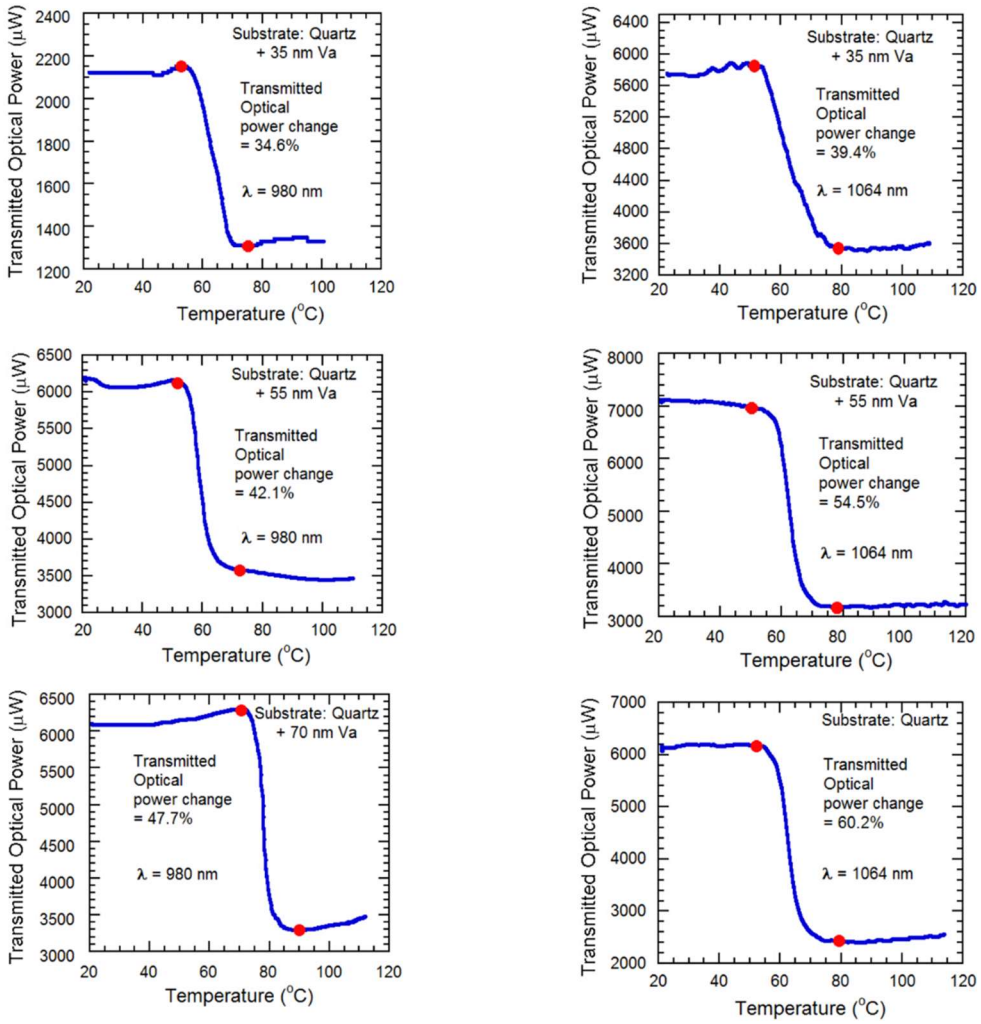

Figure 4.6: Transmitted optical power for two laser wavelengths (980 and 1064 nm), plotted against temperature, for the VO_2 thin films grown on AT-cut quartz, with deposited vanadium thickness (a, d) 35 nm, (b, e) 55 nm, (c, f) 70 nm as they undergo metal-insulator transition (SMT). The transmitted optical power change, along with the beginning and end (red dots), corresponding to beginning and end transition temperatures are shown for all the samples.

Table 4.2: Summary of the transmitted optical power change for VO_2 films on sapphire and quartz substrates in the near infrared wavelength range.

Substrate	Reference	Synthesis method	Wavelength (nm)	Film thickness (nm)	Transmitted power change (%)	Crystal type
Sapphire	Radue et al. [60]	Reactive bias target ion beam deposition	785	80	44.4	Polycrystalline
	This paper	**Direct oxidation**	**1550**	**140**	**80.84**	**Polycrystalline**
	Ma et al. [47]	Reactive magnetron sputtering	2000	20 50	33 50	Dual orientation
	Bian et al. [28]	Pulsed laser deposition	980 1064	200 200	48 44	Monocrystalline
	Zhang et al. [9]	DC magnetron sputtering	2500	140-185	52	Monocrystalline
Quartz	Liu et al. [61]	Reactive Pulsed laser ablation	1250	-	32	Amorphous
	Dejene et al. [56]	Reactive KrF laser ablation	1500 1800	500 500	40.9 48.8	Polycrystalline
	Zhang et al. [9]	DC magnetron sputtering	2500	140-185	41	-
	Radue et al. [60]	Reactive Biased Target Ion Beam Deposition	785	80	61.1	Polycrystalline
	Zhang et al. [49]	RF plasma assisted O-MBE	2000 2500	60 60	58 61	Polycrystalline
	This paper	**Direct oxidation**	**1550**	**140**	**81.86**	**Polycrystalline**

SiO2/Si	**This paper**	**Direct oxidation**	**1550**	**140**	**82.8**	**Polycrystalline**
GaN/AlGaN /GaN/Si	**This paper**	**Direct oxidation**	**1550**	**140**	**85.33**	**Polycrystalline**
Muscovite	**This paper**	**Direct oxidation**	**1550**	**140**	**80**	**Polycrystalline**

CHAPTER FIVE

ELECTRIC FIELD INDUCED MID-INFRARED OPTICAL MODULATION USING NANOSCALE VO_2 THIN FILM DIAPHRAGM

Optical properties of VO_2 thin film have enabled it to be an excellent choice of a wide variety of applications, like temperature and infrared (IR) sensing [67], smart windows [68], and for temperature based optical switches for waveguides at RF. Frequencies [69], including being the primary material required for the optical modulator we have designed and developed as reported in this work. In addition, VO_2 has become an integral material for designing a waveguide switch [70]. That involves utilizing the properties and characteristics of VO_2 film in response to the incident light beam, ranging from ultraviolet to infrared regions in the electromagnetic wave spectrum. The semiconducting state of VO_2 enables it as a highly transparent medium for infrared waves, allowing us to use the VO_2 as a regular waveguide. However, the metallic state of VO_2 film is highly reflective to the incident IR beam, causing it to block most of the incident wave [71] - [73]. This particular property of VO_2 film allows it to be implemented as a waveguide switch, an argument further supported by the fast and reversible transition of phase and state of the VO_2 film, which causes the change of refractive index of the VO_2 film ([74], [75]). The difference of responsiveness of VO_2 film to the incident and transmission of optical beam leads to the applications of implementation of VO_2 film for optical beam modulation, which is the primary focus of our work here.

Previously we had observed how VO_2 film can directly and almost instantaneously influence the transmission of IR beam through itself, especially when the VO_2 film is undergoing transition of phase and semiconducting to metallic transition (and vice versa) [31]. We had applied external heat to the VO_2 film to vary the temperature of the film and instigate the transition. Also we had observed the influence of mechanical strain on a flexible VO_2 film [57] and the responses of its optical characteristics. However, if we try to initiate the SMT and the phase transition with electric field only, it takes a huge amount of voltage even for causing a barely noticeable transition, sometimes that also does not work properly with stability and reversibility [76] – [77].

VO_2 diaphragm fabrication

Therefore, we had to make some modifications in the structure of our working chip, almost similar to what we reported in [78]. First we designed and developed the robust system for synthesizing the VO_2 films which ensures an excellent quality compared to the film we had to use beforehand, displayed in Figure 2.5 ([31], [78]). We have synthesized VO_2 film on an exceptionally small circular area of substrate, rather than the large area of substrates from our previous works ([31], [57]). Also in order to release diaphragm-like structure with the VO_2 film, we have removed the bottom layer of silicon from both the substrates (SiO2 (100 nm) / Si / SiO2 / Si and GaN (1.3 μm / Si), and later patterned the VO_2 film with two sets of densely deposited interdigitated metal fingers, each set having a microscopically small extension to be used as electrode shown

in Figure 5.1-5.2. These steps freed the VO_2 films from an additional unnecessary silicon layer for allowing better percentage of IR beam transmission through the VO_2 film, also allowed us to apply only a very small amount of electric voltage, without any external heating, for instigating the SMT and the phase transition. The externally applied voltage creates electric field along the VO_2 film, and the interdigitated metal electrodes creates some internal heating throughout the VO_2 film surface which aids in the SMT and the phase transition. Because of their coil-like design, the densely deposited interdigitated metal fingers effectively conserve the small amount of the intrinsic heat created by the electric field, and assists further into the transition, simultaneously lowering the external voltage to a minimal amount of 6V, compared to the required external 800 V as reported in (p f wang). This specially designed VO_2 film based diaphragms exhibits an instantaneous SMT and phase transition due to a very small amount of external electric field which was never possible with our previously developed VO_2 films due to applying external heating (azad1). Finally, we subjected our VO_2 film based diaphragms to the incidence and transmission of near-IR and mid-IR continuous beams, and utilized the diaphragms to periodically pulse the incoming IR beam, and the change of response in percentage of modulation depth.

Two particular substrates were chosen for this purpose in order to hold the VO_2 membrane (silicon on insulator – non-piezoelectric and GaN/AlGaN/Si – piezoelectric). Afterwards, VO_2 thin film was synthesized on both the substrates by direct oxidation technique inside our low pressure furnace, maintaining the VO_2 layer thickness of 140

nm [31] as we discussed in Chapter Two. Interdigitated 10 um wide metal fingers distant of 15 µm from each other have been deposited on the VO_2 thin films with layer thicknesses of Ti (20 nm) / Au (250 nm). At the end, Bosch process was implemented to remove the Si substrate layer and release the VO_2/SOI and VO_2/GaN diaphragms [78].

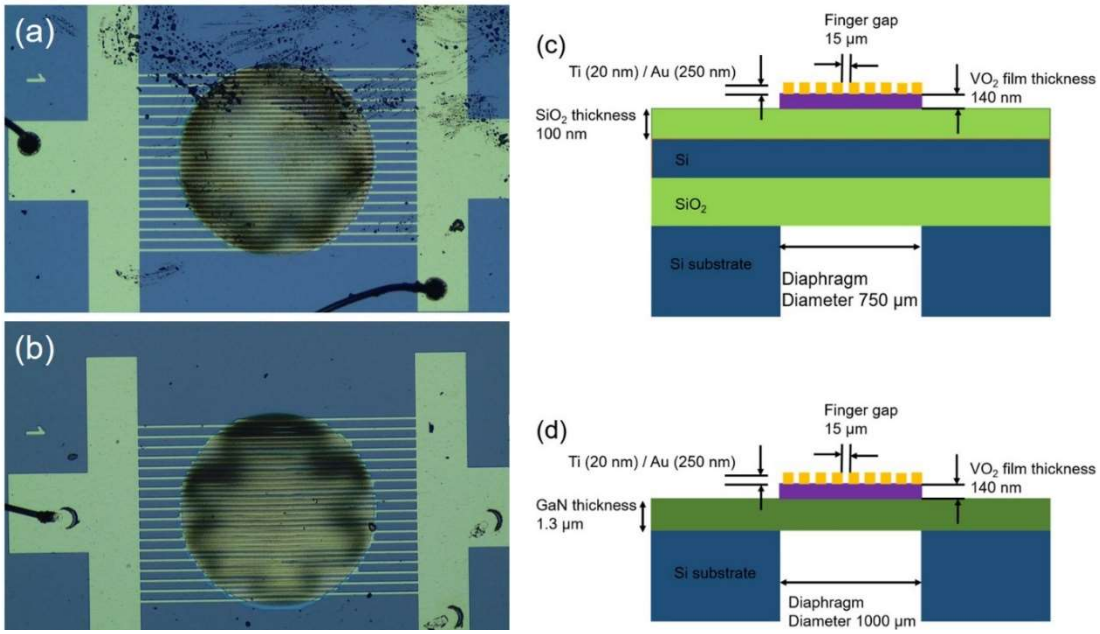

Figure 5.1 (a) and (b) Optical microscopic images (50× magnification) of VO_2 membranes on substrates SOI and GaN after removal of substrate layer of silicon (111). Polycrystalline circular patches (750 um and 1000 um diameter) of VO_2 films (70 nm thick vanadium metal) have been synthesized on SiO_2/Si substrates and GaN/AlGaN/GaN/Si substrates by direct oxidation method. Following the patterning the VO_2 thin with overlapped Ti/Al fingers, the silicon layer has been removed from underneath of the surface by Bosch process. The scale bar: 500 µm. (c) and (d) The schematic side view VO_2 membranes on substrates SiO_2 and GaN

After releasing the VO_2/SiO_2 and VO_2/GaN diaphragms by implementation of Bosch process, we loaded them on 28-pin chip carriers (from Spectrum Semiconductors Inc.) with a 0.6 cm diameter annular hole in the middle of it. The reason for choosing the

holed chip carrier is to ensure a free path for laser beam to pass through and reach the photodetector, after the beam is transmitted through the VO_2 diaphragms. Then each set of interdigitated fingers are connected to the chip carrier pin by implementing wirebonding method in our laboratory, with a wirebonder K&S 4524A Digital.

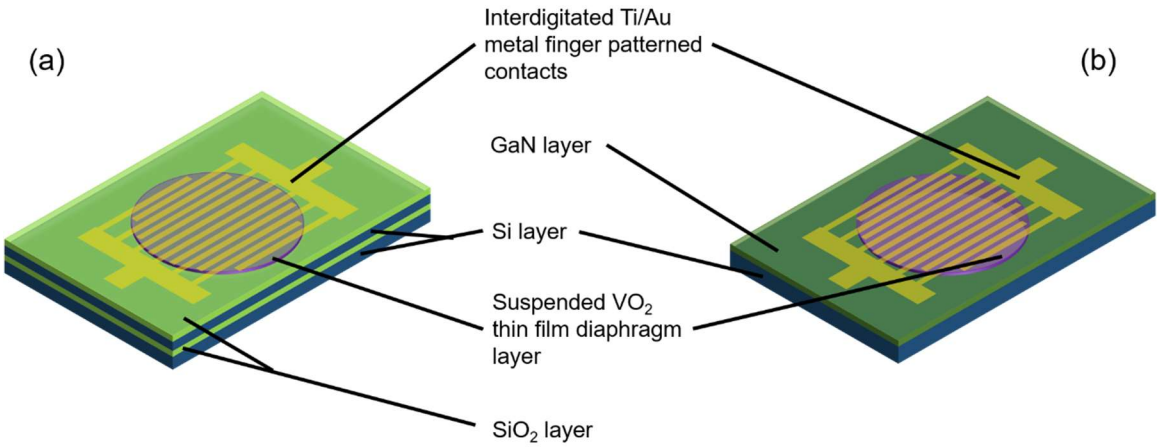

Figure 5.2: Schematic diagram of VO_2 membranes on substrates (a) SiO_2 and (b) GaN after removal of substrate layer of silicon (111).

Material characterization of VO_2 diaphragms

Prior to deposition of Ti/Au finger patterned metal contacts on the circular patterned synthesized VO_2 thin film, the film was subjected to quality testing and verification by letting it undergo surface and structural characterization. We captured atomic force microscopic (AFM) images from the VO_2 thin film with Atomic Force Microscope Veeco Dimension 3100 and analyzed the images to calculate the RMS roughness of the VO_2 film surface. The RMS roughness provided us with an acceptable estimate of the surface quality of the synthesized VO_2 thin film. Atomic force microscopic (AFM) images of 5 um x 2.5 um dimensions were captured from the VO_2

thin film. We found that the RMS roughness of the VO_2 thin films on the substrates SiO2 and GaN as 7.37 nm and 9.75 nm respectively. Such a low roughness of the thin films indicates that they can be used for depositing the metal contacts on themselves.

Further extensive structural characterization was performed on the synthesized VO_2 thin films, by performing x-ray diffraction (XRD) using Rigaku Ultima IV system. XRD pattern provided us with the crystalline quality of the VO_2 film. After analyzing the XRD pattern, we found the VO_2 thin films possess a high quality of polycrystalline nature, at XRD angles of 38.42° (020) and 38.52° (020), with full width half max width only 0.16° and 0.16°. This indicates the absolute dominant presence of polycrystalline VO_2 in the samples, having a near-monocrystalline orientation [31].

After these two types of characterization of our VO_2 thin films, we went for the next steps in order to fabricate the VO_2 diaphragms patterned with interdigitated metal fingers. Following the fabrication and preparation of the diaphragms, the pin configuration of each set of VO_2 diaphragm devices were verified prior to subjecting them to electrical and optical characterization.

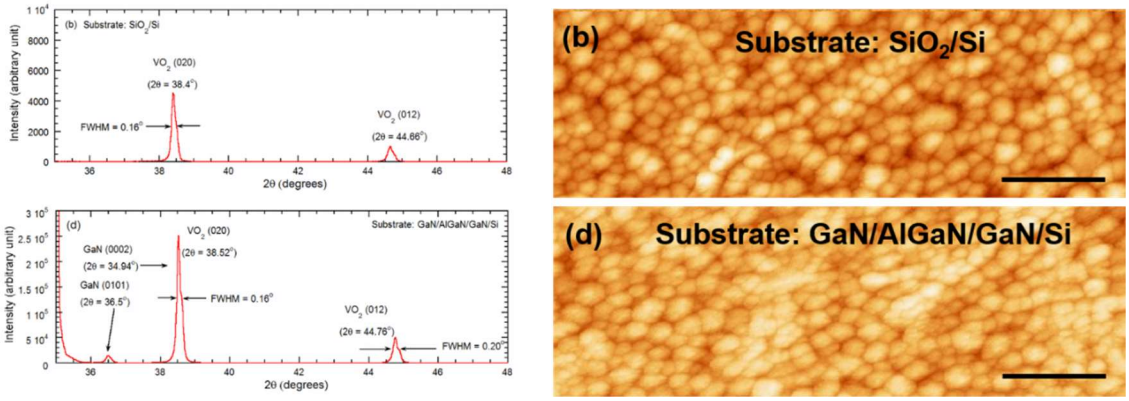

Figure 5.3: (a) and (c) X-ray diffraction peaks are presented for the VO_2 thin films synthesized on (b) SiO2/Si, (d) GaN/AlGaN/GaN/Si substrates. The VO_2 (020) and VO_2 (012) peaks, along with their respective full width at half maxima (FWHM), are pointed out with arrows. (b) and (d) show surface morphology images (5 × 2.5 μm) of thin films synthesized from 70 nm Vanadium deposited on SiO2/Si and GaN/AlGaN/GaN/Si substrates

Electrical characterization of VO_2 diaphragms

We have designed and prepared an experimental setup of vertical arrangement in order to characterize our fabricated VO_2 diaphragm devices electrically and optically, as shown in Figure 5.4. In order to apply electric field for initiating the semiconductor to metal (SMT) transition, a source measurement unit is connected to the designated pins which was wirebonded with the metal finger sets deposited on the VO_2 diaphragm. A Newport 918D-IR-003R (range 780 to 1800 nm) photodetector is placed underneath the chip carrier so that the active area of the PD is directly in line with the annular hole and the IR-transparent aperture of the VO_2 diaphragm. A downward pointing near-IR laser of wavelength 1550 nm (model AlphaNov 17A79) is placed above the VO_2 diaphragm so that the emitted IR-beam can transmit through the VO_2 diaphragm and be incident upon the photodetector active area. The photodetector is synchronized with a power meter

(Newport 1918-R) which directly measures the optical power of transmitted beam in watts.

The electrical characterization provides us with the resistance transition ratio which indicates the expected switching quality of the VO_2 thin film used in the device. The transition voltage indicates the minimum electric field required to initiate the SMT. Following the deposition of the Ti/Au interdigitated finger patterns and removal of Si layer from the substrate and releasing the VO_2/SiO_2 and VO_2/GaN membranes and wirebonding them on the chip carriers, our VO_2 thin film diaphragms are ready to be characterized for electrical characterization and optical characterization. We placed the chip carrier in the setup as shown in Figure 5.4 and held it with adjustable clamps. Next we connected the SMU with the correct pins of the chip carrier, which we connected by wires with the finger patterned metal terminals of the VO_2 diaphragms. In order to prevent excessive flow of current and damage of the membranes, we connected the SMU to an external resistor of 220 Ω in series with the VO_2 diaphragm. Following that, we applied variable electric field to the VO_2 diaphragm by gradually varying input bias voltage from the SMU, ranging from 0 to 14V (and the opposite direction) for the VO_2/SOI and 0 to 8V (and the opposite direction) for the VO_2/GaN. Simultaneously we measured and recorded the varying resistance of the VO_2 diaphragms with the SMU, later plotting the resistance vs input voltage as shown in Figure 5.4. We can observe that kilo-ohm level resistances of the VO_2 membranes undergo a huge reduction of resistance ratio around 50 abruptly to reach a level of a few ohms due to a particular electric field when

we were gradually increasing the input voltage (Figure 5.5). There occurs a hysteresis if we allow the electric field go back to its initial level by gradually decreasing the input voltage, but nevertheless the resistance of the VO_2 diaphragms returns to its initially high level abruptly. The phenomenon validates our hypothesis that VO_2 diaphragms undergo the semiconductor to metallic transition (SMT) and vice versa, similar to what we had experienced when we attempted SMT on the blanket VO_2 thin films [31].

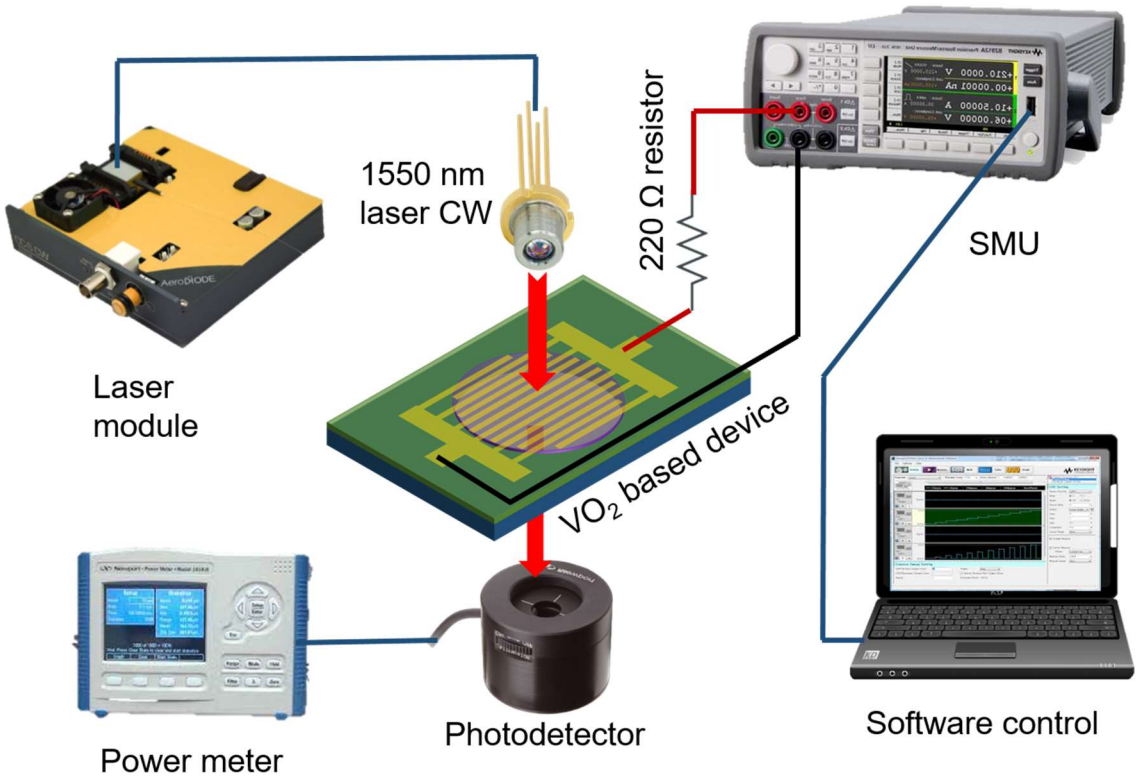

Figure 5.4 Experimental setups for electrical and optical characterizations and optical modulations of the VO_2 thin film based diaphragms. The laser is shone from the top, while a photodetector at the bottom (along with a power meter) measures the transmitted laser power as phase transition occurs, with laser wavelength 1550 nm

However, the most prominent difference is that, in our initial works, we had applied controlled heating on large area VO_2 thin films to initiate SMT and recorded the

electrical characterization as a function of resistance vs surface temperature, and observed a highly sloped but gradual transition region (Figure 3.6). But in this work, we avoided applying any heat or used any means to initiate the SMT thermally, rather we applied only electric field to initiate SMT on the micrometer level small area VO_2 diaphragms, and recording the electrical characterization as a function of resistance and electric field. Compared to the highly sloped gradual transition we had observed for large area VO_2 films [31], here we are experiencing infinite sloped abrupt transition for small area VO_2 diaphragms. These traits from electrical characterization helps us to expect the abrupt SMT when we will be applying pulsed electric field on the diaphragms.

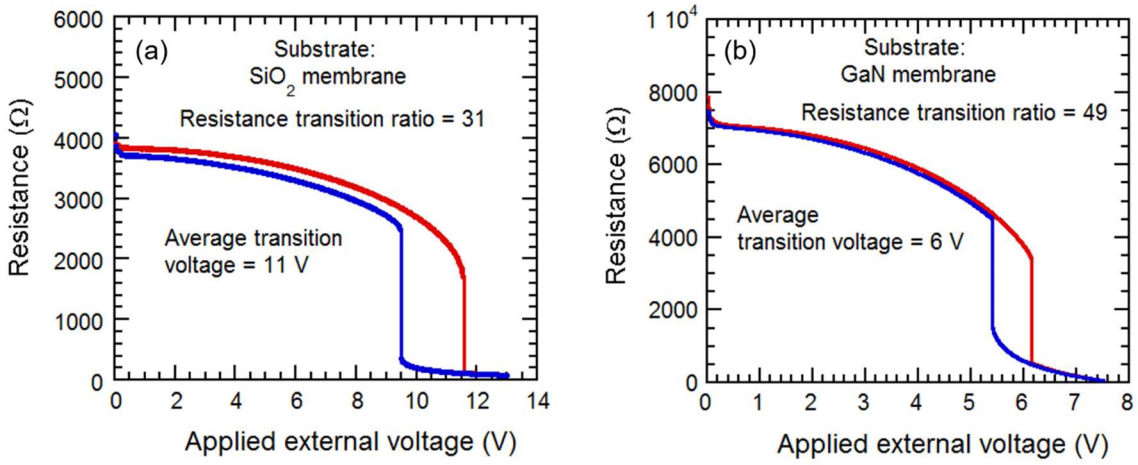

Figure 5.5: Plots of resistance variation as a function of external voltage for the VO_2 thin film based diaphragms grown on substrates (a) SiO_2/Si and (b) GaN/AlGaN/GaN/Si as they undergo semiconductor-metal transition (SMT). The resistance transition ratios and average transition voltages are shown for both the diaphragms.

Unlike Figure 3.5, there is no way to use a thermocouple to record any temperature change in our microscopic VO_2 diaphragm here. Therefore, in order to get a

correct temperature profile of the VO_2 diaphragms during the phase transition by solo electric field, we record some real-time infrared microscopic images by an IR microscope (Inframetrics SC1000 Thermacam) and measure the change in temperature at various applied biases, as shown in Figure 5.6.

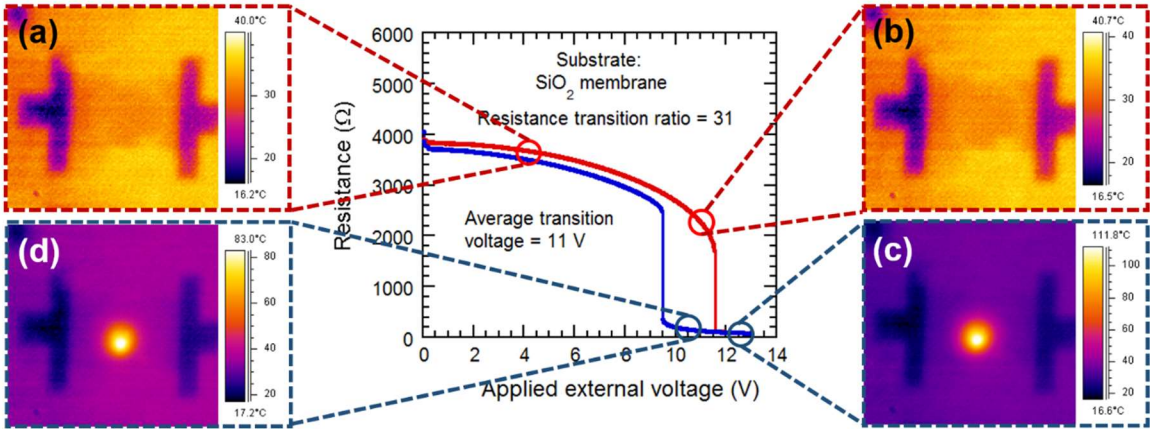

Figure 5.6: IR microscopic images captured during resistance variation as a function of external voltage for the VO_2 thin film based diaphragms grown on SiO_2/Si substrate, as it undergoes semiconductor-metal transition (SMT). (a) shows the IR image during low external input voltage, with diaphragm temperature 30 C and (b) immediately before semiconductor to metal transition, along the forward curve, with diaphragm temperature still 30 C, (c) immediately after semiconductor to metal transition, along the forward curve, with diaphragm temperature abruptly near 111 C, (d) immediately before metal to semiconductor transition, along the reverse curve, with diaphragm temperature around 83 C

An important point we should mention, in one of our previous works with VO_2/GaN diaphragms, the electrical characterization provided the ratio of transition ~5 only [78], but for the diaphragms we have prepared for this work, the ratio of transition is ~50. This considerably high ratio indicates the superior quality of VO_2 material used our diaphragms, which was synthesized using an efficiently designed setup [31], compared to the setup and method used for the VO_2 material of the older diaphragms [79].

Optical characterization of VO_2 diaphragms

In order to check how the VO_2 diaphragm can affect a continuous wave IR beam transmitted through it, we have performed optical characterization. We are using the same setup of the electrical characterization (Figure 5.4), now adding the photodetector underneath the chip carrier for capturing the IR beam and convert it to electrical signal, and the power meter for measuring the detected signal as optical power and recording it. Then we ensured that the 1550 nm IR laser, held by clamp above the VO_2 diaphragm, is pointing vertically downward to the diaphragm, and properly focused. We varied the input electric field at the finger patterned terminals of the VO_2 diaphragm by gradually varying the input voltage from the SMU, as we did for electrical characterization.

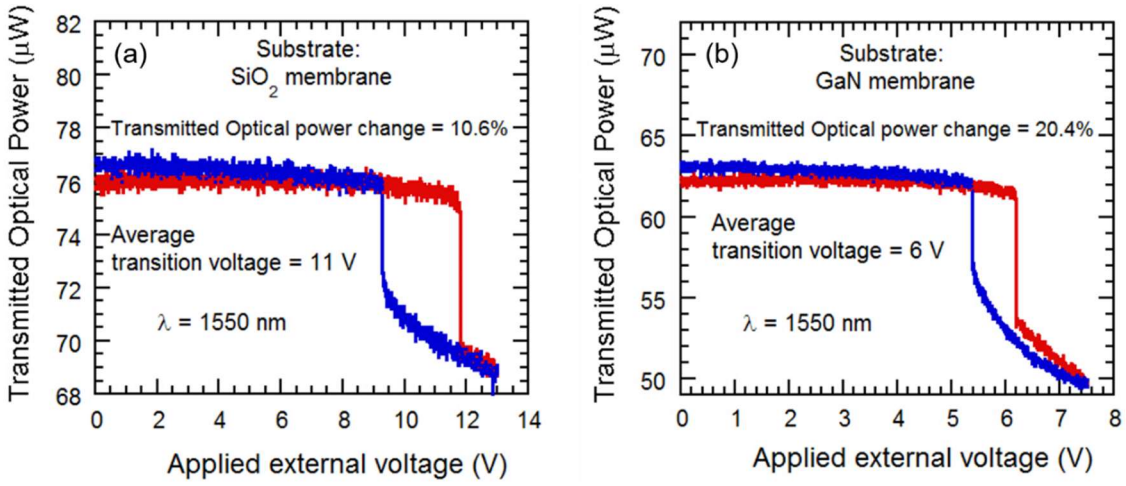

Figure 5.7: Transmitted optical power at laser wavelength 1550 nm, plotted against bias voltage applied at VO_2 membranes, fabricated from the VO_2 thin films grown on SiO_2, and GaN, as they undergo metal-insulator transition (SMT). The transmitted optical power change, along with the average transition voltages are shown for both the membranes.

As we expected, at transition voltage, the VO_2 membrane underwent semiconductor to metallic transition, and had a direct effect on the continuously transmitted IR beam through it. At the transition voltage, the transmitted optical power reduced drastically, and it went back to the initial level when we gradually reduced the input biasing voltage of the VO_2 diaphragm and allowed it to return to the semiconducting state (with an asymmetric hysteresis). The phenomenon is similar to what we experienced when we had applied heat to the large area VO_2 thin film to initiate SMT, as reported in ([31], [57]), also reported by others ([80] – [82]). After we plotted the transmitted optical power versus the input electric field as shown in Figure 5.7, we found that the transmitted power changes by 10% for the VO_2/SiO2, and 22% for the VO_2/GaN at the transition voltage.

Modulation of transmitted optical beam by VO_2 diaphragm

The similar setup shown in Figure 5.4 is implemented for the optical modulation of the transmitted IR beam by applying pulsed electric field of different pulse widths from the SMU set at an optimum analog frequency and digital data rate. The levels of the pulsed signal are decided on basis of the transition voltages of the semiconductor to metal transition (and vice versa) that we found from the electrical and optical characterizations.

Our goal is to periodically excite the VO_2 diaphragm and make it undergo SMT periodically with pulsed input electric field, and utilize this phenomenon to periodically modulate the incoming continuous IR beam transmitting through the diaphragm. The

electric field has a designated analog period of 5 milliseconds, with a particular pulse width. The pulse level is varied from 9V to 13V for the VO_2/SiO_2 (average transition voltage 11 V as shown in Figure 5.5), and 2V to 6V (average transition voltage 4V as shown in Figure 5.5. we have ensured that within the pulse level range we are setting, it should cover both the forward and reverse transitions of SMT, that is, the entire transition region including the hysteresis is captured by our input pulse.

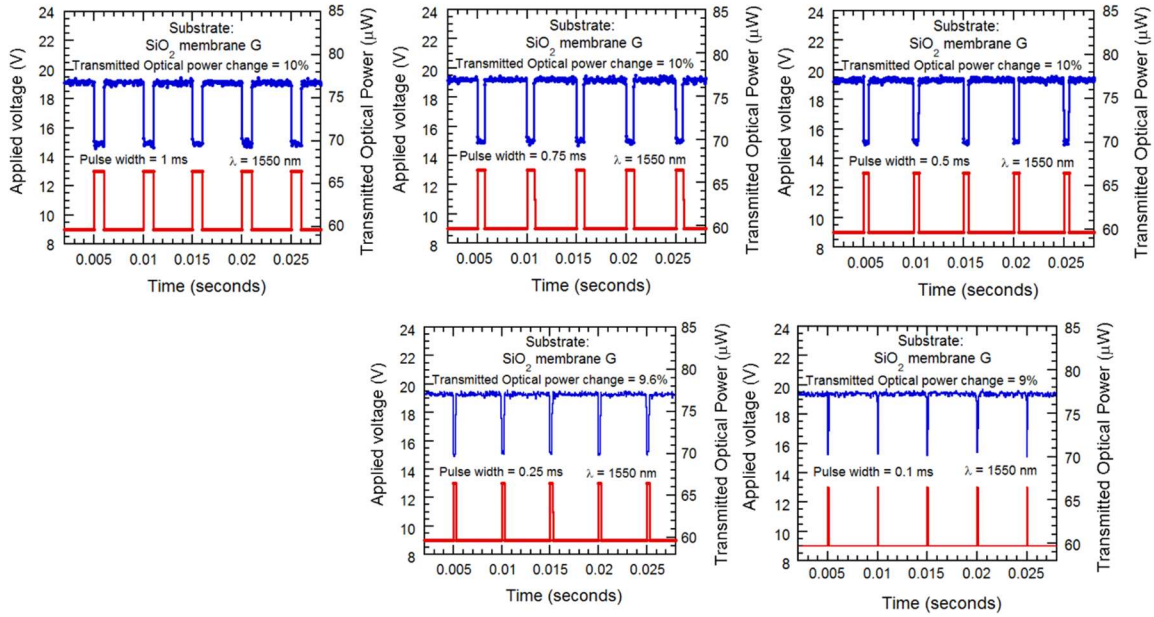

Figure 5.8: Modulation of transmitted optical power through VO_2 thin film membrane on SiO_2/Si substrate for continuous laser wavelength 1550 nm. The phase transition of the VO_2 film was initiated through applying pulsed electric signal to the VO_2 membrane. During the electric signal changing its level for each pulse, it changes the phase of the VO_2 from semiconducting to metallic and vice versa. The pulse widths for the electric signals are selected as 1 ms, 0.75 ms, 0.5 ms, 0.25 ms and 0.1 ms. For all the differently wide electric pulses, the continuously transmitted laser gets modulated by maintaining the similar pulse widths.

First we turn on the continuous IR laser of wavelength of 1550 nm to transmit through the VO_2 diaphragm, and then we initiate the periodic electric field based SMT

transition of the VO_2 membrane. We have witnessed that the resistance of the VO_2 diaphragm fluctuates periodically because of the pulsing SMT, locked at the exact same frequency of the input field. Simultaneously the previously continuous transmitted optical power is pulsing at the same input signal frequency, acting like as if emitting from a pulsed laser. This incident validates our assumption that we can cause a VO_2 diaphragm to undergo SMT at a particular frequency and pulse width by applying periodic electric field, and because of the phenomenon of the periodically pulsing SMT, it can cause periodic change to the continuously transmitted optical power [83]. Even though some literature reports their modulation depth more than 90%, actually their SMT was performed by a dual combination of external homogeneous heating and electric field. Moreover, there was no particular transition point of their VO_2 based optical switches, and they had to allow the VO_2 to undergo transition all the way from the very initial stage of semiconducting state to the final stage of the metallic state, and vice versa. On the other hand, our VO_2 diaphragms have a distinct transition voltage, which allows it to undergo semiconductor to metallic state within a very short range of external electric field, and no external heating was required.

We selected different pulse widths for the input electric voltage, as summarized in Table 5.1 With the 1550 nm laser, we have observed almost similar resistance pulse level ratios and percentages of modulation depth for all the pulse widths we have varied. That shows our VO_2 diaphragm can successfully modulate a transmitted continuous IR beam

of communication wavelength 1550 nm and construct a similar scenario of like it would be if the laser could emit pulsed IR beam.

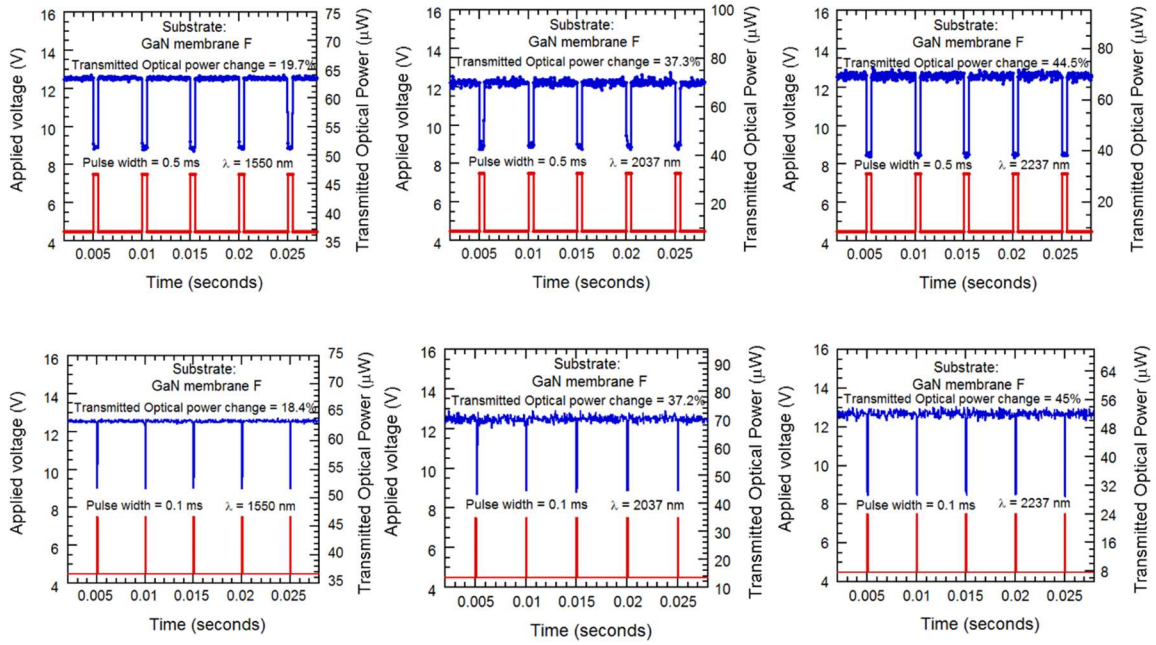

Figure 5.9: Modulation of transmitted optical power through VO_2 thin film membrane on GaN substrate for different continuous laser wavelengths 1550 nm, 2037 nm, 2237 nm, 2426 nm and 2601 nm. The phase transition of the VO_2 film was initiated through applying pulsed electric signal to the VO_2 membrane. During the electric signal changing its level for each pulse, it changes the phase of the VO_2 from semiconducting to metallic and vice versa. The pulse widths for the electric signals are selected as 1 ms, 0.75 ms, 0.5 ms, 0.25 ms and 0.1 ms. For all the differently wide electric pulses, the continuously transmitted laser gets modulated by maintaining the similar pulse widths.

However, in our lab, we do not have lasers with wavelengths more than 1550 nm. For higher wavelengths close to the mid-IR range, we collaborated with another research group and used their variable wavelength laser (model IPG HPTLM Cr:ZnS/Se) to emit continuous IR beam at our desired higher wavelengths and a different photodetector (model Thorlabs InGaAs PDA10D2, range 900 nm to 2600 nm). None of these two

groups have any power meter which is compatible with the photodetector (PDA10D2) which we had to use at their facilities. Therefore, we had to use an advanced digital oscilloscope (Tektronix, model TDS 3014C) to measure and record the optical beam detected by the photodetector. This experimental setup orientation is horizontal (Figure 5.10) compared to the vertical version we had used for 1550 nm laser at the facility of our group.

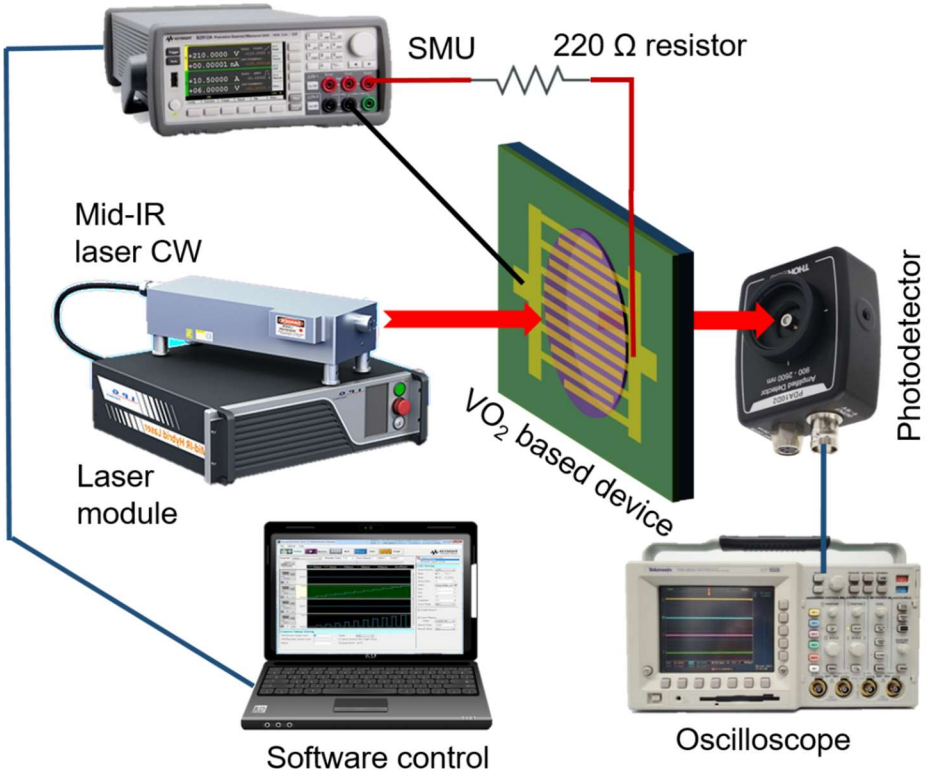

Figure 5.10: Experimental setup for optical characterizations and optical modulations of the VO_2 thin film based diaphragms in mid-IR range. The laser is shone from the left, while a photodetector at the right (along with a digital oscilloscope) measures the transmitted laser power as phase transition occurs, with laser variable wavelength (2037 nm, 2237 nm, 2416 nm and 2601 nm)

In order to observe the effect of VO_2 diaphragms on the laser beams with wavelengths close to mid-IR, we moved our experiment to the horizontally oriented setup as shown in Figure 5.10. We repeated the experiment for wavelengths 2037 nm, 2237 nm, 2426 nm and 2601 nm. For the input electric signal with analog frequency as we had for the previous step, we selected the exact same pulse widths as we did for the 1550 nm laser. For 2600 nm laser wavelength, other reports showed transmission change by 48%, which was excited by external heating to initiate transition in VO_2 [84]. On the other hand, our VO_2 diaphragms required no external heating, and they exhibited modulation depth of 52% for IR laser with 2601 nm wavelength. No matter the laser wavelength is, the periodic SMT can cause frequency locked periodic modulation of the transmitting continuous beam of IR laser. However, there is an interesting point to note, that is, the percentage of modulation depth changes with respect to the wavelength of the laser.

Table 5.1: Summary of the optimized material synthesis parameters for VO_2 diaphragms fabricated on substrates SiO_2/Si and GaN/AlGaN/GaN/Si

Parameters	SiO2 substrate	GaN substrate
VO_2 film thickness	140 nm	140 nm
Diameter of the diaphragm	0.75 mm	1 mm
RMS roughness from AFM images	7.37 nm	9.75 nm
2θ angles of prominent XRD peaks (FWHM)	69.28° (202) (0.06°)	38.52° (020) (0.16°)

2θ angles of common XRD peaks (FWHM)	38.42° (202) (0.16°)	38.52° (020) (0.16°)
Resistance transition ratio	31	49
Transmitted Optical power variation at laser1550 nm wavelength	10.6%	20.3%
Average transition voltage	11 V	6 V

The similar phenomenon was observed when we had optically characterized large area VO_2 thin films by initiating external heat induced semiconductor to metallic transition, as reported in [31]. The calculation of the modulation depths is summarized in Table 5.2. We can surmise that for laser beams of different wavelengths in IR region can be modulated periodically by causing SMT in the VO_2 membrane periodically, which is done by an externally applied pulsed electric field at different pulse widths, ranging down to 0.1 milliseconds only. Also, there appears to be a relationship between the percentage of modulation depths with respect to the wavelength of the continuous beam laser, as shown in Figures 5.11 and 5.12.

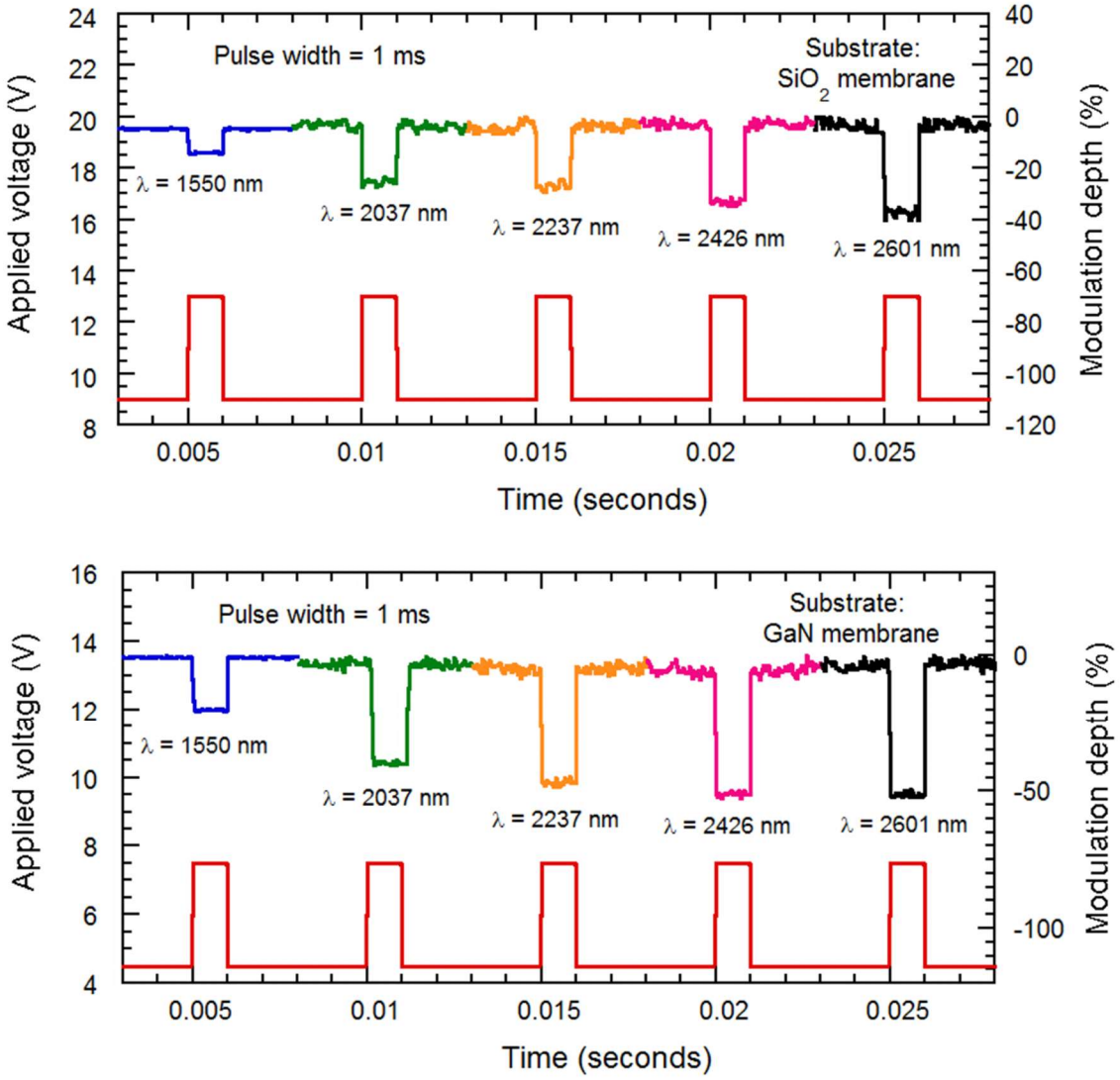

Figure 5.10: Percentage of modulation depth of transmitted optical power through VO_2 thin film membrane on (a) SiO_2 and (b) GaN substrates plotted against different continuous laser wavelengths 1550 nm, 2037 nm, 2237 nm, 2426 nm and 2601 nm. The pulse widths for the electric signals is selected as 1 ms. For all the differently wide electric pulses, the continuously transmitted laser gets modulated by maintaining the similar pulse widths. There is a trend of percentage of modulation changes linearly with the wavelength of the IR laser, irrespective of pulse width of the input voltage signal.

Power consumption during semiconductor to metal transition of VO_2 diaphragms

For VO_2/SiO2 at semiconducting state, due to applying external voltage 9 V, the voltage across the VO_2 diaphragm is 8.433 V. In this condition, the diaphragm draws 2.75 mA current, and consumes 23.19 mW of electric power. At metallic state, the applied external voltage is 13 V, and the voltage across the VO_2 diaphragm is 3.272 V only. In this condition, the diaphragm draws 47.3 mA current, and consumes 154.8 mW of electric power.

However, for VO_2/GaN at semiconducting state, due to applying external voltage 4.5 V, the voltage across the VO_2 diaphragm is 4.32 V. In this condition, the diaphragm draws 7.4 mA current, and consumes 31.97 mW of electric power. At metallic state, the applied external voltage is 7.5 V only, and the voltage across the VO_2 diaphragm is 2.469 V only. In this condition, the diaphragm draws 27.2 mA current, and consumes 67.1 mW of electric power.

We are reporting on the functionality of VO_2 diaphragms as optical modulators and their SMT due to externally applied electric field in room temperature. The membranes have been patterned with interdigitated finger contacts and the close proximity of the fingers play an important role for enabling the VO_2 undergo SMT with electric field only, without applying any external heat or change of temperature. The device is so responsive to electric field that the resistance pulsates in the exact same frequency of the externally pulsed electric field applied for initiating the SMT.

Simultaneously, the near-IR beam of communication wavelength 1550 nm which is transmitted through the VO_2 film, also the percentage of the modulation depth in the same frequency and duty cycle of the external field. The device can respond to pulses as small as those with width of 0.1 milliseconds. The similar type of responses for the transmitted IR beam is observed for the near mid-IR wavelengths of lasers, where we observe the greater modulation depth percentage for the higher wavelengths. The observed trend of modulation depth percentage increasing because of increasing the laser wavelength is supports the possibility of opening a new area of application of VO_2 as a gas sensing material at mid-IR wavelengths of the lasers, since we have observed that a wide range of variety of gases and compounds, which functions best at optimum wavelengths near mid-IR can be detected because of periodic phase transition of VO_2 thin film.

Table 5.2: Summary of the of the modulation depths by VO_2 diaphragms fabricated on substrates SiO2/Si and GaN/AlGaN/GaN/Si for different near-IR and mid-IR wavelengths, at different pulse widths

Laser wavelength		1064 nm	1550 nm	2037 nm	2237 nm	2416 nm	2601nm
Pulse width	VO_2 substrate						
1 ms	SiO2	-	9.8%	23.3%	28.3%	33.5%	36.1%
	GaN	9.09%	20.3%	37.3%	44.9%	47.3%	52.2%

0.75 ms	SiO2	-	10.1%	23.1%	28.3%	33.3%	36.3%
	GaN	9.3%	20.1%	37.2%	45%	47.2%	52.1%
0.5 ms	SiO2	-	10.4%	23.4%	28.1%	33.2%	36.3%
	GaN	9.1%	20.4%	38.1%	4.8%	47.3%	52.1%
0.25 ms	SiO2	-	10.4%	23.1%	27.9%	33.4%	36.2%
	GaN	8.97%	19.8%	37.1%	44.3%	47.1%	51.9%
0.1 ms	SiO2	-	9.9%	23.2%	28.1%	33.2%	36.1%
	GaN	8.94%	20.2%	37.2%	44.2%	47.15%	52.2%

CHAPTER SIX

CONCLUSION AND FUTURE WORK

In conclusion, high quality VO_2 film synthesis technique is reported using direct oxidation technique, on piezoelectric and flexible substrates. They are compared them to the films synthesized on two traditional substrates, sapphire and SiO_2/Si. Our VO_2 films are subjected to structural, electrical and optical characterization and their quality is foun to be mostly better than the VO_2 films grown by applying other techniques. The VO_2 films synthesized on both piezoelectric GaN/AlGaN/GaN/Si and AT-cut quartz substrates and flexible muscovite substrate display the great quality of the thin films. The parameters for VO_2 thin film growth were optimized carefully. In this research, direct oxidation technique has been implemented and optimized for VO_2 thin film synthesis and ensuring high quality polycrystalline structure. Electron beam evaporation was used to deposit Vanadium metal films on the substrates. Subsequently, they were oxidized in the low pressure system we have designed and developed at appropriate temperature, chamber pressure and gas flow rates. The time frame of oxidation, condition for cooling and substrate orientation are important in this regard. Substrates of large surface area and small patterned surface area were selected and compared. VO_2 films were subjected to material characterization techniques such as atomic force microscopy and x-ray diffraction and Raman spectroscopy to verify the crystalline quality. The synthesized polycrystalline VO_2 films were patterned with interdigitated metal fingers and later the bottom layer of the substrate was removed by Bosch process.

We have induced SMT by a high powered laser. Instead of applying heat with the ceramic heater used in this research, which heats the whole VO_2 film and impossible to control and contain the heat spatially and periodically, the high powered laser comes to rescue. The high powered laser focuses on a quite small area of the VO_2 film surface, thus allowing us to select and decide which portion of the surface we want to induce SMT. Also, we can apply periodic pulse to the laser, allowing it to be on or off periodically at any frequency, and consequently allowing the laser pointed area of the VO_2 surface to undergo SMT periodically.

The synthesized VO_2 films were characterized electrically and resulted in high resistivity transition ratio. The and smoothness of the resistivity vs. temperature plots. From the XRD pattern, the great crystal quality of the thin films is indicated by high intensity peaks with low FWHM indicates, also from the Raman spectroscopy plots. The modulation depth of infrared transmission reduction caused by the VO_2 films are evidence of the possibility for VO2 based optical modulators.

We have successfully used the VO_2 film as optical chopper or modulator and reported on the functionality of VO_2 diaphragms as optical modulators and their SMT due to externally applied electric field in room temperature. Allowing a continuous IR beam through the VO_2 and applying a periodic voltage on the VO_2 with finger pattern can induce SMT in the VO_2 in a periodic manner. The continuous IR beam experiences the

semiconducting and metallic VO_2 in a periodic manner, which will make the transmission through the film periodically high and low. We can control the input voltage frequency and trigger the SMT in the VO_2 according to our choice, leading to the VO_2 film being a fast and robust optical modulator.

The membranes have been patterned with interdigitated finger contacts and the close proximity of the fingers play an important role for enabling the VO_2 undergo SMT with electric field only, without applying any external heat. The device is so responsive to electric field that the resistance pulsates in the exact same frequency of the externally pulsed electric field applied for initiating the SMT. Simultaneously, the near-IR beam of communication wavelength 1550 nm which is transmitted through the VO_2 film, also the percentage of the modulation depth in the same frequency and duty cycle of the external field. The device can respond to pulses as small as those with width of 0.1 milliseconds. The similar type of responses for the transmitted IR beam is observed for the near mid-IR wavelengths of lasers, where we observe the greater modulation depth percentage for the higher wavelengths. The observed trend of modulation depth percentage increasing because of increasing the laser wavelength is supports the possibility of opening a new area of application of VO_2 as a gas sensing material at mid-IR wavelengths of the lasers, since we have observed that a wide range of variety of gases and compounds, which functions best at optimum wavelengths near mid-IR can be detected because of periodic phase transition of VO_2 thin film.

Future plans

1) **Surface acoustic wave based optical modulators**

The SMT of the our VO_2 films are triggered by applying heat, but they can be triggered by electric field and laser heating and mechanical strain as well. The SMT induction by electric field removes the necessity of extra heating to use the VO_2 film in switching applications. When the applied electric field crosses the threshold field, the VO_2 undergoes SMT, shifts its phase and turn on or off the switch as it is designed. Periodic electric field into a VO_2 with finger pattern on a piezoelectric substrate can generate surface acoustic waves on the surface. This acoustic waves can create periodic mechanical strain on the VO_2 film, which can induce phase transition in a periodic fashion. Combined with the properties of the VO_2 film based diaphragms that we have fabricated, we are planning to make a novel type of surface acoustic wave based IR modulators. They will play efficient and significant roles in a wide area of applications such as cellular disintegration, DNA sensing, detection of small molecules and so on. This proposed VO_2-GaN based surface acoustic wave generator is a new prototype of device which is highly stable, and highly sensitive simultaneously. It will become a reliable sensing device in the realm of biomedical applications.

2) **Strain induced deflection sensors**

We are also planning to design and fabricate microcantilever and bridge structures coated with VO_2 thin film. In a vacuum environment, the cantilevers and the bridges can be deflected very easily and make them experience mechanical strain. This strain can

induce SMT in the VO_2 film on the cantilever, and can be used to detect deflections of microcantilevers and films for sensing applications.

3) Highly sensitive room temperature deflection sensors

We have observed that metal doped VO_2 has a much lower transition temperature rather than the undoped VO_2. This can enable us to synthesize VO_2 film with appropriate amount of metal doping so that the transition temperature is as close as the room temperature. This will lead to fabrication of highly sensitive thermal sensor, which can undergo SMT at a quite low temperature and provide high precision temperature detection.

4) Gas sensing using infrared optical transmission

It is also in our plan to implement VO_2 thin films and diaphragms for sensing gases such as CO_2, H_2S, H_2, NH_3 and others, both in ambient temperature, also in harsh high temperature and polluted environment. Since we have discovered and displayed how VO_2 can regulate and modulate near-IR and mid-IR beams, and the IR beams are commonly used for gas sensing and detection, therefore VO_2 can play a highly important role in gas sensing.

Undoubtedly, VO_2 is a highly promising material with a new unexplored realm of possibilities. If we are successful to meet all our research agenda described above, we can guarantee that it will lead to a revolution in semiconductor based sensing industry.

REFERENCES

[1] P. Guo, A. Sarangan, E. Agha, A Review of Germanium-Antimony-Telluride Phase Change Materials for Non-Volatile Memories and Optical Modulators, Applied Sciences, vol. 9:530, 1-26 (2019)

[2] S. V. Ovsyannikov, D. M. Trots, A. V. Kurnosov, W. Morgenroth, H. –P. Liermann, and L. Dubrovinsky, Anomalous compression and new high-pressure phases of vanadium sesquioxide, V2O3", Journal of Physics: Condensed Matter, vol. 25:385401, 1-10 (2013)

[3] Kang et al. "Metal-insulator transition without structural phase transition in V2O5 film", Applied Physics Letters, vol. 98:131907, 1-4 (2011)

[4] Zhou et al. "Heteroepitaxial VO_2 thin films on GaN: Structure and metal-insulator transition characteristics", Journal of Applied Physics, vol. 112:074114, 1-9 (2012)

[5] Singer et al. "Nonequilibrium Phase Precursors during a Photoexcited Insulator-to-Metal Transition in V_2O_3", Physics Review Letters, vol. 120:207601, 1-6 (2018)

[6] Kang et al. "Metal-insulator transition without structural phase transition in V_2O_5 film", Applied Physics Letters, vol. 98:131907, 1-4 (2011)

[7] L. L. Fan, S. Chen, Y. F. Wu, F. H. Chen, W. S. Chu, X. Chen, C. W. Zou, and Z. Y. Wu, Growth and phase transition characteristics of pure M-phase VO_2 epitaxial film prepared by oxide molecular beam epitaxy, Applied Physics Letter, vol. 103, no. 131914, 1-6 (2013)

[8] Ming et al. "Hydrothermal Synthesis of VO_2 Polymorphs", Advanced Science News, 1701147, 1-25 (2017)

[9] Shao et al. "Recent progress in the phase-transition mechanism and modulation of vanadium dioxide materials", NPG Asia Materials, vol. 10, 581-605 (2018)

[10] Xu et al. "A Thermal Tuning Meta-Duplex-Lens (MDL): Design and Characterization", Nanomaterials, vol. 10:1135, 1-12 (2020)

[11] Kim et al. Mott Switching and Structural Transition in the Metal Phase of VO_2 Nanodomain, ACS Applied Electronic Materials, vol. 3, no. 2, 605-610 (2021)

[12] Grandi et al, Unraveling the Mott-Peierls intrigue in vanadium dioxide, Physical Review Research, vol. 2, 013298 (2020)

[13] Hofstetter et al, Relation between energy-level statistics and phase transition and its application to the Anderson model, Physical Review B, vol. 49, 14726 (1994)

[14] M. A. Baqir, and P. K. Choudhury, On the VO_2 metasurface-based temperature sensor, Journal of the Optical Society of America, vol. 36, no. 8, F123-F130 (2019).

[15] Y. Cui, Y. Ke, C. Liu, Z. Chen, N. Wang, L. Zhang, Y. Zhou, S. Wang, Y. Gao, and Y. Long, Thermochromic VO_2 for energy-efficient smart windows, Joule Cellpress Reviews, 1707-1746 (2018).

[16] J. Lee, D. Lee, S. J. Cho, J. –H. Seo, D. Liu, C. –B. Eom, and Z. Ma, Epitaxial VO_2 thin film-based radio-frequency switches with thermal activation, Applied Physics Letter, vol. 111, no. 063110, 1-5 (2017).

[17] D. Torres, T. Wang, J. Zhang, X. Zhang, S. Dooley, X. Tan, H. Xie, and N. Sepúlveda, VO_2-based MEMS mirrors, Journal of Microelectromechanical Systems, vol. 25, no. 4, 780-787 (2016).

[18] D. Gajula, F. Bayram, I. Jahangir, D. Khan, and G. Koley, Dynamic response of VO_2 mesa based GaN microcantilevers for sensing applications, Proc. IEEE Sensors (2019).

[19] C. Piccirillo, R. Binions, and I. P. Parkin, Synthesis and functional properties of vanadium oxides: V_2O_3, VO_2, and V_2O_5 deposited on glass by aerosol-assisted CVD, Chemical Vapor Deposition vol. 13, 145-151 (2007).

[20] L. Kang, Y. Gao, H. Luo, A novel solution process for the synthesis of VO_2 thin films with excellent thermochromic properties, Applied Materials and Interfaces, vol. 1, no. 10, 2211-2218 (2001).

[21] C. Zhang, C. Koughia, O. Günes, J. Luo, N. Hossain, Y. Li, X. Cui, S. –J. Wen, R. Wong, Q. Yang, and S. Kasap, Synthesis, structure and optical properties of high-quality VO_2 thin films grown on silicon, quartz and sapphire substrates by high temperature magnetron sputtering: Properties through the transition temperature, Journal of Alloys and Compounds, 848, 156323 (1-13) (2020).

[22] Ch. V. R. Reddy, E. H. Walker Jr, S. A. Wicker, Q. L. Williams, R. R. Kaluru, Synthesis of VO_2 (B) nanorods for Li battery application, Current Applied Physics, vol. 9, 1195-1198 (2009).

[23] M. J. Powell, I. J. Godfrey, R. Queseda-Cabrera, Qualitative XANES and XPS analysis of substrate effects in VO_2 thin films: A route to improving chemical vapor deposition synthetic methods? The Journal of Physical Chemistry, vol. 121, 20345-20352 (2017).

[24] D. –Q. Liu, W. –W. Zheng, H. –F. Cheng, and H. –T. Liu, Thermochromic VO_2 thin film prepared by post annealing treatment of V_2O_5 thin film, Advanced Materials Research, 79-82, 747-750 (2009).

[25] O. A. Novodvorsky, L. S. Parshina, and O. D. Karamova, Influence of the conditions of pulsed laser deposition on the structural, electrical, and optical properties of VO_2 thin films, Bulletin of the Russian Academy of Sciences, vol. 80, no. 4, 376-380 (2016).

[26] B. Guo, D. Wan, A. Ishaq, H. Luo, and Y. Gao, Direct synthesis of high-performance thermal sensitive VO_2 (B) thin film by chemical vapor deposition for using in uncooled infrared detectors, Journal of Alloys and Compounds, vol. 715, 129-136 (2017).

[27] J. Vlček, D. Kolenatý, J. Houška, T. Kozák and R Čerstvý, Controlled reactive HiPIMS—effective technique for low-temperature (300 °C) synthesis of VO_2 films with semiconductor-to-metal transition, Journal of Physics D: Applied Physics, vol. 50, no. 38, 1-7

[28] J. Houska, D. Kolenaty, J. Vlcek, and R. Cerstvy, Properties of thermochromic VO_2 films prepared by HiPIMS onto unbiased amorphous glass substrates at a low temperature of 300 °C, Thin Solid Films, vol. 660, 463-470 (2018).

[29] J. Houska, D. Kolenaty, J. Vlcek, T. Barta, J. Rezek, and R. Cerstvy, Significant improvement of the performance of $ZrO_2/V_{1-x}W_xO_2/ZrO_2$ thermochromic coatings by utilizing a second-order interference, Solar Energy Materials and Solar Cells, vol. 191, 365-371 (2019).

[30] D. Kolenatý, J. Vlček, T. Bárta, J. Rezek, J. Houška and S. Haviar, High-performance thermochromic VO_2-base coatings with a low transition temperature deposited on glass by a scalable technique, Scientific Reports, vol. 10, no. 11107, 1-12 (2020).

[31] S. Chen, J. Lai, J. Dai, H. Ma, H. Wang, and X. Yi, Characterization of nanostructured VO_2 thin films grown by magnetron controlled sputtering deposition and post annealing method, Optics Express, vol. 17, no. 26, 24153-24161 (2009).

[32] D. Li, M. Li, J. Pan, Y. X. Zhang, and G. H. Li, Thermal Oxidation of V_2O_3 Nanocrystals: A Template Method for the Fabrication of Monoclinic Phase VO_2 Nanocrystals, Journal of Nanoscience and Nanotechnology, vol. 13, 5469-5473 (2013).

[33] X. Liu, R. Ji, Y. Zhang, H. Li, and S. –W. Wang, Annealing process and mechanism of glass based VO_2 film from V oxidation in pure oxygen atmosphere, Optical and Quantum Electronics, 48, article 453, 1-10 (2016).

[34] L. Rongrong, H. Peng, H. Wanxia, Y. Jiazhen, and C. Jinghan, Optical switching and color changing properties of VO_2 films on muscovite substrate, Rare Metal Materials and Engineering, vol. 41, issue 8, 1327-1330 (2012).

[35] R. Lindstrom, V. Maurice, S. Zanna, L. Klein, H. Grault, L. Perrigaud, C. Cohen and P. Marcus, Thin films of vanadium oxide grown on vanadium metal: oxidation conditions to produce V_2O_5 films for Li-intercalation applications and characterization by XPS, AFM, RBS/NRA, Surface and Interface Analysis, vol. 38, 6-18 (2006).

[36] T. Lin, J. Wang, G. Liu, L. Wang, X. Wang and Y. Zhang, influence of discharge current on phase transition properties of high quality polycrystalline VO_2 thin film fabricated by HiPIMS, Materials, vol. 10, no. 633, 1-12 (2017).

[37] M. R. Bayati, R. Molaei, F. Wub, J. D. Budai, Y. Liu, R. J. Narayan and J. Narayan, Correlation between structure and semiconductor-to-metal transition characteristics of VO_2/TiO_2/sapphire thin film heterostructures, Acta Materialia, vol. 61, 7805-7815 (2013).

[38] Y. Zhao, J. H. Lee, Y. Zhu, M. Nazari, C. Chen, H. Wang, A. Bernussi, M. Holtz, and Z. Fan, Structural, electrical, and terahertz transmission properties of VO_2 thin films grown on c-, r-, and m-plane sapphire substrates, Journal of Applied Physics, vol. 111, 053533 (2012).

[39] P. Markov, R. E. Marvel, H. J. Conley, K. J. Miller, R. F. Haglund Jr., and S. M. Weiss, Optically monitored electrical switching in VO_2, ACS Photonics, 2, 1175-1182 (2015).

[40] Z. Yang, C. Ko, and S. Ramanathan, Metal-insulator transition characteristics of VO_2 thin films grown on Ge (100) single crystals, Journal of Applied Physics, 108, 07308 (1-7) 2010.

[41] S. Rathi, J. –H. Park, In. –y. Lee, J. M. Baik, K. S. Yi, and G. –H. Kim, Unravelling the switching mechanisms in electric field induced insulator–metal transitions in VO_2 nanobeams, Journal of Physics D: Applied Physics, 47, 295101 (1-9) (2014).

[42] L. Q. Mai, B. Hu, T. Hu, W. Chen, and E. D. Gu, Electrical property of Mo-doped VO_2 nanowire array film by melting-quenching sol-gel method, The Journal of Physical Chemistry B, 110, 19083-19086 (2006)

[43] C. Chen, Y. Zhao, X. Pan, V. Kuryatkov, A. Bernussi, M. Holtz, and Z. Fan, Influence of defects on structural and electrical properties of VO_2 thin films, Journal of Applied Physics, 110, 023707 (1-7) (2011).

[44] C. N. Berglund, and H. J. Guggenheim, Electronic properties of VO_2 near semiconductor-metal transition, Physical Review, Bell Telephone Laboratories, vol. 185, no. 3, 1022-1033 (1969).

[45] J. Wei, Z. Wang, W. Chen and D. H. Cobden, New aspects of the metal–insulator transition in single-domain vanadium dioxide nanobeams, Nature Technology, vol. 4, 420-424 (2009).

[46] S. Kumar, J. P. Strachan, M. D. Pickett, A. Bratkovsky, Y. Nishi, and R. S. Williams, Sequential electronic and structural transitions in VO_2 observed using x-ray absorption spectromicroscopy, Advanced Materials, 26, 7505-7509 (2014).

[47] R. T. Singh, D. Khan, D. Gajula, F. Bayram, and G. Koley, Synthesis and characterization of VO_2 on III nitride thin films using low pressure chemical vapor deposition for sensing applications, Proceedings of IEEE 13th Nanotechnology Materials and Devices Conference, 1-4 (2018).

[48] S. Azad, R. Singh, M. Munna, F. Bayram, D. Khan, H. Li, and G. Koley, Investigation of VO_2 thin film grown on III-nitride epitaxial layer, Proceedings of IEEE Nano 2020, 315-318 (2020).

[49] M. Qazi, III-V nitride based piezoresistive microcantilever for sensing applications, Applied Physics Letter, vol. 99, 99–103 (2011).

[50] T. Slusar, J.–C. Cho, B.–J. Kim, S. J. Yun, and H.–T. Kim, Epitaxial growth of higher transition temperature VO_2 films on AlN/Si, Applied Physics Letters Materials, vol. 4, 026101, 1-8 (2016).

[51] H. Harima, Properties of GaN and related compounds studied by means of Raman scattering, Journal of Physics: Condensed Matters, vol. 14, 967-993 (2002).

[52] D. Zhang, H.–J. Sun, M.–H. Wang, L.–H. Miao, H.–Z. Liu, Y.–Z. Zhang, and J. M. Bian, VO_2 thermochromic films on quartz glass substrate grown by RF-plasma-assisted oxide molecular beam epitaxy, Materials, 10, 3174 (1-10) (2017).

[53] Joushaghani, J. Jeong, S. Paradis, D. Alain, Wavelength-size hybrid Si-VO_2 waveguide electroabsorption optical switches and photodetectors, Optics Express, vol. 23, no. 3 (2015).

[54] S. Yu, S. Wang, M. Lu, and Lei Zuo, A metal-insulator transition study of VO_2 thin films grown on sapphire substrates, Journal of Applied Physics, vol. 122, no. 235102, 1-6 (2017).

[55] J. Jian, X. Wang, L. Li, M. Fan, W. Zhang, J. Huang, Z. Qi, and H. Wang, Continuous tuning of phase transition temperature in VO_2 thin films on c-cut sapphire substrates via strain variation, Applied Materials and Interfaces, vol. 9, no. 6, 5319-5327 (2017).

[56] J. Bian, L. Miao, S. Zhao, X. Li, C. Zou, D. Zhang, and Y. Zhang, Vanadium oxide films deposited on sapphire substrate with in situ AlN stress layer: structural, electric, and optical properties, Journal of Material Science, vol. 50, 5709-5714 (2015).

[57] G. J. Kovács, D. Bürger, I. Skorupa, H. Reuther, R. Heller, and H. Schmidt, Effect of the substrate on the insulator–metal transition of vanadium dioxide films, Journal of Applied Physics, vol. 109, no. 063708, 1-6 (2011).

[58] T. –H. Yang, R. Aggarwal, A. Gupta, H. Zhou, R. J. Narayan, and J. Narayan, Semiconductor-metal transition characteristics of VO_2 thin films grown on c- and r- sapphire substrates, Journal of Applied Physics, vol. 107, no. 053514, 1-7 (2010).

[59] B. G. Chae, D. H. Youn, H. T. Kim, S. L. Maeng, and K. Y. Kang, Fabrication and electrical properties of pure VO_2 phase films, Journal of the Korean Physical Society, vol. 44, no. 4, 884-888 (2004).

[60] D. Bhardwaj, A. Goswami, and A. M. Umarji, Synthesis of phase pure vanadium dioxide (VO_2) thin film by reactive pulsed laser deposition, Journal of Applied Physics, vol. 124, no. 135301, 1-7 (2018).

[61] D. –H. Youn, J. –W. Lee, B. –G. Chae, H. –T. Kim, S. –L. Maeng, and K. –Y. Kang, Growth optimization and electrical characteristics of VO_2 films on SiO_2/Si amorphous substrates, Journal of Applied Physics, vol. 95, no. 1407, 1-6 (2004).

[62] F. B. Dejene, and R.O. Ocaya, Electrical, optical and structural properties of pure and gold-coated VO_2 thin films on quartz substrate, Current Applied Physics, vol. 10, 508-512 (2010).

[63] H. Kizuka, T. Yagi, J. Jia, Y. Yamashita, S. Nakamura, N. Taketoshi, and Y. Shigesato, Temperature dependence of thermal conductivity of VO_2 thin films across metal–insulator transition, Japanese Journal of Applied Physics, vol. 54, no. 053201, 1-6 (2015).

[64] Y. Dang, D. Wang, X. Zhang, L. Ren, B. Li, and J. Liu, Structure and thermochromic properties of Mo-doped VO_2 thin films deposited by sol–gel method, Inorganic and Nano Metal Chemistry, vol. 49, no. 4, 120-125 (2019).

[65] M. Taha, S. Walia, T. Ahmed, D. Headland, W. Withayachumnankul, S. Sriram and M. Bhaskaran, Insulator–metal transition in substrate-independent VO_2 thin film for phase-change devices, Scientific Reports, vol. 7:178999, 1-10 (2017).

[66] D. –Q. Liu, C. Haifeng, Z. Wenwei, and Z. Chaoyang, Infrared thermochromic properties of VO_2 thin films prepared through aqueous sol-gel process, Journal of Wuhan University of Technology-Maters, vol. 10, no. 5, S61-S65 (2012).

[67] J. Ma, G. Xu, L. Miao, M. Tazawa, and S. Tanemura, Thickness-dependent structural and optical properties of VO_2 thin films, Japanese Journal of Applied Physics, vol. 50, 020215 (1-4) (2011).

[68] E. Radue, E. Crisman, L. Wang, S. Kittiwatanakul, and J. Lu, Effect of a substrate-induced microstructure on the optical properties of the insulator-metal transition temperature in VO_2 thin films, Journal of Applied Physics, vol. 113, 233104 (1-7) (2013).

[69] A. Lochbaum, A. Dorodnyy, U. Koch, S. M. Koepfli, S. Volk, Y. Fedoryshyn, V. Wood, and J. Leuthold, "Compact Mid-Infrared Gas Sensing Enabled by an All-Metamaterial Design", Nano Letters, vol. 20, 4169-4176 (2020).

[70] T. Jin, J. Zhoua, and P. T. Lin, "Real-time and non-destructive hydrocarbon gas sensing using mid-infrared integrated photonic circuits", RSC Advances, vol. 10, 7452-7459 (2020).

[71] Y. Wang, K. Zheng, F. Song, F. K. Tittel, and C. Zheng, "Mid-infrared absorption spectroscopy for gas sensing and application," 2020 IEEE 5th Optoelectronics Global Conference (OGC) (2020).

[72] R. S. El Shamy, D. Khalil, and M. A. Swillam, "Mid Infrared Optical Gas sensor using Plasmonic Mach-Zehnder interferometer," Scientific Reports 10, 1293 (2020).

[73] Y. Yamamoto, M. Oshita, S. Saito, and T. Kan, "Near-infrared spectroscopic gas detection using a surface plasmon resonance photodetector with 20 nm resolution," ACS Applied Nano Materials 4, 13405–13412 (2021).

[74] X. Tan, H. Zhang, J. Li, H. Wan, Q. Guo, H. Zhu, H. Liu, and F. Yi, "Non-dispersive infrared multi-gas sensing via nanoantenna integrated narrowband detectors," Nature Communications 11, (2020).

[75] X. Chong, K.-J. Kim, E. Li, Y. Zhang, P. R. Ohodnicki, C.-H. Chang, and A. X. Wang, "Near-infrared absorption gas sensing with metal-organic framework on optical fibers," Sensors and Actuators B: Chemical 232, 43–51 (2016).

[76] X. Yin, M. Gao, R. Miao, L. Zhang, X. Zhang, L. Liu, X. Shao, and F. K. Tittel, "Near-infrared laser photoacoustic gas sensor for simultaneous detection of CO and H2S," Optics Express 29, 34258 (2021).

[77] Q. Chen, L. Liang, Q. Zheng, Y. Zhang, and L. Wen, "On-chip readout plasmonic mid-IR Gas Sensor," Opto-Electronic Advances 3, 190040–190040 (2020).

[78] Y. Suematsu, "Long-wavelength optical fiber communication," Proceedings of the IEEE 71, 692–721 (1983).

[79] G. Li, Y. Song, H. Zhao, E. Dong, J. Li, L. Jia, Y. Liu, S. Zhang, and F. Zhao, "A near-infrared multi-gas sensor based on IWTD-CEEMDAN and WOA-BiLSTM for detection of CH4 and NH3 leaked in industrial production," Infrared Physics & Technology 131, 104695 (2023).

[80] B. Li, Z. Wang, S. Zhao, C. Hu, L. Li, M. Liu, J. Zhu, T. Zhou, G. Zhang, J. Jiang, and C. Zou, "Enhanced Pd/a-WO3/VO_2 Hydrogen Gas Sensor Based on VO_2 Phase Transition Layer," Small Methods 6, 2200931 (2022).

[81] P.-G. Su and L.-Y. Yang, "NH 3 gas sensor based on Pd/SNO 2 /RGO ternary composite operated at room-temperature," Sensors and Actuators B: Chemical 223, 202–208 (2016).

[82] M. A. Baqir and P. K. Choudhury, "On the VO_2 metasurface-based temperature sensor," Journal of the Optical Society of America B 36, (2019).

[83] Y. Cui, Y. Ke, C. Liu, Z. Chen, N. Wang, L. Zhang, Y. Zhou, S. Wang, Y. Gao, and Y. Long, "Thermochromic VO_2 for energy-efficient smart windows," Joule 2, 1707–1746 (2018).

[84] J. Lee, D. Lee, S. J. Cho, J.-H. Seo, D. Liu, C.-B. Eom, and Z. Ma, "Epitaxial VO_2 thin film-based radio-frequency switches with thermal activation," Applied Physics Letters 111, 063110 (2017).

[85] R. Basu, V. Srihari, M. Sardar, S. K. Srivastava, S. Bera, and S. Dhara, "Probing phase transition in VO_2 with the novel observation of low-frequency collective spin excitation," Scientific Reports 10, (2020).

[86] C. Aurelian, V. T. Vinod, O. Jean-Christophe, and B. Annie, "Fast electrical and optical activation of RF switches integrating vanadium dioxide (VO_2) phase change material," 2021 IEEE MTT-S International Microwave Workshop Series on Advanced Materials and Processes for RF and THz Applications (IMWS-AMP), 118-120 (2021).

[87] M. Rini, A. Cavalleri, R. W. Schoenlein, R. Lopez, C. Feldman, R. Haglund, L. A. Boatner, and T. E. Haynes, "Giant, ultrafast optical switching based on an insulator-to-metal transition in VO_2 nano-particles: Photo-activation of shape-controlled plasmons at 1.55 μm," https://escholarship.org/uc/item/68n8x41j.

[88] K. A. Hallman, K. J. Miller, A. Baydin, S. M. Weiss, and R. F. Haglund, "Sub-picosecond response time of a hybrid VO_2:Silicon Waveguide at 1550 nm," Advanced Optical Materials 9, 2001721 (2020).

[89] B. Janjan, M. Miri, A. Zarifkar, and M. Heidari, "Design and simulation of compact optical modulators and switches based on si–VO_2 –si horizontal slot waveguides," Journal of Lightwave Technology 35, 3020–3028 (2017).

[90] P. Markov, R. E. Marvel, H. J. Conley, K. J. Miller, R. F. Haglund, and S. M. Weiss, "Optically monitored electrical switching in VO_2," ACS Photonics 2, 1175–1182 (2015).

[91] D. Chauhan, G. T. Mola, and R. P. Dwivedi, "An ultra-compact plasmonic modulator/switch using VO_2 and elasto-optic effect," Optik 201, 163531 (2020).

[92] D. Chauhan, Z. Sbeah, R. Adhikari, M. S. Thakur, S. H. Chang, and R. P. Dwivedi, "Theoretical analysis of VO_2 filled double rectangular cavity-based coupled resonators for Plasmonic Active Switch/Modulator and band Pass Filter Applications," Optical Materials 125, 112078 (2022).

[93] H. M. Wong, Z. Yan, K. A. Hallman, R. E. Marvel, R. P. Prasankumar, R. F. Haglund, and A. S. Helmy, "Broadband, integrated, micron-scale, all-optical si3N4/VO_2 modulators with PJ switching energy," ACS Photonics 6, 2734–2740 (2019).

[94] S. Cueff, J. John, Z. Zhang, J. Parra, J. Sun, R. Orobtchouk, S. Ramanathan, and P. Sanchis, "VO_2 nanophotonics," APL Photonics 5, 110901 (2020).

[95] B. Wu, A. Zimmers, H. Aubin, R. Ghosh, Y. Liu, and R. Lopez, "Electric-field-driven phase transition in vanadium dioxide," Physical Review B 84, 241410 (2011).

[96] P.-F. Wang, Q. Hu, T. Zheng, Y. Liu, X. Xu, and J.-L. Sun, "Optically monitored electric-field-induced phase transition in vanadium dioxide Crystal Film," Crystals 10, 764 (2020).

[97] Y. Zhao, J. H. Lee, Y. Zhu, M. Nazari, C. Chen, H. Wang, A. Bernussi, M. Holtz, and Z. Fan, "Structural, electrical, and terahertz transmission properties of VO_2 thin films grown on c-, r-, and m-plane sapphire substrates", Journal of Applied Physics, vol. 111, 053533 (2012).

[98] I. Olivares, L. Sánchez, J. Parra, R. Larrea, A. Griol, M. Menghini, P. Homm, L.-W. Jang, B. van Bilzen, J. W. Seo, J.-P. Locquet, and P. Sanchis, "Optical switching in hybrid VO_2/si waveguides thermally triggered by lateral microheaters," Optics Express 26, 12387 (2018).

[99] E. K. Barimah, A. Boontan, D. P. Steenson, and G. Jose, "Infrared Optical Properties modulation of VO_2 thin film fabricated by ultrafast pulsed laser deposition for Thermochromic Smart Window applications," Scientific Reports 12, (2022).